SUPPLEMENTO
AL VOLUME XI, SERIE X, DEL
NUOVO CIMENTO
A CURA DELLA SOCIETÀ ITALIANA DI FISICA

1959 | 1° Trimestre | N. 1

The Earth's Simple Shadow Effect on Cosmic Radiation (*).

J. E. KASPER

State University of Iowa - Iowa City, Iowa

(ricevuto il 22 Aprile 1958)

CONTENTS. — **1. Introduction.** – **2. Definition of the simple shadow cones.** 1. Pencils of trajectories with properties *A*. 2. Pencils of trajectories with properties *B*. 3. Relations of pencils with properties *A* and *B* to features of cone diagrams. 4. Families of trajectories with properties *C* and their relation to pencils with properties *A* and *B*. 5. Generation of simple shadow cones. 6. Definition of a simple shadow cone. 7. Restrictions on the variables for validity of the definition. – **3. Computation of trajectories and of simple shadow cones.** 1. Computation of trajectories. 2. Interpolations performed on trajectories. 3. Reduction of trajectory data to simple shadow cones. – **4. Discussion.**

1. – Introduction.

This paper describes a new investigation of the earth's simple shadow effect on the cosmic radiation. A reexamination of this problem has long been called for by several considerations. One of these is that experimentalists have for many years believed the previously published simple shadow cones to be grossly in error because of their inherent unreasonableness. Another is that it can be shown easily without reference to any computed trajectories that at least parts of some of those cones are indeed incorrect quantitatively (vide infra). Further, it has recently been shown by numerical integration of the equations

(*) Assisted by the National Science Foundation, I.G.Y. Project 32.1.

of motion that a trajectory which should be in an earth's simple shadow region according to the published cones, is not in such a region [1].

Despite such considerations, the urgency of the need for new computations of the cones has not been great enough to have justified undertaking the large program of numerical work required for the integration of the equations of motion hundreds of times over and for the reduction of the integrations to actual simple shadow cones. However, in pursuing other and more elaborate goals, the author recently computed some 2 000 trajectories of charged particles in the field of a magnetic dipole with the use of an IBM Type 704 computer, some 500 of these trajectories having direct applicability to the problem of the shadow cones. This availability of the required trajectories, together with an awareness of the need for a recomputation of the cones, prompted performance of the work discussed in this paper.

There are given here a definition of the concept of the simple shadow cone, a discussion of some theoretical aspects of the subject, a set of newly computed cones, and a brief discussion of some of the significance of these cones for interpretation of cosmic ray observations.

Since even a partially self-contained paper on this subject would necessarily contain excessively lengthy preliminary explanations which are generally and readily available, there will be assumed familiarity with the older work on aspects of geomagnetic theory. Familiarity with the manner of treatment, and with the principal results of that treatment, of the problem of the reduced motion of a charged particle in the meridian plane of a magnetic dipole, as carried out by LEMAITRE and VALLARTA [2], and by SCHREMP [3,4] will be assumed. It will be assumed in particular that the contents of the second paper of 1938 by SCHREMP [4] are known.

The mathematical symbolism used by the writers referred to will be employed without explanation where it is uniform among them; otherwise explicit new conventions will be adopted. All symbols not defined here are defined in the papers of the writers named [2-4].

---

[1] (*a*) M. SCHWARTZ: *Bull. Am. Phys. Soc.*, II, **1**, no. 7, 319 (1956). This work is more fully described in a paper to be published soon by M. SCHWARTZ. (*b*) At the completion of this paper, a recent note by VALLARTA, GALL and LIFSHITZ has come to our attention (*Phys. Rev.*, **109**, 1403 (1958)). These authors have considered the influence of the quadrupole component of the earth's magnetic field on the simple shadow cone for several values of latitude, longitude and magnetic rigidity. They get results very near to ours, and attribute the discrepancy with Schremp to the quadrupole component. Our work shows that in fact this discrepancy is mostly due to serious errors in Schremp's work.

[2] G. LEMAITRE and M. S. VALLARTA: *Phys. Rev.*, **49**, 719 (1936).

[3] E. J. SCHREMP: *Phys. Rev.*, **54**, 153 (1938).

[4] E. J. SCHREMP: *Phys. Rev.*, **54**, 158 (1938).

It will be assumed that the earth is spherical and its magnetic field will be taken to be that of a magnetic dipole located at the geometrical center of the earth. The dipole strength is incorporated in the Størmer unit of length and need be specified. Latitudes (λ) referred to are geomagnetic latitudes defined with respect to the magnetic dipole axis, and are to be understood to be northern latitudes ($\lambda \geqslant 0°$) throughout this paper.

2. – Definition of the simple shadow cones.

2·1. *Pencils of trajectories with properties A.* – We begin by claiming that for at least some values x_0 and λ_0 of the variables x and λ, and for some values of the parameter γ_1, the pencil of trajectories in the x, λ plane issuing from the point x_0, λ_0 will have the following properties: 1) If the initial value η_0 of the angle η at the point x_0, λ_0 is such that $90° < \eta_0 < 270°$, the associated trajectory immediately upon issuance from the point lies in a region where $x < x_0$. 2) As η_0 decreases monotonically from 90° a continuum of trajectories associated with that continuum of values of η_0 occurs, all of which immediately upon issuance from the point x_0, λ_0 lie in a region where $x > x_0$ and all of which return after traversal or such a region to a region where $x < x_0$ with no points of inflection or extrema in x or λ in the region where $x > x_0$ except for a relative maximum in x followed by a relative maximum in λ, or except for a relative maximum in x only. 3) The continuum of trajectories referred to in (2), above, is terminated when η_0 reaches a value η_{SR} for which the associated trajectory issues into a region where $x > x_0$ and is a self-reversing trajectory with no points of inflection or extrema in x or λ between x_0, λ_0 and the self-reversal point at the contour $P = 0$ (upper branch). 4) As η decreases from η_{SR} monotonically, a continuum of associated trajectories occurs, all of which immediately upon issuance from x_0, λ_0 lie in a region where $x > x_0$ and which return after traversing such a region to a region where $x < x_0$ with no points of inflection or extrema in x or λ except for a relative maximum in λ followed by a relative maximum in x. 5) The continuum of trajectories referred to in 4), above, is terminated when η_0 reaches a value η_T^N for which the associated trajectory differs from those in 4) only in that on returning to the value x_0 for x, it there has a point of tangency with the line $x = x_0$. Such a trajectory will be called a trajectory of the second kind, following Schremp, as will certain others presently to be specified. The properties 1) through 5) will be referred to as properties A in the balance of this paper.

The existence of points with the properties A has not been shown with analytic rigor, nor can such a pencil with the required infinitely large population be produced by computation. However, the claim can be regarded as a postulate, and arguments adduced to lend it a high degree of plausibility.

The author settles the matter in the following brief way: in Figure 1 are shown some members of a pencil of trajectories for $x_0 = -0.08$, $\lambda_0 = 10°$, and $\gamma_1 = 0.92$ produced by numerical integration of the equations of motion. Although neither the self-reversing trajectory referred to in 3) above nor the trajectory of the second kind referred to in 5) above were computed, it is apparent that those sketched in with broken lines, and that the entire pencil has the properties *A*. One sees this by considering the form of the contour map over which the motions take place, the manner in which the x-minima for the trajectories move uniformly to the right as η_0 decreases from 90°, and the role played by the self-reversing trajectories in separating families which turn in a clockwise sense near the curve $P = 0$ from those which turn in a counter clockwise sense near there.

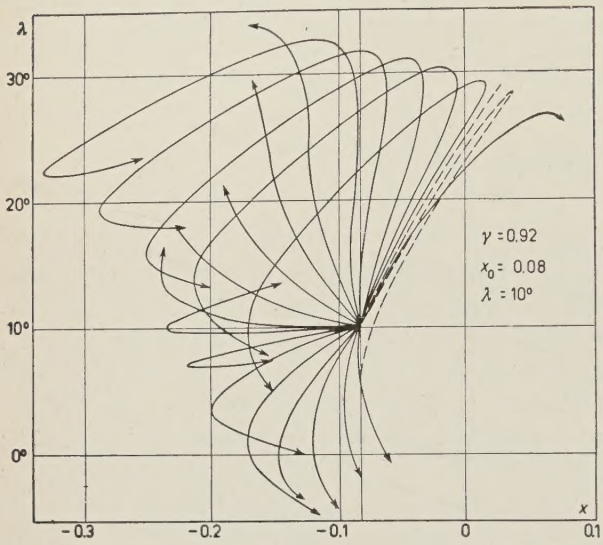

Fig. 1. – Pencil of trajectories issuing from $x_0 = -0.08$, $\lambda_0 = 10°$, for $\gamma_1 = 0.92$.

When such a point exists, then all trajectories issuing from the point x_0, λ_0 with $270° > \eta_0 > \eta_T^N$ are said to lie in the earth's simple shadow. The line $x = x_0$ can be interpreted as representing the earth's surface in these coordinates, and the point x_0, λ_0 as an observation point on the earth, while the reversibility of the motions in the x, λ plane with respect to the independent variable σ makes the trajectories open to interpretation as trajectories arriving at the point x_0, λ_0, so that those which lie in the earth's simple shadow correspond to paths for charged particles in the earth's magnetic dipole field which have to traverse part of the impenetrable earth in order to arrive at the observation point.

2·2. *Pencils of trajectories with properties B.* – The further claim is made that at least for some values x_0, λ_0 of x, λ and for some values of γ_1, the pencil issuing from the point x_0, λ_0 will have the following characteristics: 1) If η_0 is such that $90° < \eta_0 < 270°$ the associated trajectory immediately upon issuance from the point x_0, λ_0 lines in a region where $x < x_0$. 2) As η_0 increases monotonically from 270° a continuum of trajectories associated with

that continuum of values of η_0 occurs, all of which immediately upon issuance from the point x_0, λ_0 lie in a region where $x > x_0$ and all of which return after traversal of such a region where $x < x_0$ with no points of inflection or extrema in x or λ in the region where $x > x_0$ except for a relative maximum in x. 3) The continuum of trajectories just referred to is terminated when η_0 reaches a value η_T^S for which the associated trajectory differs from those in 2) only in that on returning to $x = x_0$, it there has a point of tangency with that line. Such a trajectory will also be called a trajectory of the second kind. Again, all trajectories from such a point with η_0 such that $90° < \eta_0 < \eta_T^S$ will be said to lie in the earth's simple shadow. The properties 1) through 3) will be called properties *B*.

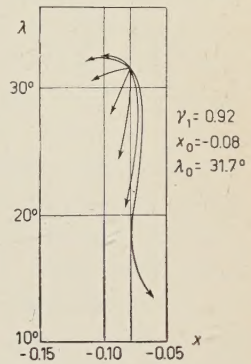

Fig. 2. – Pencil of trajectories issuing from $x_0 = -0.08$, $\lambda_0 = 31.7°$, for $\gamma_1 = 0.92$.

The validity of the claim is supported by examination of computed trajectories, together with considerations of the effects of the contours $P =$ costant on the forms of the trajectories as η_0 varies, as was the validity of the first claim. An example of such a point is shown in Figure 2 for $x_0 = -0.08$, $\lambda_0 = 31.7°$, $\gamma_1 = 0.92$.

A special kind of points of the first type described above exist when the self-reversing trajectory referred to in 3) itself has a point of tangency with the line $x = x_0$ at the initial point x_0, λ_0 and is thus identical with the trajectory referred to in 5), so that $\eta_{SR} = \eta_T^N$ and the continuum referred to in (4) is empty of members. Another special kind of point exist when families with properties *A* and *B* exist simultaneously for one point. Examples will be omitted.

2·3. *Relations of pencils with properties A and B to features of cone diagrams.* – It is to be noticed that for any point for which η_T^N exists, the corresponding values of x_0, λ_0, and γ_1 determine a value of the quantity $\sin\theta$, the horizontal coordinate in a cone diagram (as a $\sin\theta$, $\cos\theta \sin\eta$ plot will be called) and that the value of η_T^N there, together with the value of θ, fixes a quantity $\cos\theta \sin\eta$, the vertical coordinate in the cone diagram. In a similar way, x_0, λ_0, γ_1 and η_T^S, if the latter quantity exists at the point in question, determine a point on a cone diagram. All points in a cone diagram on a line $\sin\theta =$ constant above a point corresponding to η_T^N or below a point corresponding to η_T^S, or both if the two points exist simultaneously, correspond to trajectories lying in the earth's simple shadow. The points themselves will also be said to be in the earth's simple shadow for simplicity of expression. Thus the line $\sin\theta =$ = const may be divided into segments, some of which represent directions of arrival at the observation point on the earth which are not physically possible.

Figure 3 is a schematic representation of typical cases. In the figure, lines of constant $\sin\theta$ are shown; these are the same as lines of costant γ_1. For $\gamma_1^{(1)}$ all points on the segment ab above a, for $\gamma_1^{(2)}$ all points on cd below c, and for $\gamma_1^{(3)}$ all on ef above e and on gh below g are in the earth's simple shadow, as are all those in the lower hemisphere ($90° < \eta_0 < 270°$) for all values of γ_1.

It should be remarked somewhat parenthetically here that it is not claimed that the trajectories corresponding to the points a, c, e, or g or to points below a, above c, or between e and g escape to infinite values of x in the x, λ plane without ever intersecting the line $x = x_0$ after having issued from the point x_0, λ_0. Thus a point such as a, for example, may have points neighboring it on *both* sides along the line $\gamma_1 = \gamma_1^{(1)}$ which correspond to trajectories which arrive at x_0, λ_0 only after traversing regions where $x < x_0$.

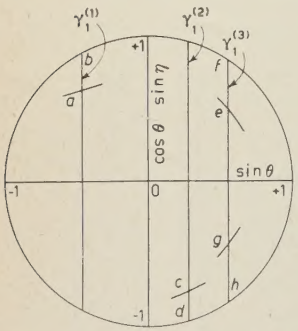

Fig. 3. – Schematic representation of points, lines, and arcs in cone diagram discussed in text.

Suppose that for some set of values of x_0, λ_0, and γ_1 a pencil having properties A exists. By virtue of the relation $e^x = 2r\gamma_1$ the family can equivalently be said to exist for certain values of r_0, λ_0, and γ_1. Now let it be supposed that while r and λ are held constant at the values r_0 and λ_0, γ_1 is allowed to vary from its initial value, which will now be called γ_{10}. It is apparent that one consequence of a minute variation of γ_1 from the value γ_{10} will be a minute variation of the topography of the x, λ plane — that is, the contour map formed by the lines $P =$ constant will change its structure slightly. A second consequence will be that a new point x, λ will correspond to the new value of γ_1 and the fixed values of r and λ, and this new point will lie embedded in the new contour map in changed relation to its features.

At least for some x_0, λ_0, γ_{10} there will exist pencils with the properties A for the new point and for all the points generated during the variation of γ_1. Also, the value of η_T^N associated with the pencils will vary continuously during the variation of γ_1. An adequate proof for these claims is the following: certainly for some x_0, λ_0, γ_{10} the trajectories in question will not pass through singular points, and therefore they will be continuous functions of the initial points and slopes and of the parameter ([5]).

Entirely similar claims are made for the continuous variation of the angle η_T^S during variation of k_1 when at least some points are considered for which pencils having properties B exist, and at least for suitably small ranges of variation of γ_1.

When variations of the kinds just discussed occur, there will be generated

([5]) E. L. Ince: *Ordinary Differential Equations* (London, 1927), ch. III.

continuous arcs on the faces of corresponding cone diagrams due to the continuous variations of θ and of η_T^N and η_T^S. Such arcs are indicated very schematically in Figure 3.

The reader will have anticipated the author's intent, at this point, to extend the claims just made sufficiently to provide for the continuous generation of an entire locus in any cone diagram as γ_1 varies continuously through its values across the face of the diagram, for given r and λ. Such a locus would be required to begin at some point on the upper edge of the cone diagram, move continuously in a clockwise sense around the diagram, and terminate at some point on the lower edge of the diagram. The loci for various values of r and λ would in fact constitute the simple shadow cones contemplated by Schremp. The generation of such loci will be discussed in a special way in the sequel. The approach to be adopted exhibits, it is believed, the manner of generation of the cones, the significance of special points on them (such as the upper initial point, the lower terminal point, and the maximum in the coordinate $\sin\theta$), and the limitations to be placed on the allowable values of r, λ, and γ_1 with clarity, and makes a meaningful definition of the simple shadow cones possible.

2·4. *Families of trajectories with properties C and their relation to pencils with properties A and B.* – We begin by discussing the properties of certain kinds of families of related trajectories. Let the segment of the line $x = x_0$ (for some value of γ_1) be considered which lies in a region where the values of P are allowed values for the motions. If, at each point on such a segment, a trajectory is initiated with $\eta_0 = 90°$ then the family resulting contains among its members all the trajectories of the second kind that can exist for those values of x and γ_1. Computed members of two such families are shown in Figures 4 and 5 for widely different values of x and γ_1. By reliable interpolations and extrapolations, one sees that in these families there occur in order with increasing λ: 1) A continuum of trajectories all of which begin at points below the point at which there appears a self-reversing trajectory with a point of tangency to the line $x = x_0$. This self-reversing trajectory has no points of inflection or extrema in x or λ between the initial point and the self-reversal point. 2) The self-reversing trajectory just referred to. 3) A continuum of trajectories all of which are trajectories of the second kind. 4) A limiting trajectory for the preceding continuum which occurs at the point at which the line $x = x_0$ intersects the curve $\mathrm{d}^2x/\mathrm{d}\sigma^2 = 0$, and which immediately upon issuing from its initial point turns to the left. 5) Above this last point a continuum of trajectories, all of which immediately turn left as did the one referred to in 4). (The region above the curve $\mathrm{d}^2x/\mathrm{d}\sigma^2 = 0$ is a region in which the x-component of the acceleration is negative.) A family with these characteristics will be said to have properties *C*.

For any value of γ_1 between 0 and 1 the curve $\mathrm{d}^2x/\mathrm{d}\sigma^2 = 0$ is given ana-

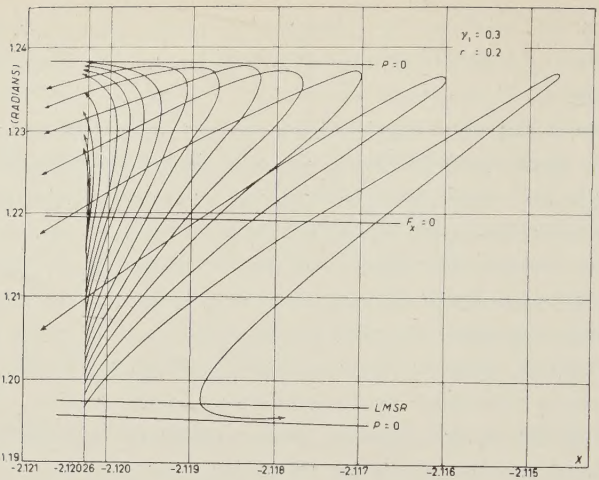

Fig. 4. – Family of trajectories with $\eta_0 = 90°$ along the line $r = 0.2$ for $\gamma_1 = 0.3$.

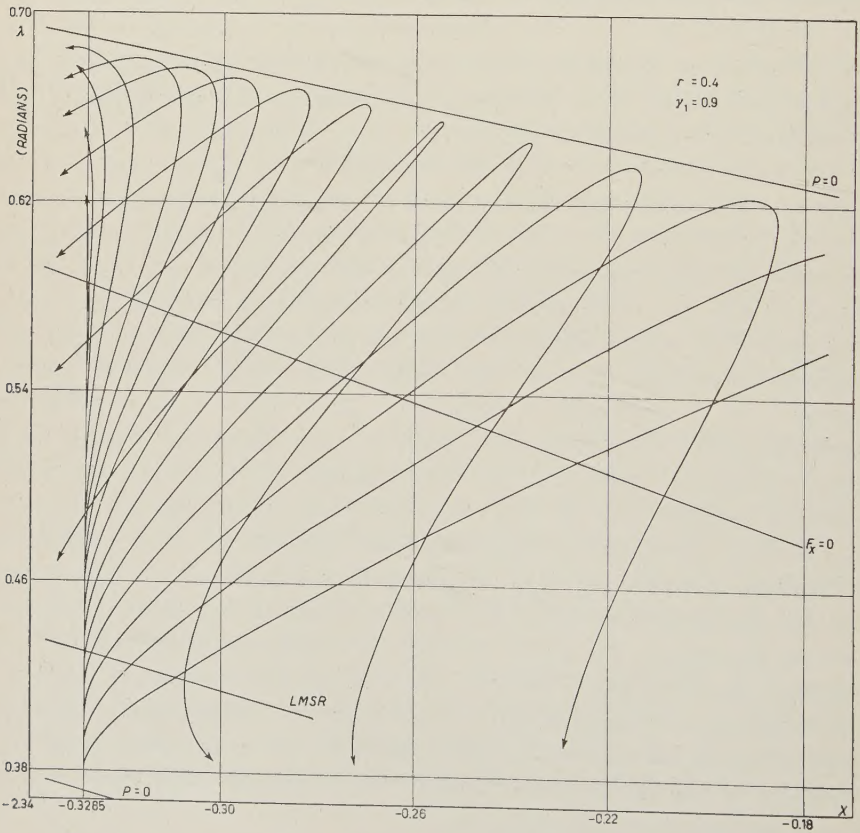

Fig. 5. – Family of trajectories with $\eta_0 = 90°$ along the line $r = 0.4$ for $\gamma_1 = 0.9$.

lytically, and it is also known that there exists a continuous locus (which for values of γ_1 near 1 may be of more than one branch) of points of first minima for self-reversing trajectories. The latter loci have been given by SCHREMP (4); any such locus will hereafter be referred to as an LMSR (for locus of minima of self-reversers). A curve of the first kind will be called $F_x = 0$.

If a line $x = x_0$ is so located for a given γ_1 that it intersects both an LMSR and $F_x = 0$, the intersection with the LMSR falls at a smaller value of λ than does the intersection with $F_x = 0$ because the LMSR must fall in a region where $F_x > 0$. It may of course happen for a given γ_1 that a line $x = x_0$ intersects only $F_x = 0$, or may intersect neither $F_x = 0$ nor the LMSR.

Now the claim is made that under the conditions to be specified immediately after this sentence the family of trajectories along $x = x_0$ with $\eta_0 = 90°$ will have properties *C*. The conditions are: 1) $0.1 \leqslant \gamma_1 \leqslant 1.0$, 2) $x = x_0$ intersects both $F_x = 0$ and the LMSR (or $F_x = 0$ and the branch of the LMSR which lies nearest the dipole if the value of γ_1 is such that the LMSR has two branches), and 3) $x = x_0$ does not intersect the upper branch of $P = 0$ to the right of the λ-minimum of that branch of $P = 0$ in the x, λ plane. (The latter restriction is made in order to avoid the supposed possibility that if the restriction is violated self-reversers may leave their self-reversal points on $P = 0$ and reach tangencies at $x = x_0$, but fail to have the simple forms required here.) The authors has in his possession some 60 such families for values of γ_1 from 0.1 to 1.0 and for widely distributed walues of x_0 (from -4.0 to $+0.4$). Examination of these families together with consideration of the contour maps for the regions of the x, λ planes involved show that the truth of the claim is overwhelmingly likely. Since such evidence cannot be adequately presented here, the claim is simply postulated.

Some properties of the trajectories in the families being discussed, which have been deduced from inspection of computed families, will be of importance later, and will be enumerated here. 1) Along the segment of the line $x = x_0$ between the LMSR and $F_x = 0$, there will be at each point one and only one trajectory of the second kind starting there with $\eta_0 \neq 90°$. 2) The segment between $F_x = 0$ and $P = 0$ can be divided into two parts, the lower of which is such that for each point on it there will be two and only two trajectories of the second kind, and the upper of which is such that for points on it there will be no trajectories of the second kind at all. 3) There is in each such family a trajectory of the second kind which begins along the line $x = x_0$ at a point at which the value of λ is greater than it is for any other point along $x = x_0$ at which a trajectory of the second kind exists. This happens, of course, at the limiting point of the segment containing points, each of which has two trajectories of the second kind issuing from it. 4) In the neighborhood below such a point along the line $x = x_0$ the two trajectories of the second kind issuing jointly from any point in the neighborhood have values of η_0 not

greatly different, and as the points approach the northernmost point these values of η_0 approch equality and attain it at that northernmost point.

Let it be understood now that when a trajectory of the second kind is mentioned, it is meant to be taken as issuing from the northernmost of its two points for which $x = x_0$. This will always mean that the trajectory issues from the earth with $\eta_0 \neq 90°$ except in the case of a trajectory of the second kind which is also a self-reversing trajectory; in such a special case $\eta_0 = 90°$. It is postulated that whenever a family of trajectories having properties C exists each trajectory of the second kind in the family issues from a point on $x = x_0$ at which there exists a pencil of trajectories having properties A or B. Further, each trajectory of the second kind terminates the pencil associated with it in the manner of one of those described in the fifth of the properties A or the third of the properties B, as may be appropriate. That is, for each such trajectory $\eta_0 = \eta_T^N$ and all trajectories in its pencil with $270° > \eta_0 > \eta_T^N$ lie in the earth's simple shadow, or else $\eta_0 = \eta_T^S$ and all trajectories in its pencil with $90° < \eta_0 < \eta_T^S$ lie in the earth's simple shadow. The validity of this postulate rests entirely on examination of available computed trajectories and generalization suggested by the intuition.

2·5. *Generation of simple shadow cones.* – Now we begin an examination of the generation of arcs in a cone diagram as γ_1 varies across the face of the diagram for fixed values of r and λ. This will be done at the outset for a more or less specific case; the mode of generation to be described is illustrated in Figure 6, which is somewhat schematic but nevertheless represents fairly accurately the case for any value of r from about 0.1 to 0.3 and for $\lambda \cong 0.6$ radians.

Since at the left edge of a cone diagram $\sin\theta = -1$ and since $\sin\theta$ is an analytically given function of r, λ, and γ_1, the value of γ_1 at the left edge is fixed. As γ_1 increases from this value, the lines $\sin\theta = \text{constant}$ are generated across the face of the diagram until that value of γ_1 is encountered for which $\sin\theta = 1$, at the right edge of the diagram. For each value of γ_1, if r and λ are held fixed, there will be a corresponding point in an x, λ plane whose position with respect to the contours $P = \text{constant}$ will depend on the value of γ_1, as will the structure of the contour map itself.

Reference should now be made to Figure 6. At the left edge of the cone diagram the point in question lies on the inner branch of the curve $P = 0$, as in (a). As γ_1 increases the point moves along the line $\lambda = \text{constant}$, and for every point x, λ generated a family with properties C exists along the vertical line through x. The point first traverses a region such that the point is always below an LMSR as in (b), where no trajectories of the second kind exist, and then moves in a region such that the point is always between an LMSR and a curve $F_x = 0$, as in (c), having somewhere between crossed an LMSR. At

that crossing occurs the first encounter by the point with a trajectory of the second kind and there the value of η_T^N is 90°. In (*c*) there is one trajectory of the second kind per point and a family with the properties A with which that trajectory is associated as a limiting trajectory. The assumptions of continuity

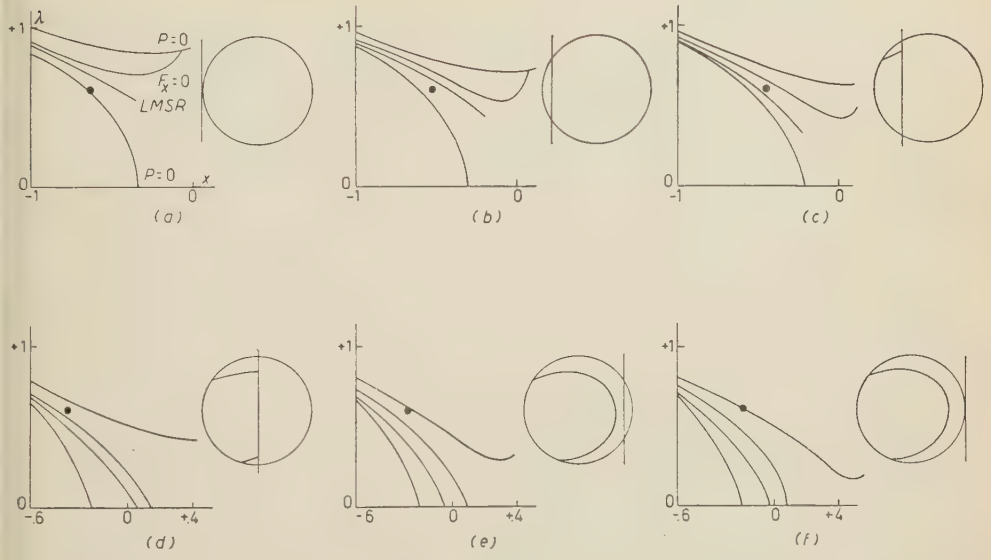

Fig. 6. – Schematic representation of motion of x, λ points (for fixed r and γ) over x, λ planes during generation of simple shadow cone, and corresponding movement of the line $\sin\theta = \sin\theta(r, \lambda, \gamma_1)$ across the cone diagram.

previously discussed are applied here and with what has just been said show that an arc starting on the upper edge of the diagram is generated continuously in this region. Next the point crosses the curve $F_x = 0$ and then traverses a region in which two trajectories of the second kind exist per point, as in (*d*). In this region there is generated a continuation of the arc already begun and a second arc in addition. This second arc begins at the lower edge of the cone diagram when the point x, λ crosses $F_x = 0$. This is true because for points after $F_x = 0$, but infinitesimally near that curve, the newly acquired second trajectories of the second kind have η_T^S infinitesimally near 270°, and these angles increase as $F_x = 0$ is left farther behind. As the point progresses through the region in which two arcs are being generated, the arcs approach each other and join smoothly together. After this a region is encountered in which no trajectories of the second kind exist at the points x, λ as in (*e*). (The reasons for the joining of the arcs and the subsequent disappearance of trajectories of the second kind will be clear because of properties of families of trajectories of the second kind previously stated.) Finally the other branch of the curve

$F_x = 0$ is met as in (*f*), and the cone diagram has then been swept over completely.

On the basis of what has preceded this analysis it is clear that the trajectories corresponding to all points above the northern arc of the curve generated on the cone diagram are in the earth's simple shadow as are all those corresponding to points below the southern arc of the curve. The points to the right of the maximum reach of the curve in $\sin\theta$ are not in the earth's simple shadow but do not correspond to physically allowable trajectories since such trajectories (when reversed) must traverse a region of the earth in order to arrive at the observation point. This claim can be regarded as only postulated here, but a little reflection convinces one of its truth. In crude language, the x, λ points corresponding to such cone diagram points are nestled so closely against the upper branch of $P = 0$ where its slope is negative that all trajectories leaving those points to the right reflect back to the left sufficiently to intersect the earth.

2·6. *Definition of a simple shadow cone.* – It will be noticed that in the case illustrated and described two salient features are present: 1) The generated points x, λ traverse in order (as γ_1 increases) the inner $P = 0$, a region below an LMSR, an LMSR, a region between an LMSR and a curve $F_x = 0$, a curve $F_x = 0$, a region between a curve $F_x = 0$ and the upper $P = 0$, and finally the upper $P = 0$. 2) Every generated point x, λ is such that a family with properties C exists along the vertical line through it. (As a consequence of a postulate made in section 2·4, above, every trajectory of the second kind which exists at any generated point x, λ is a limiting trajectory for a pencil with properties A, or with properties B.) Whenever the values of r and λ are such that these two features are properties of the generated x, λ points as γ_1 varies across the face of the corresponding cone diagram the curve developed in the cone diagram will be called a simple shadow cone.

For some values of r and λ it may happen that the generation of a curve in a cone diagram begins in the manner in which it begins when the curve is a simple shadow cone as just defined, but that the value 1 for the parameter γ_1 occurs before generation of a complete curve is accomplished. In any such case the segment (or segments) up to the line $\gamma_1 = 1$ will also be called a simple shadow cone. All trajectories corresponding to points above the northern reach of such a cone or below the southern reach, if the latter exists, will be in the earth's simple shadow. Trajectories corresponding to points on or to the right of the line $\gamma_1 = 1$ will be said to be Størmer dark. For some values of r and λ generation of a cone is not begun before γ_1 reaches the value 1, and for others the value of γ_1 at the left edge of the cone diagram is equal to or greater than 1. In either of these cases it will be considered that no simple shadow cones exist, and it will be said that they are prevented from existing

by the Størmer condition. Any trajectory for which $\gamma_1 \geqslant 1$ and which has its initial point inside the closed region of the x, λ plane where motions can occur is not (when reversed) a physically allowable trajectory for cosmic ray particles coming from the outer, open region, as is well known.

2·7. *Restrictions on the variables for validity of the definition.* – The values of r and λ for which a simple shadow cone can exist must yet be specified. To decide whether it is possible for a simple shadow cone to exist for a given r and λ the range through which γ_1 must vary in moving across the face of the cone diagram, and traces the course of the generated x, λ points. One then observes whether the sequence of traversals of special curves and regions required by the definition occurs or not, and whether families with properties C exist for each generated x.

The author has thus determined that for all latitudes such that $30° \leqslant \lambda \leqslant 60°$ for all values of r not greater than 0.6, and for all latitudes such that $60° < \lambda \leqslant 80°$ for all values of r not greater than 0.4, simple shadow cones exist, provided they are not prevented from existing by the Størmer condition.

These ranges of r and λ can be extended, but no practical gain is to be effected by their extension because of the negligible practical importance of the cones for smaller values of λ; the computed cones given later in this paper may be consulted in this connection. However, it is of importance to observe that while those ranges can be extended, they cannot be extended very widely. One limitation effective for a given value of λ is that when $r^2 > \cos \lambda$ there can be no simple shadow cone for such r at that λ, as has been pointed out by SCHREMP (4). A second limitation that must be mentioned is the following: as long as r is small enough or λ large enough, the points x, λ generated during variation of γ_1 will lie well up in the « neck » between the branches of the curve $P = 0$ where the vertical line through x must intersect both branches of $P = 0$, an LMSR, and $F_x = 0$, but for larger values of r and for latitudes near the equator this is no longer so because for some locations of the points x, λ the vertical lines through such points may fail to intersect an LMSR, and even may lie entirely in a region where $F_x < 0$.

The above consideration leads directly to the claim that some of the cones shown by SCHREMP (4) are either not simple shadow cones (generated by trajectories of the second kind), or else are numerically incorrect simple shadow cones. It is easy to show by elementary calculations that at a value of roughly 0.86 for γ_1 the $F_x < 0$ region of the x, λ plane touches the equator at a small positive value of x. For larger values of γ_1 (but values less than 1) such regions cover extended segments of the equator, so that for any value of x along segments, vertical lines lie entirely in regions where $F_x < 0$, between branches of the curve $P = 0$. Whenever a set of values for r, λ and γ_1 is considered which corresponds to a point on such a line in such a region it is obvious that no

trajectories of the second kind exist along that line. Now measurements on Schremp's figures and easy computations show that in some cases all points on parts of his cones are such that the values of r, λ and γ_1 associated with those parts require that the corresponding points in the x, λ planes fall in regions of the kinds just mentioned. This is in contradiction with the claim that the points correspond to trajectories of the second kind. One example of such a case is the most easterly arc of Schremp's cone for $r = 0.8$, $\lambda = 10°$, as can be readily verified by the reader.

3. – Computation of trajectories and of simple shadow cones.

3·1. *Computation of trajectories.* – As Schremp [4] has pointed out, the calculation of simple shadow cones can be carried out if one computes sufficiently extensively families of trajectories of the second kind like those shown in Figures 4 and 5. The method used by the author depends on integration of the equations of motion to produce such families, but differs from the method of Schremp in by-passing the λ, η interpolations mentioned by him as having been used to reduce data taken from his trajectories to points on cone diagrams.

All trajectories used were computed with the use of IBM Type 704 computers. Of the approximately 550 trajectories of the second kind computed, about 500 were computed personally by the author with a program written by him and used on the computer at the General Motors Technical Center, Detroit, Michigan. The rest were computed for him by personnel of Martin Aircraft Company, Baltimore, Maryland at the request of RIAS, Inc. of that city, with an independently prepared program. In addition, some 100 other trajectories were used in the associated investigations.

The method used by the author for the numerical integrations was Gill's modification of the Kutta-Runge method [6]. The precision of the trajectories was checked by several investigations: 1) Machine produced results were compared with known trajectories, such as those given by Stormer [7]. 2) Trajectories of great lengths in σ and of convoluted forms were run forwards and backwards and the results compared; this constitutes a severe test. 3) Trajectories were computed independently by the author and the Martin group and compared. 4) Trajectories were computed several times over, with different step sizes in the independent variable σ. It was concluded that the machine produced values of x, λ and η along the trajectories of the second kind, all of which were short and had simple forms, could be considered to be precise to at least five digits. This precision is very adequate for application of the trajectories to the computation of the cones.

---

[6] S. Gill: *Proc. Camb. Phil. Soc.*, **47**, 96 (1951).

[7] C. Stormer: *Norske Videnskaps Akademi i Oslo*, Mat.-Nat. Kl., no. 1, 5 (1947).

Each family of trajectories of the second kind was computed by picking values of r and γ_1 (and hence of x) and starting the integrations of the members of the family at points distributed between the LMSR and the curve $F_x = 0$ along the vertical line through x. The values of r used were 0.1, 0.2, 0.3, 0.4, and 0.6. For each value of r the values of γ_1 used were from 0.1 to 1.0 in steps of 0.1, except that the value 1.0 was not used for $r = 0.6$. An average of about 10 members per family was computed.

3·2. *Interpolations performed on trajectories.* – The trajectories calculated with the General Motors computer were produced by a program written with an object in mind other than the computation of simple shadow cones, and no provision was made in the program for printing out values of x, λ and η precisely at the points on the trajectories at which they return to the earth after starting out with $\eta_0 = 90°$. Instead, values of those variables were printed out after each increment in the independent variable σ. The increment in σ was constant during each trajectory computation; for about 40 of the trajectories it was 0.003 166 666 6, for about 120 it was 0.006 333 333 3, and for the rest, 0.05. (The smaller step sizes were used when large negative values of x were involved.) As a result, print-outs occurred on each trajectory extremely near the line $x = x_0$ when the trajectories returned to the earth, and linear interpolations were done between printed points bracketing the line $x = x_0$ in order to find the values of λ and η at $x = x_0$. The points at which x, λ and η were printed out near the earth fell at x-values differing from $x = x_0$ by roughly 0.000 05 or less in about half the cases, by about 0.000 05 to 0.000 5 in about two thirds of the remaining cases, and by larger amounts to a maximum of about 0.001 in the rest of the cases. Thus the interpolations were done over small arcs of the trajectories. The interpolative procedure was subjected to an analysis in which estimates were made with liberality of the maximum possible errors that could be incurred in the angles λ and η. These estimates were checked in two ways: 1) Trajectories were computed with $\Delta\sigma = 0.05$ and with much smaller step sizes, and the interpolations made on the various runs of single trajectories were compared, and 2) some trajectories computed by the author were recomputed by the Martin group, whose program provided for print-out of values of the angles at the earth. It was concluded that the maximum possible errors in λ (in radians) were less than 0.000 1 in all but 16 cases. In the 16 cases referred to it was of the order of 0.001. The maximum possible errors in η (in radians) were of the order 0.001 or less in all but about 100 of the cases. In all but 20 of those 100 they were from 0.001 to 0.01. In those 20 cases (in which the trajectories were turning rapidly near the earth and so varying rapidly in η) the data were not used when they seemed inconsistent with the other data.

The question of importance in connection with the possible errors in the

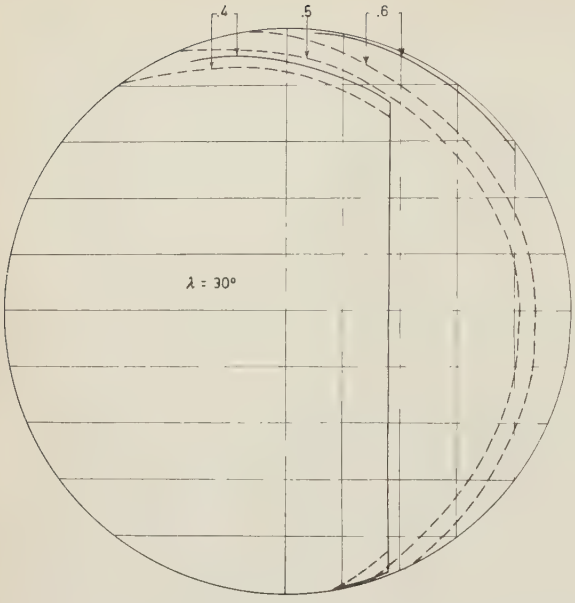

Fig. 7. – Newly computed simple shadow cones (solid curves) and simple shadow cones of Schremp (4) (broken curves) for $r_{\frac{1}{2}}$ values shown, and for $\lambda = 30°$.

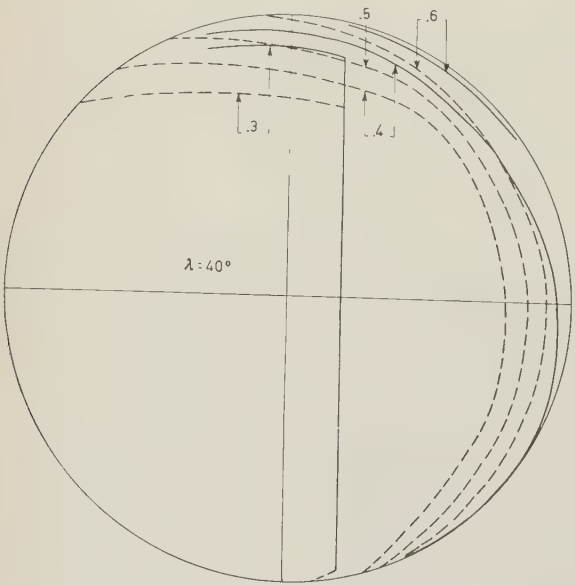

Fig. 8. – Same as Fig. 7, but for $\lambda = 40°$.

interpolated angles λ and η is that of their effects on the coordinates $\sin\theta$ and $\cos\theta \sin\eta$. The effects depend on the sizes of the angles as well as on the sizes of the errors because of the trigonometric functions involved, and because of the errors in λ were smallest at large latitudes. The conclusions are summarized by the assertion that the values of the coordinates for all points computed are believed to be correct to within ± 0.02.

3·3. *Reduction of trajectory data to simple shadow cones.* – One way to utilize the r, λ, η data taken from the trajectories is that described by SCHREMP (4), which involves interpolations over the λ, η values for each family of trajectories of the second kind. This method was tried with exercise of care and it was found by making fair and reasonable estimates of the errors introduced that the procedure was essentially unproductive of simple shadow cones. Errors in the coordinates of points on the resulting cones as large as 0.1 were estimated to be possible.

For this reason a different method was used for

much more direct determination of the cones. It was observed that a consequence of the choices of the values of r and γ_1 made was that points $\sin\theta$, $\cos\theta\sin\eta$ (computed by use of the values of r, λ, η, γ_1 taken from the trajectories) resulted which generally could be divided into subgroups for each group pertaining to one value of r, such that the points in each subgroup pertained to latitudes nearly equal. This made it easy to draw in segments of simple shadow cones for any latitude included in subgroups with sufficient precision by plotting the $\sin\theta$, $\cos\theta\sin\eta$ points on cone diagrams and letting the pencil be guided by them. The table exhibits the values of r, λ, $\sin\theta$ and $\cos\theta\sin\eta$ for all points used.

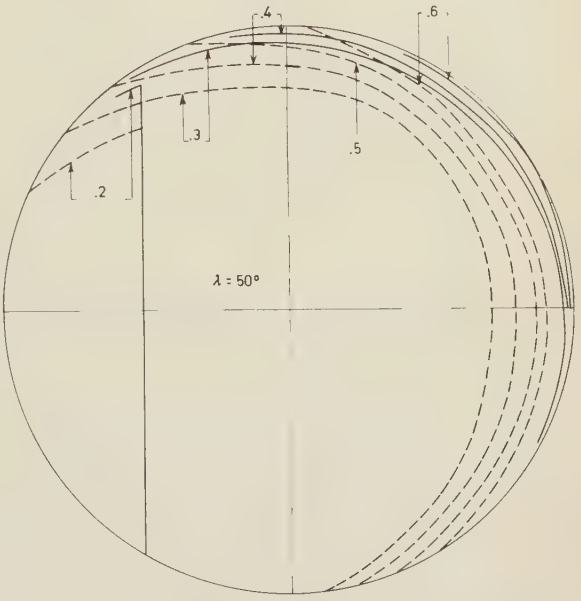

Fig. 9. – Same as Fig. 7, but for $\lambda = 50°$.

For a given r this process fixed segments of cones of various lengths lying along different parts of the rims of the cone diagrams. When all those segments were plotted together in one diagram, the interrelations between them made it possible often to extend the lengths of segments with good reliability, and also made a consistency check possible.

When all the simple shadow cones for one value of r were thus determined, the process was repeated for the other values of r. Then for each value of r, interpola-

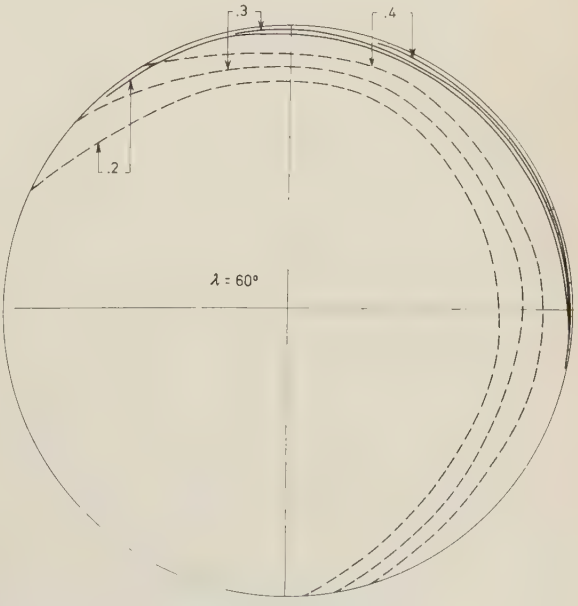

Fig. 10. – Same as Fig. 7, but for $\lambda = 60°$.

tions between the cones (which fell at unpreselected latitudes) to find the cones for any special desired latitudes (such as 30°, 40°, 50°, and so on) could be readily done because the number of cones was large and they were not spread very widely over the cone diagrams.

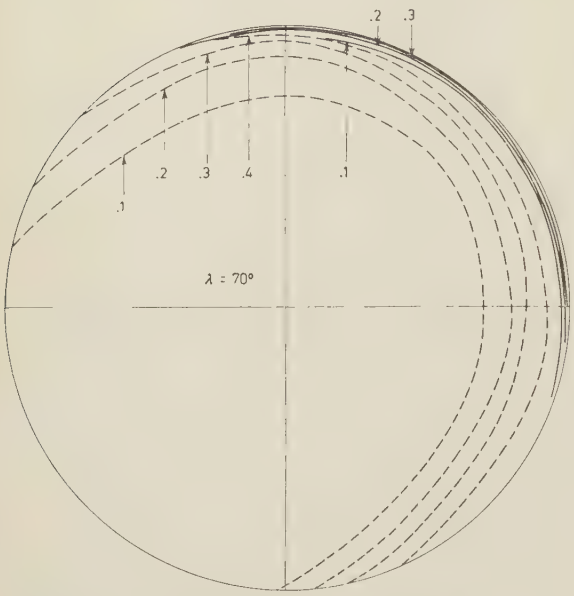

Fig. 11. – Same as Fig. 7, but for $\lambda = 70°$.

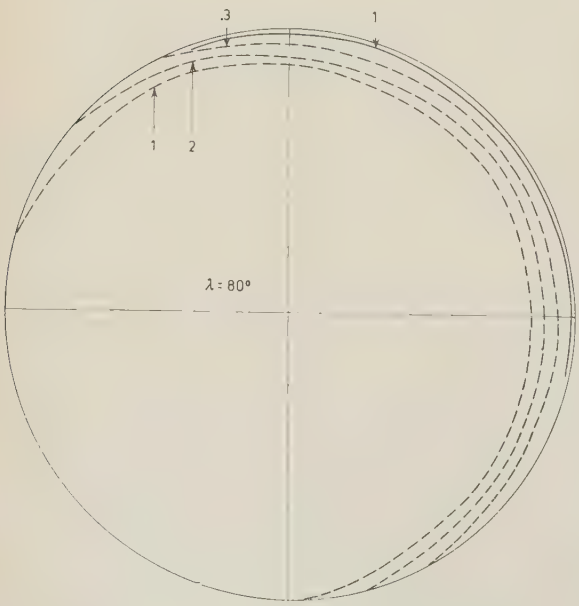

Fig. 12. – Same as Fig. 7, but for $\lambda = 80°$.

The terminal points of the cones on the lower and upper edges of the cone diagrams were not given by this procedure. The lower terminal points were not given by this procedure. The lower terminal points were computed from the relation $F_x = 0$ and the cones extended down to such points. The upper terminal points depend on locating accurately the self-reversing trajectory for each family of trajectories of the second kind, or on knowing accurately the LMSR for each of the values of γ_1 involved. In this work, such self-reversers were not computed, and it is not known whether the loci of minima of self-reversers given by SCHREMP [4] are accurate. However, the cones are so small that there exists no practical need for carrying out the rather extensive investigations necessary for finding those terminals.

In Figures 7 through 12 are shown simple shadow cones produced as described in this section for latitudes at 10° intervals from 30° to

80°. When a section of a cone approaches the rim of a diagram very closely, such a section is not shown, as in the cases $r = 0.2$, 0.3, 0.4 at $\lambda = 60°$, and when entire cones are very near the edge, they are not shown, as in the cases $r = 0.2$ and 0.3 at $\lambda = 80°$. This has been done to avoid obscuring the drawings.

There are also shown in the figures some of the cones of Schremp in broken curves for comparison. These were drawn with fair precision by expanding the published cones with an optical projector and tracing the images. The southern terminal points for the cones of Schremp apply to the new cones.

4. – Discussion.

One striking feature of the new simple shadow cones is that they differ greatly from those of Schremp. It is, of course, necessarily the author's contention that the old cones were badly in error. Some evidence for the incorrectness of the old cones has already been mentioned (the work of Schwartz, and the evident faults in the old cones for large r values and latitudes). More evidence could be given — for example, visual inspection of families of trajectories of the second kind shows that most simple shadow cones must be considerably « fatter » in their northern reaches than in their southern, whereas Schremp's cones tend to near-symmetry about their sin θ axes in their easterly parts — however, it is not desired to belabor this matter.

An associated question is that of the origin of the errors in the old cones. It is not intended to produce here a list of possible origins, since that would at least partially involve conjecture. However, it ought to be pointed out that at least one certain and strong criticism can be made. The values of γ_1 needed for the production of the earlier published cones can be readily computed and compared with the values used by SCHREMP [4], which were from 0.62 to 0.98 in steps of 0.04. On finds that the cones for $r = 0.1$ and latitudes greater than roughly 70°, $r = 0.2$ and latitudes greater than roughly 65°, $r = 0.3$ and latitudes greater than about 60°, $r = 0.4$ and latitudes greater than about 50°, and other cones, require values of γ_1 between 0 and 0.6. How such cones were obtained is an open question. (Schremp does not mention extrapolations, which would in any event have been extremely dubious over such a wide range of missing γ_1 values.)

A brief commentary on the newly computed simple shadow cones will be appended here. It is clear that for experimentalists these cones will ordinarily be considered as negligible because the fractions of the sky made dark by them are small, and because they fall at large zenith angles where investigation of azimuthal effects is very difficult.

At high latitudes the penumbral region is known to be nearly completely a region of allowed directions of arrival at the observation point. In such

cases the simple shadow cones are so small that the total allowed cones will probably be viewed as being given by the Størmer cones alone.

At intermediate latitudes the simple shadow cones are again negligible for practical purposes and the entire region outside any main cone will probably be considered a penumbral region.

No simple shadow cones are given for latitudes below 30°. However, the omission of these cones is of no real importance. The cones of Schremp for these latitudes are doubtless too large, but even they only slightly affect the main cones, and it is known that with decreasing latitude the penumbral region tends toward a condition of complete darkness. Thus at low latitudes the total allowed cones reduce essentially to the main cones.

TABLE I. – *Co-ordinates and values of r and λ, for all cone diagram points.*

λ (°)	sin θ	cos θ sin η	λ (°)	sin θ	cos θ sin η
	$r = 0.1$			$r = 0.1$	
81.766	— .357	.932	76.102	.959	— .274
81.928	.201	.977	76.088	.912	— .406
82.021	.527	.847	76.071	.853	— .520
82.080	.736	.673	76.026	.701	— .713
82.117	.868	.493	75.977	.531	— .847
82.139	.946	.317	75.915	.321	— .947
82.151	.990	.013	73.702	.444	.880
82.147	.975	— .199	73.817	.833	.533
82.134	.927	— .372	73.859	.977	.167
82.122	.886	— .463	73.861	.983	— .151
82.077	.726	— .688	73.840	.912	— .406
82.021	.527	— .850	73.793	.758	— .651
81.954	.292	— .956	73.753	.616	— .788
78.747	.984	— .020	73.698	.432	— .902
78.746	.980	— .119	73.681	.374	— .927
78.742	.966	— .238	71.704	.461	.866
78.725	.906	— .419	71.858	.979	.150
78.711	.855	— 5.18	71.859	.983	— 1.55
78.664	.694	— .720	71.836	.906	— .418
78.607	.495	— .869	71.798	.778	— .627
78.540	.263	— .965	71.751	.619	— .785
75.816	— .018	.988	71.713	.491	— .871
75.937	.393	.903	71.630	.214	— .977
76.009	.640	.751	69.873	.462	.858
76.064	.829	.545	70.029	.979	1.43
76.093	.929	.352	70.029	.979	— .170
76.101	.957	.248	70.005	.900	— .429
76.108	.982	.005	69.968	.776	— .629
76.110	.986	— .137	69.918	.611	— .792

TABLE I (*continued*).

λ (°)	$\sin\theta$	$\cos\theta\sin\eta$	λ (°)	$\sin\theta$	$\cos\theta\sin\eta$
	$r = 0.1$			$r = 0.1$	
69.862	.427	— .904	63.733	.936	— .326
69.800	.222	— .975	63.705	.847	— .514
68.172	.471	.849	63.691	.804	— .586
68.281	.828	.489	63.655	.891	— .721
68.324	.969	— .211	63.600	.516	— .856
68.304	.901	— .426	63.538	.323	— .946
68.265	.773	— .632	63.470	.111	— .994
68.215	.610	— .791			
68.158	.424	— .906		$r = 0.2$	
68.096	.223	— .975			
66.444	.070	.966	79.029	.497	.865
66.570	.475	.842	79.269	.716	.695
66.640	.701	.664	79.423	.859	.508
66.684	.844	.484	79.513	.944	.324
66.718	.954	.025	79.551	.980	.010
66.720	.962	— .021	79.541	.970	— .148
66.707	.917	— .362	79.466	.899	— .436
66.681	.834	— .540	79.316	.759	— .651
66.654	.747	— .657	79.002	.472	— .882
66.635	.687	— .726	73.551	— .016	.994
66.584	.520	— .854	73.963	.333	.917
66.523	.325	— .946	74.257	.588	.770
66.463	.132	— .991	74.413	.726	.653
64.921	.079	.961	74.617	.908	.406
65.047	.478	.835	74.677	.962	.255
65.117	.702	.660	74.717	.993	.023
65.161	.843	.458	74.708	.990	— .101
65.184	.918	.284	74.670	.955	— .290
65.197	.958	— .120	74.539	.838	— .545
65.196	.956	— .136	74.335	.657	— .754
65.176	.891	— .401	74.095	.447	— .894
65.167	.863	— .482	73.859	.244	— .970
65.147	.797	— .598	69.304	— .347	.930
65.114	.694	— .719	69.990	.213	.963
65.059	.518	— .855	70.315	.485	.857
64.999	.325	— .946	70.559	.693	.674
64.933	.119	— .993	70.669	.813	.516
63.507	.225	.930	70.818	.916	.353
63.588	.480	.829	70.890	.979	— .183
63.661	.708	.650	70.848	.942	— .339
63.702	.839	.464	70.704	.817	— .575
63.731	.932	.280	70.503	.645	— .764
63.746	.978	— .039	70.264	.442	— .897
63.734	.942	— .221	70.021	.239	— .971

TABLE I (*continued*).

λ (°)	$\sin\theta$	$\cos\theta \sin\eta$	λ (°)	$\sin\theta$	$\cos\theta \sin\eta$
	$r = 0.2$			$r = 0.2$	
66.225	— .157	.971	60.918	.192	— .981
66.768	.280	.937	57.176	— .198	.957
67.087	.651	.813	58.099	.035	.954
67.337	.749	.641	58.522	.352	.880
67.466	.857	.418	58.907	.644	.704
67.533	.913	.310	59.111	.801	.528
67.583	.955	.092	59.235	.897	.346
67.568	.942	— .184	59.306	.952	.156
67.583	.955	— .295	59.343	.981	.007
67.457	.850	— .508	59.321	.964	— .168
67.399	.800	— .598	59.281	.932	— .399
67.192	.628	— .778	59.238	.899	— .422
66.951	.428	— .904	59.057	.759	— .647
66.672	.201	— .980	58.845	.596	— .802
62.342	— .834	.551	58.583	.397	— .918
66.672	.201	— .980	58.356	.227	— .974
62.342	— .834	.551	54.740	— .574	.791
63.260	— .059	.973	55.626	.055	.942
63.868	.340	.908	56.117	.412	.844
64.199	.607	.758	56.440	.652	.684
64.400	.770	.592	56.845	.955	.160
64.545	.888	.387	56.868	.973	— .031
64.609	.940	.201	56.854	.962	— 1.68
64.647	.970	.059	56.814	.932	— .318
64.631	.959	— .168	56.768	.897	— .425
64.612	.944	— .299	56.562	.742	— .666
64.526	.873	— .464	56.336	.574	— .818
64.424	.789	— .612	56.092	.394	— .919
64.212	.617	— .787	55.800	.181	— .983
63.964	.418	— .908	52.363	— .528	.810
63.691	.201	— .980	53.222	.064	.929
59.790	— .655	.743	53.709	.409	.832
60.667	.001	.965	54.050	.653	.668
61.148	.370	.886	54.250	.798	.502
61.481	.630	.728	54.386	.897	.315
61.684	.791	.560	54.455	.947	.139
61.804	.887	.393	54.482	.968	— .036
61.878	.945	.204	54.473	.961	— .167
61.919	.978	.034	54.433	.931	— .319
61.863	.934	— .317	54.185	.751	— .655
61.809	.891	— .433	53.931	.567	— .823
61.634	.751	— .657	53.688	.394	— .919
61.453	.609	— .792	53.389	.182	— .893
61.199	.410	— .912	50.742	— .017	.922

TABLE I (*continued*).

λ (°)	$\sin\theta$	$\cos\theta\sin\eta$
	$r = 0.2$	
51.620	.584	.709
52.006	.855	.390
52.148	.955	.066
52.145	.953	— .207
52.047	.885	— .443
51.874	.762	— .642
51.634	.594	— .803
51.386	.422	— .907
51.123	.241	— .971
50.914	.099	— .955
	$r = 0.3$	
77.589	.714	.699
78.161	.970	.240
78.166	.972	— .234
77.808	.810	— .586
69.174	— .200	.978
70.519	.292	.951
71.249	.576	.811
71.750	.778	.619
72.231	.978	— .202
71.928	.851	— .524
71.427	.647	— .762
70.800	.400	— .916
64.663	— .082	.986
65.827	.334	.929
66.531	.597	.786
67.030	.789	.597
67.280	.887	.407
67.493	.971	.204
67.231	.868	— .483
67.035	.791	— .611
66.496	.584	— .812
65.852	.344	— .939
59.919	— .249	.957
61.231	.193	.961
62.127	.509	.835
62.677	.710	.675
63.066	.854	.479
63.297	.941	.295
63.374	.970	— .009
63.380	.973	— .088
63.116	.873	— .479
62.539	.659	— .752
62.236	.548	— .836
61.574	.313	— .950
56.692	— .032	.974
57.765	.323	.913
58.569	.598	.760
59.042	.764	.600
59.387	.888	.400
59.561	.951	.195
59.645	.981	.026
59.628	.975	— .161
59.340	.871	— .483
59.873	.704	— .708
58.364	.527	— .850
57.669	.290	— .957
51.296	— .551	.822
53.333	.063	.958
54.307	.373	.879
55.113	.638	.714
55.552	.786	.556
55.890	.902	.350
56.043	.955	.166
56.106	.977	— .037
56.878	.967	— .175
55.818	.877	— .470
55.331	.712	— .701
54.615	.474	— .881
54.028	.283	— .959
48.316	— .372	.895
50.009	.121	.936
51.020	.429	.835
51.665	.632	.701
52.151	.788	.532
52.519	.908	.315
52.671	.958	.125
52.721	.975	— .057
52.682	.962	— .206
52.393	.867	— .488
51.888	.703	— .709
51.234	.496	— .868
50.479	.263	— .965
45.061	— .298	.905
46.667	.147	.912
47.712	.450	.803

TABLE I (*continued*).

λ (°)	$\sin\theta$	$\cos\theta\sin\eta$
	$r = 0.3$	
48.425	.664	.649
48.909	.812	.475
49.208	.904	.293
49.374	.956	.110
49.416	.970	— .067
49.378	.958	— .219
49.040	.852	— .510
48.518	.692	— .719
47.753	.462	— .887
47.028	.251	— .968
41.660	— .270	.894
43.269	.150	.889
44.362	.449	.778
45.095	.656	.628
45.607	.804	.455
45.922	.896	.279
46.097	.947	.094
46.151	.964	— .068
46.104	.950	— .229
45.770	.851	— .508
45.183	.681	— .729
44.428	.466	— .884
43.610	.242	— .970
37.916	— .315	.865
39.765	.132	.865
40.851	.409	.768
41.721	.639	.610
42.229	.776	.458
42.608	.880	.272
42.797	.933	.106
42.873	.954	— .073
42.840	.945	— .218
42.508	.853	— .499
41.894	.685	— .724
41.102	.474	— .880
40.215	.245	— .969
	$r = 0.4$	
77.642	.998	.055
77.624	.994	— .114
77.527	.965	— .262
77.361	.918	— .397
76.850	.776	— .631

λ (°)	$\sin\theta$	$\cos\theta\sin\eta$
	$r = 0.4$	
70.828	— .530	.844
77.593	.984	.159
77.136	.855	— .519
68.270	.387	.920
70.440	.894	.443
70.745	.971	— .224
70.283	.856	— .518
69.145	.584	— .812
62.106	.282	.953
63.650	.605	.786
64.589	.814	.569
65.124	.937	— .344
64.782	.858	— .514
63.095	.487	— .874
53.916	— .285	.955
56.911	.251	.954
58.541	.570	.803
59.558	.781	.603
60.161	.910	.383
60.508	.986	— .063
60.074	.891	— .450
59.144	.694	— .720
57.847	.432	— .902
51.143	.064	.978
53.036	.399	.888
54.524	.681	.699
55.354	.844	.495
55.848	.945	.278
55.995	.975	— .155
55.419	.857	— .510
54.349	.647	— .763
52.992	.391	— .920
44.189	— .298	.938
47.319	.188	.945
49.178	.504	.817
50.403	.723	.637
51.183	.868	.432
51.620	.952	.214
51.706	.968	— 1.97
51.040	.841	— .535
49.906	.633	— .774
40.093	— .206	.946
43.041	.221	.917
44.919	.517	.786

TABLE I (*continued*).

λ (°)	$\sin\theta$	$\cos\theta\sin\eta$	λ (°)	$\sin\theta$	$\cos\theta\sin\eta$
	$r = 0.4$			$r = 0.4$	
46.179	.727	.607	31.360	.519	.646
46.993	.882	.385	34.571	.926	.035
47.451	.949	.196	34.329	.893	— .394
47.530	.964	— .208	33.363	.766	— .630
46.787	.832	— .547	29.911	.351	— .936
45.525	.617	— .786			
34.981	— .239	.924		$r = 0.6$	
38.188	.177	.903			
40.285	.476	.781	60.903	.706	.708
41.710	.692	.611	62.730	.910	.415
42.655	.842	.414	63.380	.987	.155
43.198	.931	.206	63.433	.994	— .112
43.366	.958	— .199	62.239	.853	— .522
42.624	.837	— .536	57.544	.994	— .075
41.176	.610	— .791	57.556	.995	— .083
39.330	.337	— .942	56.912	.926	— .377
27.988	— .423	.864	55.318	.763	— .647
32.151	.024	.895	49.951	.803	.589
34.785	.346	.806	51.780	.975	— .215
36.632	.592	.657	49.180	.734	— .679
37.895	.770	.473	43.993	.782	.604
38.689	.887	.268	45.416	.899	— .435
39.146	.955	— .148	40.577	.523	— .852
38.423	.847	— .512	27.892	.185	.967
36.849	.622	— .781	37.149	.713	.662
34.701	.335	— .942	40.891	.987	— .092
25.825	— .071	.854	38.850	.833	— .552
28.996	.250	.783	35.394	.598	— .802

* * *

The author must ask many individuals who helped him in carrying out this work to accept his thanks without specific mention because of the number of such people. He must, however, especially thank Dr. J. A. VAN ALLEN, Head, Physics Department, State University of Iowa, for encouragement and for supporting him liberally during the performance of this work and of making arrangements for him to use the IBM computer at the General Motors Technical Center and to have trajectories computed by Martin Aircraft Corporation at the request of RIAS, Inc. He further thanks Dr. E. C. RAY, Physics Department, State University of Iowa, for many stimulating discussions and for several

useful suggestions. He is very grateful to the General Motors Corporation and to Dr. R. C. Herman, General Motors Research Staff, Detroit, Michigan, for making the General Motors IBM computer accesible to him, and to Mr. D. Hart and personnel of the Data Processing Group, General Motors Technical Center, Detroit, Michigan, for invaluable help in programming. He owes a debt of gratitude to Drs. G. Groetzinger and P. Schwed of RIAS, Inc., for their cooperation in obtaining machine-computed trajectories for him. During the early part of the time spent by the author on this project he was supported by a fellowship granted him by the Aerojet General Corporation, Azusa, California, and he wishes to express his appreciation for the generosity shown by that organization . Finally, he wishes to acknowledge the very considerable contribution of Mrs. W. Bottacini and Mr. G. L. Hockey, both of Iowa City, Iowa, who carried out extensive hand calculations and performed many other onerous tasks for the author.

SUPPLEMENTO AL VOLUME XI, SERIE X
DEL NUOVO CIMENTO

N. 1, 1959
1° Trimestre

Penumbra and Simple Shadow Cone of Cosmic Radiation (*).

M. SCHWARTZ (**)

Department of Physics, State University of Iowa - Iowa City, Ia.

(ricevuto il 22 Aprile 1958)

1. – Introduction and summary.

Since the earth has a magnetic field, it acts as a magnetic analyzer for charged cosmic ray particles. The earliest work on the effect of the earth's magnetic field on the motion of charged particles was done by STORMER [1] in his auroral studies. In this work, he used a dipole as a model for the earth's field. Because of the cylindrical symmetry of the dipole field, STORMER was able to derive the first integral from which he deduced the forbidden cones of radiation now bearing his name.

Størmer's simple theory did not take into account the effect of an impenetrable earth. It was LEMAITRE and VALLARTA [2] who first did that. Using

(*) Assisted by joint program of the Office of Naval Research and the U.S. Atomic Energy Commission.

(**) Now at School of Physics, University of Minnesota, Minneapolis, Minnesota.

(1) Størmer's work on this subject dates back to 1904. For a conveniently available summary of much of his work pertaining to this subject, along with extensive references, the reader is referred to C. STØRMER: *The Polar Aurora* (London, 1955).

(2) G. LEMAITRE and M. S. VALLARTA: (*a*) *Phys. Rev.*, **43**, 87 (1933); (*b*) **49**, 719 (1936); (*c*) **50**, 493 (1936). For a complete summary of the work of LEMAITRE and VALLARTA and their collaborators see (*d*) M. S. VALLARTA: *An outline of the theory of the allowed cone of cosmic radiation* (Toronto, 1938).

the dipole model, they showed the existence of the cones of full light, called the main cones, which consist only of trajectories arriving (unobstructed) at the earth having come directly from infinity without making loops representing turning away and turning toward the dipole. For each point on the earth, they showed that the region between the main cone and the STORMER cone consists of alternating bands of allowed and forbidden trajectories which respectively either arrive at the earth from infinity unobstructed by the earth or do not. Because of the analogy with optics, they called this region the penumbra. They also pointed out the existence of the simple shadow cones which may bound either the main cones or penumbral regions. The region between the STORMER cones and the simple shadow cones consists entirely of forbidden trajectories. The boundary orbits which determine a simple shadow cone are ones which graze the earth in a fashion to be described later.

Main cones and penumbral regions have been calculated numerically by BOUCKAERT [3] in the geomagnetic latitude range from 0° to 20°. LEMAITRE and VALLARTA, using the BUSH differential analyzer, have calculated the main cones at geomagnetic latitudes 0°, 20° and 30°. HUTNER [4], also using the Bush analyzer, has made extensive calculations of the penumbral regions over the whole sky at 20° geomagnetic latitude. SCHREMP [5], also using the Bush analyzer, calculated the simple shadow cones at latitude intervals of 10° from the equator to the pole. The results of LAMAITRE and VALLARTA and SCHREMP will be found plotted in a convenient form in a paper by ALPHER [6].

In this paper, we extend the investigation of the main cone and the penumbra to higher latitudes. We present the results of calculating penumbral bands in the vertical direction at 30°, 35°, 41°, 45°, 50° geomagnetic latitudes; and in the north, east, south and west directions for zenith angles of 45° and 60° at 41° geomagnetic latitude. The results were obtained from trajectory calculations made by the high speed digital computer, Avidac, at Argonne National Laboratory. It was decided to concentrate on 41° geomagnetic latitude because much experimental work is done there and because WINCKLER and ANDERSON [7] had made azimuthal studies at high zenith angles around that latitude.

We have used our vertical direction results to fit total vertical intensity data, thereby determining an integral rigidity spectrum and at the same time defining effective rigidity cut-offs. The rigidity spectrum determined from the vertical data is compared with the 60° zenith angle measurements of WINCKLER and ANDERSON [7] and is found to agree with them within experimental error.

[3] L. BOUCKAERT: *Ann. Soc. Scient. Bruxelles*, **54**, 174 (1934).
[4] R. A. HUTNER: *Phys. Rev.*, **55**, 15, 614 (1939).
[5] E. J. SCHREMP: *Phys. Rev.*, **54**, 158 (1938).
[6] R. A. ALPHER: *Journ. Geophys. Res.*, **55**, 437 (1950).
[7] J. R. WINCKLER and K. ANDERSON: *Phys. Rev.*, **93**, 596 (1954).

The Winckler-Anderson measurements, when compared with Schremp's results at 40° geomagnetic latitude exhibited strong disagreement with them. The present calculations show that the disagreement was not with geomagnetic theory, but arose because of large errors in Schremp's results at 40° geomagnetic latitude.

2. – Penumbral bands.

2·1. *Method of calculation.* – The motion of a charged particle in a magnetic dipole field separates mathematically into motion in meridian plane and the rotation of the meridian plane about the symmetry axis of the field.

In cylindrical coordinates, the equations for the motion in the meridian plane are

$$\varrho'' = \left(\frac{2\gamma}{\varrho} - \frac{\varrho\cos\lambda}{r^3}\right)\left(\frac{2\gamma}{\varrho^2} + \frac{\cos\lambda}{r^3} + \frac{3\varrho^2\cos\lambda}{r^5}\right), \tag{1}$$

$$Z'' = -\left(\frac{2\gamma}{\varrho} - \frac{\varrho\cos\lambda}{r^3}\right)\left(\frac{3\varrho z\cos\lambda}{r^5}\right), \tag{2}$$

where γ is the Størmer parameter, λ denotes geomagnetic latitude, $\varrho = r\cos\lambda$, $Z = r\sin\lambda$, and r represents distance from the origin as measured in Størmer units. The Størmer unit is defined by the equation

$$r = (R/M)^{\frac{1}{2}} L = (mcv/ZeM)^{\frac{1}{2}} L\,, \tag{3}$$

where $R = mvc/Ze$ is the magnetic rigidity in statvolts, M is the earth's magnetic dipole moment in gauss-cm^3 and L is the length in cm to which r in Størmer units corresponds.

The solutions to Eqs. (1) and (2) are subject to the well-known accessibility restrictions imposed by Størmer's integral,

$$\pm\cos\omega = \frac{2\gamma}{r\cos\lambda} - \frac{\cos\lambda}{r^2}\,, \tag{4}$$

where (+) is used for positively charged particles and (—) is used for negatively charged particles. The angle ω is the angle which the negative of the velocity vector makes with the east-west line at a point of observation and is measured from the east.

In the discussion which follows we will assume that the reader has a working acquaintance with geomagnetic theory.

Since (except for the case of the equatorial plane) solutions to the equations of motion in a magnetic dipole field have not been found in terms of elementary

or tabulated functions, one must generally resort to numerical integrations in order to obtain trajectories. The numerical integrations used in the present work were performed on Avidac, the high speed digital computer at Argonne National Laboratory. Each trajectory took, on the average, about three minutes to compute.

We used the following approach for determining the principal structure of the penumbra. We fix a direction of observation at a given latitude. Negatively charged particle trajectories are started out from the earth in the chosen direction. The trajectories thus obtained will be the same as those traversed by positively charged particles with the same magnetic rigidity, but travelling in the opposite direction. Now for arbitrary longitude, the initial conditions for any trajectory will be completely specified by giving values for ϱ', Z', and any two of the variables r, λ and γ. Therefore, we may generate the entire class of trajectories associated with a fixed direction and latitude by varying either r or γ.

Since we are not interested in rigidities below the Stormer cut-off, we find it convenient to vary γ in order to easily guarantee not going beyond $\gamma = 1$. Let R_m denote the rigidity associated with the main cone cut-off. Let γ_m denote the value of γ associated with R_m. We start with a value of γ below γ_m and increase the value by small increments until the Stormer cut-off is reached with $\gamma = 1$. In this fashion, we may generate the entire allowed and forbidden band structure of the penumbral region (and at the same time determine R_m). As a guide in choosing an initial value of γ below γ_m for each fixed direction and latitude, we used trajectories calculated by STORMER ([8]), the published curves of LEMAITRE and VALLARTA ([2]) and HUTNER ([1]), the published curves of MALMFORS ([9]) which are based on his model experiments, and the author's own trajectory calculations made with a desk computer.

The next important step was to decide on what size increment in γ would be sufficient for determining R_m and the boundaries of the principal allowed and forbidden regions of the penumbra to a satisfactory degree of accuracy. A study of Stormer's trajectories ([8]) indicated that an increment of $\Delta\gamma = .003$ might be sufficient (at latitudes from 30° to 41°) to determine the boundaries of the main cone and the main penumbral bands correct to there figures in r with a small error in the fourth figure. A trial run, made at $\lambda = 41°$, indicated that $\Delta\gamma = .003$ would be satisfactory.

To conclude this section on the method of calculation, we will say a few words about the program used on the machine for calculating trajectories. The basic program was one originally devised for the work of F. S. JORY ([10]).

([8]) Figs. 144–146 of Størmer's book.
([9]) K. G. MALMFORS: *Ark. Mat., Astron., o. Fys.*, **32**, no. 8 (1945).
([10]) F. S. JORY: *Phys. Rev.*, **103**, 1068 (1956).

The numerical integrations were based on Eqs. (1) and (2). A trajectory was started out from the earth and the calculation was continued until either of three things occured:

1) A distance $r = 1$ was reached.
2) The trajectory returned to the earth.
3) The trajectory turned through a relative maximum of r for the fifth time.

As soon as any one of the above three conditions occured in a trajectory, the calculation was stopped. In the first case, the distance $r = 1$ exceeds the maximum distance from the dipole of the region where maxima of r can exist. Hence, such trajectories will proceed to infinity and will be allowed. Trajectories in the second class are forbidden. In the third case, trajectories were « left in mid-air » because of the possibility that they would pass through many more maxima and minima of r before coming under either case (1) or case (2); continuing the calculation we would have run the risk of having truncation errors become significant as well as adding considerably to the expense of the project.

Not every trajectory point was printed out. Besides the initial and final points of a calculation, those points corresponding to maxima or minima of r were the only ones printed out. This procedure saved a good deal of calculating time while still allowing for the possibility of obtaining a rough idea of the structure of the calculated trajectories.

We believe the above method of calculation is relatively simple and straightforward. Accurate results may be obtained directly from the machine calculations without time consuming trajectory plotting and slope measuring. One is limited mainly by the expense of computing machine time.

2·2. *Results on the penumbra.* – 1) The above program has been carried out for the latitudes and directions of observation mentioned in the introduction. The results of the calculation are given in Tables I-XIII. The first line of each table refers to the main cone cut-off and the last line to the Störmer cut-off. A set of footnotes which explain the entries has been included with the tables. However, some further amplifying remarks are necessary.

(α) The entries in the tables refer to positively charged particles arriving in the northern hemisphere. From the symmetry properties of the equations of motion, it follows that the north and south directions should be interchanged when using the tables for positively charged particles arriving in the southern hemisphere; when using the tables for negative particles arriving in the northern hemisphere, east and west should be interchanged; when using the tables for negative particles arriving in the southern hemisphere, both east and west directions and north and south directions should be interchanged.

TABLE I. – *Allowed and forbidden regions at* $\lambda = 30°$, *vertical.*

Boundaries (γ)	Boundaries (r_e in millistørmers) [a]	Relative uncertainty [b] (%)	Δr_e (millistørmers)	R_e [c] (GV)	ΔR_e (GV)	Allowed [d]
0.892 (**)	420.4	—	0.1	10.43	0.00	No
0.8923	420.3			10.43		
0.8923 (**)	420.3	—	0.6	10.43	0.03	Yes
0.8935	419.7			10.40	0.03	
0.8935	419.7	—	0.4	10.40	0.02	No
0.8943	419.3			10.38		
0.8943	419.3	± 0.1	3.1	10.38	0.16	Yes
0.901	416.2			10.22		
0.901	416.2	± 0.1	13.8	10.22	0.66	No [e]
0.932	402.4	± 0.1		9.57		
0.932	402.4	± 0.1	3.7	9.557	0.171	Yes
0.9405	398.7	± 0.1		9.386		
0.9405	398.7	± 0.1	1.5	9.386	0.071	No
0.944	397.2	± 0.1		9.315		
0.944	397.2	± 0.1	1.0	9.315	0.047	Yes
0.9465	396.2	± 0.1		9.268		
0.9465	396.2	± 0.1	6.4	9.268	0.301	No
0.962	389.8	± 0.1		8.967		
0.962	389.8	± 0.1	1.0	8.967	0.042	Yes
0.9645	388.8	± 0.1		8.925		
0.9645	388.8	± 0.1	2.4	8.967	0.112	Yes
0.9705	386.4	± 0.1		8.813		
0.9705	386.4	± 0.1	1.2	8.813	0.053	Yes
0.9735	385.2	± 0.1		8.760		
0.9735	385.2	± 0.1	6.0	8.760	0.271	No
0.989	379.2	± 0.1		8.489		
0.989	379.2	± 0.1	3.4	8.489	0.154	Yes
0.998	375.8	± 0.1		8.335		
0.998	375.8	± 0.1	0.3	8.335	0.035	No
1.0	375.0			8.300		

Total $\Delta r_e = 45.4$ [f] Total $\Delta R_e = 2.13$ [f]

TABLE II. - *Allowed and forbidden regions at* $\lambda = 35°$, *vertical.*

Boundaries (γ')		Boundaries (r_e in millistormers) [a]	Relative uncertainty [b] (%)	Δr_e (millistormers)	R_e [c] (GV)	ΔR_e (GV)	Allowed [d]
0.9345	[*]	359.0	—	0.1	7.609	0.006	No
0.9347		358.9			7.603		
0.9347		358.9	—	0.1	7.603	0.006	Yes
0.9352		358.8			7.597		
0.9352	[**]	358.8	—	0.2	7.597	0.006	No
0.9355		358.6			7.591		
0.9355	[**]	358.6	—	0.2	7.591	0.006	Yes
0.936		358.4			7.585		
0.936		358.4	—	19.8	7.585	0.820	No [e]
0.991		338.6			6.765		
0.991	[**]	338.6	—	3.1	6.765	0.118	No
1.0		335.5			6.647		
Total $\Delta r_e = 23.5$ [f]					Total $\Delta R_e = 0.962$ [f]		

TABLE III. – *Allowed and forbidden regions at* $\lambda = 41°$, *vertical.*

Boundaries (γ')		Boundaries (r_e in millistormers) [a]	Relative uncertainty [b] (%)	Δr_e (millistormers)	R_e [c] (GV)	ΔR_e (GV)	Allowed [d]
0.9429		302.0	—	0.1	5.384	0.004	No
0.9433		301.9			5.380		
0.9433	[**]	301.9	—	0.5	5.380	0.018	Yes
0.9448		301.4			5.362		
0.9448	[**]	301.4	$\pm$ 0.1	0.1	5.362	0.003	No
0.9452		301.3			5.359		
0.9452	[**]	301.3	$\pm$ 0.1	3.1	5.359	0.110	Yes
0.9505		298.2	$\pm$ 0.2		5.249		
0.9505	[**]	298.2	$\pm$ 0.2	4.3	5.249	0.150	No [e]
0.969		293.9	$\pm$ 0.1		5.099		
0.969	[**]	293.9	$\pm$ 0.1	3.6	5.099	0.125	Yes
0.981		290.3	$\pm$ 0.1		4.974		
0.981		290.3	$\pm$ 0.1	0.4	4.974	0.013	No
0.9825		289.9	$\pm$ 0.1		4.961		
0.9825		289.9	$\pm$ 0.1	1.4	4.961	0.048	Yes
0.987		288.5	$\pm$ 0.1		4.913		
0.987		288.5	$\pm$ 0.1	1.7	4.913	0.058	No
0.993		286.8			4.855		
0.993		286.8	—	2.0	4.855	0.067	No
1.0	[**]	284.8			4.788		
Total $\Delta r_e = 17.2$ [f]					Total $\Delta R_e = 0.596$ [f]		

TABLE IV. – *Allowed and forbidden regions at* $\lambda = 45°$, *vertical.*

Boundaries (γ)	Boundaries (r_e in millistørmers) [3]	Relative uncertainty [b] (%)	Δr_e (millistørmers)	R_e [c] (GV)	ΔR_e (GV)	Allowed [d]
0.919 (**) 0.9193	272.0 271.9	—	0.1	4.367 4.364	0.003	No
0.9193 (**) 0.9200	271.9 271.7	—	0.2	4.364 4.358	0.003	Yes
0.9200 (**) 0.9206	271.7 271.6	—	0.1	4.358 4.355	0.003	No
0.9206 0.938	271.6 266.5	—	5.1	4.355 4.192	0.163	Yes
0.938 0.962	266.5 259.9	± 0.1	6.6	4.192 3.987	0.205	No [e]
0.962 0.968	259.9 258.3	± 0.1 ± 0.15	1.6	3.987 3.938	0.049	Yes
0.968 0.972	258.3 257.2	± 0.15 ± 0.15	1.1	3.938 3.905	0.033	No
0.972 0.980	257.2 255.1	± 0.15 ± 0.2	2.1	3.905 3.842	0.063	Yes
0.980 (*) 0.984	255.1 254.1	± 0.2 ± 0.2	1.0	3.842 3.812	0.030	No
0.984 (**) 0.988	254.1 253.0	± 0.2	1.1	3.812 3.779	0.033	Yes
0.988 (**) 0.993	253.0 251.8	—	1.2	3.779 3.743	0.036	No
0.993 (**) 0.997	251.8 250.8	—	1.0	3.743 3.713	0.030	Yes
0.997 0.999	250.8 250.3	—	0.5	3.713 3.698	0.015	Yes
0.999 (**) 1.0	250.3 250.0	—	0.3	3.698 3.689	0.009	No
Total $\Delta r_e = 22.0$ [f]				Total $\Delta R_e = 0768$ [f].		

TABLE V. – *Allowed and forbidden regions at* $\lambda = 50°$, *vertical* (°).

Boundaries (γ)	Boundaries (r_e in millistormers) (a)	Relative uncertainty (b) (%)	Δr_e (millistormers)	R_e (c) (GV)	ΔR_e (GV)	Allowed (d)
0.927	222.9	—	3.8	2.933	0.100	Yes
0.943	219.1			2.833		
0.943	219.1	—	3.7	2.833	0.094	No (e)
0.959	215.4			2.739		
0.959	215.4	—	7.8	2.739	0.195	Yes
0.995	207.6			2.544		
0.995	207.6	—	1.0	2.544	0.025	No
1.0	206.6			2.519		
Total $\Delta r_e = 16.3$ (f)				Total $\Delta R_e = 0.414$ (f)		

(°) The results presented in this table for the allowed and forbidden regions are believed by the author to be good guesses of the main structure of the penumbra for $\lambda = 50°$, vertical. The guesses are based upon seven trajectories, which were all the data the author had available for this case. No attempt has been made to estimate the relative uncertainty in the boundary assignments. The reader should consult the text for further discussion of this table.

TABLE VI. – *Allowed and forbidden regions at* $\lambda = 41°$ N, $\zeta = 45°$ N (°).

Boundaries (γ)	Boundaries (r_e in millistormers) (a)	Relative uncertainty (b) (%)	Δr_e (millistormers)	R_e (c) (GV)	ΔR_e (GV)	Allowed (d)
0.888 (**)	320.7	—	0.1	6.068	0.000	No
0.8884	320.6			6.068		
0.8884 (**)	320.6	—	0.4	6.068	0.017	Yes
0.8895	320.2			6.051		
0.8895	320.2	—	0.4	6.051	0.012	No
0.8905	319.8			6.039		
0.8905 (*)	319.8	—	7.5	6.039	0.282	Yes
0.912	312.3			5.757		
0.912	312.3	—	26.6	5.757	0.939	No (e)
0.997	285.7			4.818		
0.997 (**)	285.7	—	0.9	4.818	0.030	No
1.0	284.8			4.788	0.030	
Total $\Delta r_e = 35.9$ (f)				Total $\Delta R_e = 1.280$ (f)		

(°) ζ is the zenith angle measured from the vertical.

TABLE VII. – *Allowed and forbidden regions at* $\lambda = 41°$ N, $\zeta = 60°$ N (°).

Boundaries (γ)		Boundaries (r_e in millistormers) (a)	Relative uncertainty (b) (%)	Δr_e (millistormers)	R_e (c) (GV)	ΔR_e (GV)	Allowed (d)
0.9565	(**)	297.7	—	0.0	5.232	0.000	No
0.9568		297.7			5.232		
0.9568	(**)	297.7	—	0.3	5.232	0.011	Yes
0.9575		297.7			5.221		
0.9575	(**)	297.4	—	0.1	5.221	0.003	No
0.958		297.3			5.218		
0.958	(*)	297.3	± 0.1	2.2	5.218	0.078	Yes
0.965		295.1			5.140		
0.965		295.1	± 0.1	2.0	5.140	0.069	No (e)
0.9715		293.1			5.071		
0.9715	(*)	293.1	± 0.3	2.2	5.071	0.076	Yes
0.979		290.9			4.995		
0.979	(*)	290.9	± 0.3	3.1	4.995	0.106	No
0.9895		287.8			4.889		
0.9895	(*)	287.8	± 0.1	2.1	4.889	0.071	Yes
0.997		285.7			4.818		
0.997	(**)	285.7	± 0.1	0.9	4.818	0.030	No
1.0		284.8			4.788		
Total $\Delta r_e = 12.9$ (f)					Total $\Delta R_e = 0.444$ (f)		

(°) ζ is the zenith angle measured from the vertical.

TABLE VIII. – *Allowed and forbidden regions at* $\lambda = 41°$, $\zeta = 45°$ E (°).

Boundaries (γ)	Boundaries (r_e in millistørmers) (a)	Relative uncertainty (b) (%)	Δr_e (millistørmers)	R_e (1) (GV)	ΔR_e (GV)	Allowed (d)
0.938 (**) 0.9383	335.7 335.5	—	0.2	6.653 6.647	0.006	No
0.9383 (**) 0.9389	335.5 335.3	—	0.2	6.647 6.635	0.012	Yes
0.9389 0.9391	335.3 335.2	—	0.1	6.635 6.635	0.000	No
0.9391 (**) 0.9396	335.2 335.0	—	0.2	6.635 6.623	0.012	Yes
0.9396 (**) 0.9402	335.0 334.7	—	0.3	6.623 6.611	0.012	No
0.9402 0.9435	334.7 333.3	± 0.1	1.4	6.611 6.558,	0.053	Yes
0.9435 (*) 0.963	333.3 325.0	± 0.1 ± 0.2	8.3	6.558 6.234	0.324 0.324	No (e)
0.963 (*) 0.9675	325.0 323.2	± 0.2 ± 0.1	1.8	6.234 6.169	0.065	Yes
0.9675 0.9715	323.2 321.5	± 0.1	—	6.169 6.104	0.065	No
0.9715 (*) 0.989	321.5 314.7	—	6.8	6.104 5.846	0.258	Yes
0.989 (*) 0.9945	314.7 312.6	± 0.15 ± 0.15	2.1	5.846 5.768	0.078	No
0.9945 0.9975	312.6 311.5	± 0.15 ± 0.1	1.1	5.768 5.728	040.0	Yes
0.9975 (**) 1.0	311.5 310.5	± 0.1	1.0	5.728 5.691	0.037	No
Total $\Delta r_e = 25.2$ (f)				Total $\Delta R_e = 0.962$ (f)		

(°) ζ is the zenith angle measured from the vertical.

TABLE IX. – *Allowed and forbidden regions at* $\lambda = 41°$, $\zeta = 60°$ E (°).

Boundaries (γ)	Boundaries (r_e in millistørmers) (a)	Relative uncertainty (b) (%)	Δr_e (millistørmers)	R_e (c) (GV)	ΔR_e (GV)	Allowed (d)
0.9245 (**)	351.8	—	0.2	7.308	0.012	No
0.9248	351.6			7.296		
0.9248 (*,*)	351.6	—	0.2	7.296	0.006	Yes
0.9253	351.4			7.290		
0.9253 (**)	351.4	—	0.3	7.290	0.012	No
0.9258	351.1			7.278		
0.9258	351.1	—	1.6	7.278	0.065	Yes
0.929	349.5			7.213		
0.929	349.5	—	5.9	7.213	0.242	No (e)
0.941	343.6			6.971		
0.941 (*)	343.6	± 0.3	3.3	6.971	0.135	Yes
0.948	340.3			6.836		
0.948	340.3	± 0.3	6.2	6.836	0.248	No
0.9615 (*)	334.1	± 0.1		6.588		
0.9615 (*)	334.1	± 0.1	11.0	6.588	0.425	Yes
0.987	323.1	± 0.2		6.163		
0.987 (*,*)	323.1	± 0.2	1.6	6.163	0.059	Yes
0.991	321.5			6.104		
0.991 (*,*)	321.5	—	1.7	6.104	0.065	No
0.995	319.8			6.039		
0.995 (*,*)	319.8	—	0.8	6.039	0.030	Yes
0.997	319.0			6.009		
0.997 (*,*)	319.0	—	1.2	6.009	0.047	No
1.0	317.8			5.962		
Total $\Delta r_e = 34.0$ (f)				Total $\Delta R_e = 1.346$ (f)		

(°) ζ is the zenith angle measured from the vertical.

TABLE X. – *Allowed and forbidden regions at* $\lambda = 41°$ N, $\zeta = 45°$ S (°).

Boundaries (γ)	Boundaries (r_e in millistormers) (a)	Relative uncertainty (b) (%)	Δr_e (millistormers)	R_e (c) (GV)	ΔR_e (GV)	Allowed (d)
0.921 (**)	309.2	—	0.1	5.643	0.003	No
0.9213	309.1			5.640		
0.9213 (**)	309.1	—	0.4	5.640	0.015	Yes
0.9225	308.7			5.625		
0.9225	308.7	—	0.3	5.625	0.011	No
0.9235	308.4			5.614		
0.9235	308.4	± 0.1	2.3	5.614	0.083	Yes
0.9305	306.1			5.531		
0.9305	306.1	± 0.1	1.0	5.531	0.036	No
0.9335	305.1	± 0.1		5.495		
0.9335	305.1	± 0.1	2.2	5.495	0.079	Yes
0.9402	302.9			5.416		
0.9402	302.9	—	8.3	5.416	0.293	No (e)
0.9667	294.6			5.123		
0.9667	294.6	± 0.2	4.3	5.123	0.149	Yes
0.981	290.3			4.974	0.149	
0.981 (**)	290.3	± 0.2	1.2	4.974	0.040	Yes
0.985	289.1			4.934		
0.985 (**)	289.1	—	1.4	4.934	0.048	No
0.990	287.7		1.4	4.886		
0.990 (**)	287.7	—	1.2	4.886	0.041	Yes
0.994	286.5			4.845		
0.994 (**)	286.5	—	0.6	4.845	0.020	No
0.996	285.9			4.825		
0.996	285.9	—	0.5	4.825	0.017	No
0.998	285.4			4.808		
0.998 (**)	285.4	—	0.6	4.808	0.020	No
1.0	284.8			4.788		
Total $\Delta r_e = 24.4$ (f)				Total $\Delta R_e = 0.855$ (f)		

(°) ζ is the zenith angle measured from the vertical.

TABLE XI. - *Allowed and forbidden regions at* $\lambda = 41°$ N, $\zeta = 60°$ S (°).

Boundaries (γ)		Boundaries (r_e in millistormers) (a)	Relative uncertainty (b) (%)	Δr_e (millistormers)	R_e (c) (GV)	ΔR_e (GV)	Allowed (d)
0.912	(**)	312.3	—	0.2	5.757	0.007	No
0.9124		312.1			5.750		
0.9124	(**)	312.1	—	0.2	5.750	0.008	Yes
0.9132		311.9			5.742		
0.9132	(**)	311.9	—	0.3	5.742	0.011	No
0.9139		311.6			5.731		
0.9139	(*)	311.6	± 0.2	6.5	5.731	0.236	Yes
0.9335		305.1			5.495		
0.9335	(*)	305.1	± 0.2	15.1	5.495	0.531	No (e)
0.982		290.0	± 0.1		4.964		
0.982	(**)	290.0	± 0.1	1.3	4.964	0.044	Yes
0.9865		288.7	± 0.1		4.920		
0.9865		288.7	± 0.1	0.9	4.920	0.031	No
0.9895		287.8	± 0.1		4.889		
0.9895	(**)	287.8	± 0.1	0.7	4.889	0.023	Yes
0.992		287.1			4.866		
0.992	(**)	287.1	—	1.2	4.866	0.041	No
0.992		285.9			4.825		
0.996	(**)	285.9	—	0.5	4.825	0.017	Yes
0.998		285.4			4.808		
0.998	(**)	285.4	—	0.6	4.808	0.020	No
1.0		284.8			4.788		
Total $\Delta r_e = 27.5$ (f)					Total $\Delta R_e = 0.969$ (f)		

(°) ζ is the zenith angle measured from the vertical.

TABLE XII. – *Allowed and forbidden regions at* $\lambda = 41°$, $\zeta = 45°$ W (°).

Boundaries (γ)	Boundaries (r_e in milli-stormers) (a)	Relative uncertainty (b) (%)	Δr_e (milli-stormers)	R_e (c) (GV)	ΔR_e (GV)	Allowed (d)
0.9203 (**) 0.9206	285.6 285.6	—	0.0	4.815 4.815	0.000	No
0.9206 0.9213	285.6 285.6	—	0.0	4.815 4.815	0.000	Yes
0.9213 (**) 0.9218	285.6 285.5	—	0.1	4.815 4.812	0.003 0.003	No
0.9218 0.928	285.5 283.7	—	1.8	4.812 4.751	0.061	Yes
0.928 0.938	283.7 281.1	—	2.6	4.751 4.665	0.086	No (e)
0.938 0.9435	281.1 279.7	± 0.1	1.4	4.665 4.618	0.047	Yes
0.9435 0.9465	279.7 279.0	± 0.1 ± 0.1	0.7	4.618 4.595	0.023	No
0.9465 (*) 0.965	279.0 274.3	± 0.1	4.7	4.595 4.441	0.154	Yes
0.965 (*) 0.9765	274.3 271.5	± 0.3	2.8	4.441 4.351	0.090	No
0.9765 0.987	271.5 269.0	± 0.3	2.5	4.351 4.271	0.080	Yes
0.987 0.996	269.0 266.9	± 0.1	2.1	4.271 4.205	0.066	No
0.996 (**) 1.0	266.9 265.9	± 0.1	1.0	4.205 4.173	0.032	No

Total $\Delta r_e = 19.7$ (f) Total $\Delta R_e = 0.642$ (f)

(°) ζ is the zenith angle measured from the vertical.

TABLE XIII. - *Allowed and forbidden regions at* $\lambda = 41°$, $\zeta = 60°$ W (°).

Boundaries (γ)	Boundaries (r_e in millistørmers) [a]	Relative uncertainty [b] (%)	Δr_e (millistørmers)	R_e [c] (GV)	ΔR_e (GV)	Allowed [d]
0.898 (**) 0.8984	287.1 287.0	—	0.1	4.866 4.862	0.004	No
0.8984 (**) 0.8992	287.0 286.8	—	0.2	4.862 4.855	0.007	Yes
0.8992 (**) 0.8997	286.8 286.7	—	0.1	4.855 4.852	0.003	No
0.8997 0.918	286.7 281.9	—	4.8	4.852 4.691	0.161	Yes
0.918 0.930	281.9 278.9	± 0.1	3.0	4.691 4.592	0.099	No [e]
0.930 (*) 0.9405	278.9 276.3	± 0.1 ± 0.1	2.6	4.592 4.506	0.086	Yes
0.9405 (**) 0.9415	276.3 276.0	± 0.1 ± 0.1	0.3	4.506 4.497	0.009	No
0.9415 0.9495	276.0 274.1	± 0.1 ± 0.1	1.9	4.497 4.435	0.062	Yes
0.9495 0.9525	274.1 273.4	± 0.1 ± 0.1	0.7	4.435 4.412	0.023	No
0.9525 0.978 (*)	273.4 267.3	± 0.1 ± 0.15	6.1	4.412 4.218	0.194	Yes
0.978 (**) 0.981	267.3 266.6	± 0.15	0.7	4.218 4.196	0.022	No
0.981 (**) 0.9885	266.6 264.9	± 0.1	1.7	4.196 4.142	0.054	Yes
0.9885 0.993	264.9 263.9	± 0.1	1.0	4.142 4.111	0.031	No
0.993 (**) 0.996	263.9 263.2	—	0.7	4.111 4.089	0.022	No
0.996 0.998	263.2 262.8	—	0.4	4.089 4.077	0.012	Yes
0.998 (**) 1.0	262.8 262.5	—	0.3	4.077 4.068	0.009	No
Total $\Delta r_e = 24.6$ [f]				Total $\Delta R_e = 0.798$ [f]		

(*) ζ is the zenith angle measured from the vertical.

Footnotes for Tables I through XIII.

([a]) r_e is the radius of the earth in milli-størmers. The values given represent the boundaries between allowed and forbidden regions. The first entry of the table represents the main cone cut-off.

([b]) This column gives the percentage uncertainty in assignments of the boundary values, r_e. The values given represent estimates of the upper limit of the uncertainty. Except for lines marked (**), no entry of the relative uncertainty means that it is considered to be less than 0.1%.

([c]) This column gives the rigidity in GV, corresponding to r_e, at 6400 km. If we neglect errors in the earth's dipole moment ($M = 8.06 \cdot 10^{25}$ G cm^3) and error from using 6400 km as the radius of the earth, the percentage error in R_e is twice that in the corresponding value of r_e.

([d]) If a region specified by Δr_e and ΔR_e is made up of allowed trajectories, we designate this with the word yes; if it is made up of forbidden trajectories, we designate this with the word no.

([e]) This is the group of trajectories which return directly to the neighborhood of the initial point on the earth after leaving the first turning point.

([f]) The total Δr_e is the distance in milli-størmers between the « main cone » cut-off and the Störmer cut-off; the total ΔR_e represents the same distance in GV.

(*) This region contains one or two trajectories which were not calculated all the way to the point of either cutting back through the earth or going to infinity. However, on the basis of the structure of surrounding trajectories, and on the basis of knowledge of the distribution of the force, and knowing where the final calculated point of these trajectories lies with respect to the force field, and in comparison with the known behavior of other trajectories such as the author's and Stormer's, these trajectories were assigned to the regions in which they appear.

(**) These regions contain no calculated trajectories. They have been included because they are expected theoretically and are exhibited by Stormer's trajectories. The positions and sizes of these regions have in some cases been estimated on the basis of a study of Størmer's trajectories.

(***) This region consists entirely of trajectories which were not calculated all the way to the point of either cutting back through the earth or going to infinity. The assignments are guesses based on a study of the trajectories to the extent that they have been calculated and on the basis of the relative sizes of the neighboring allowed and forbidden regions. The nearness to the Størmer cut-off has also been considered as a weighting factor in some cases. These assignments are intended solely as guesses of what the main structure, with respect to allowedness or forbiddenness, of these regions is. No attempt is made to estimate the relative uncertainty in the boundary assignments.

(β) The band marked with a superscript e on the tables generally constituted the largest forbidden band (and, with a few exceptions, also the largest band) for the directions studied. The trajectories in this band are centered about an orbit which leaves the earth in one hemisphere, proceeds directly to the forbidden region boundary determined by $\cos\omega = 1$ in the opposite hemisphere where it bounces off at right angles and retraces its original path back to the earth. One can obtain an idea of how this band arises by studying the Størmer trajectories referred to previously ([8]).

(γ) In computing the trajectories for the vertical direction at $\lambda = 45°$, $\Delta\gamma = .004$ was used because it was considered adequate for this latitude.

(δ) It was not originally intended to investigate the situation extensively for the vertical direction at $\lambda = 50°$ because the penumbra was expected to be predominantly light. Therefore, only six trajectories were calculated for this case. The primary purpose was to determine R_m; however, as a check on the expectation of the predominance of light, γ was varied from 0.930 to 0.990 in steps of $\Delta\gamma = .01$ (omitting $\gamma = .970$). This choice of values for γ turned out to be fortunate because the structure of the calculated trajectories made it possible to outline the boundaries of the predominant band structure. The value of R_m was estimated by noting that according to JORY ([10]), $r_e = 0.225$ stormers (where r_e denotes the radius of the earth in Störmer units) is allowed in the vertical direction at $\lambda = 50°$ with the corresponding value of R being greater than R_m:

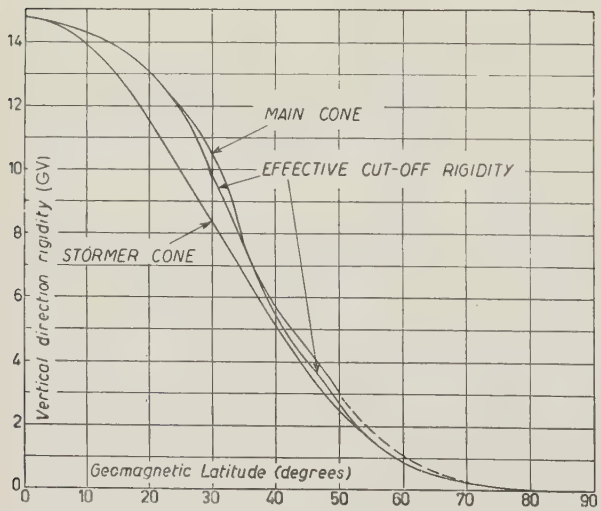

Fig. 1. – Low rigidity limits for the vertical direction.

(ε) In converting from Størmer units to rigidity, we used a magnetic dipole moment of $8.06 \cdot 10^{25}$ G cm^3 and an effective radius of the earth of 6400 km.

(η) A total of 374 trajectories was computed on the machine.

2) The following remarks pertain to the curves in Figs. 1 through 6. The upper curve of Fig. 1 is a plot of R_m for the vertical direction as a function of latitude. The points in the latitude range from 0° to 30° and are determined from the published curves of LEMAITRE and VALLARTA ([5b,c]). The points in the

latitude range from 30° to 50° were determined from the first lines of Tables I through V. The meridian plane curves of LEMAITRE and VALLARTA ([2b]) were used as guides from $\lambda = 30°$ to $\lambda = 45°$. The dashed part of the curve represents an extrapolation to 90°. The lowest curve is a plot of R_s *vs.* latitude (where R_s denotes the rigidity corresponding to the Störmer cut-off) while the middle curve is a plot of effective cut-off rigidity in the vertical direction *vs.* latitude. (Effective cut-off rigidities are discussed in the next Section).

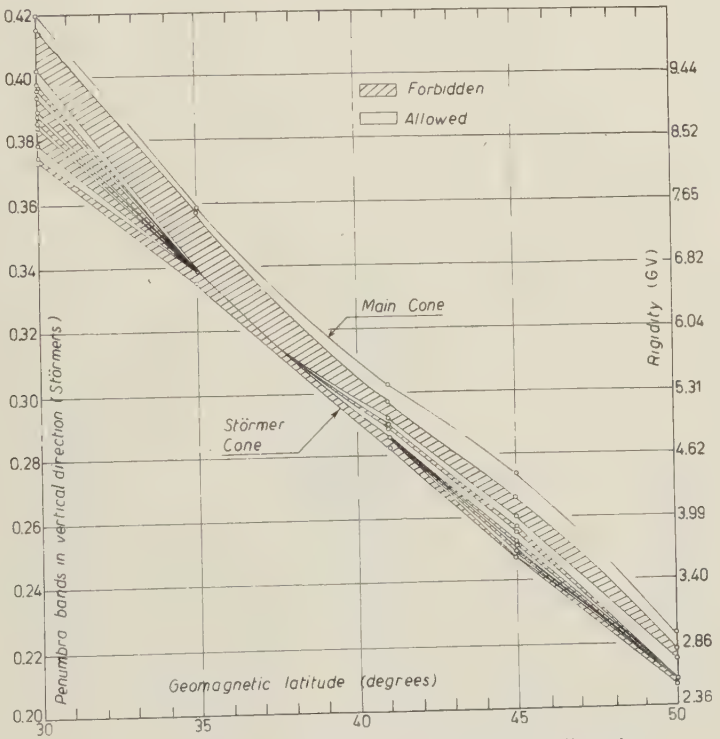

Fig. 2. – Penumbral bands in the vertical direction.

The curves of Figs. 2 through 6 were constructed as follows. First the data given in Tables I through XIII were plotted-with certain narrow bands omitted because they would not show up well on the curves. The size of these omitted bands was generally less than four milli-stormer. Then the uppermost curve (corresponding to R_m) and the lowest curve (corresponding to R_s) were drawn in. As an aid in drawing the curves for R_m at $\lambda = 41°$, we used estimates based on Jory's data ([10]) for zenith angles 16° east, 32° north and 32° south at $\lambda = 40°$. The curves showing the banded structure were drawn by joining those calculated bands which consisted of trajectories having the same structure. The curves for R_m and R_s were used as guides.

2·3. *Discussion of errors* ([11]). – 1) The initial conditions for each trajectory were fed into the machine to six significant figures. The machine handled ten figures for a given quantity so round-off errors were negligible. Apart from possible machine failures, the main source of error in the numerical integrations would then be the truncation error. The step-size was taken sufficiently small and varied as the trajectory curvature varied so that it is expected that the final point calculated for each trajectory is good to at least four significant figures.

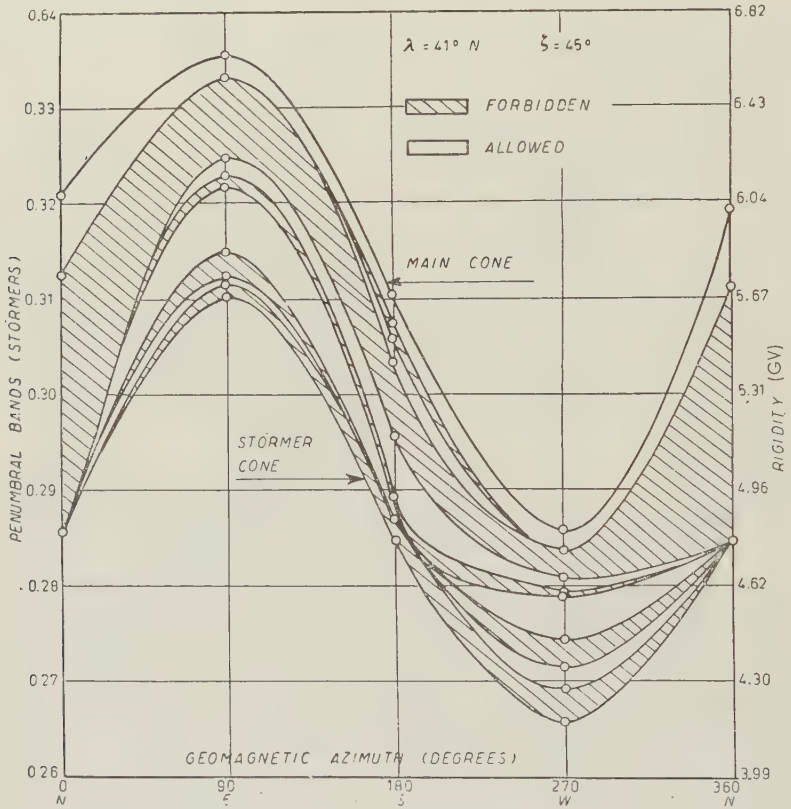

Fig. 3. – Penumbral bands for 45° zenith angle at $\lambda = 41°$.

To check this, the turning points of three machine calculated trajectories were compared with the turning points of the same three trajectories as calculated with a desk computer. The two calculations agreed to four significant figures.

([11]) For a more detailed discussion of errors see the author's thesis, State University of Iowa (1958).

A qualitative check on the accuracy of the machine calculations was made by studying the consistency with which the trajectory structure changed as $\gamma \to 1$ for fixed observation direction and fixed λ. Each such set of trajectories satisfied this check.

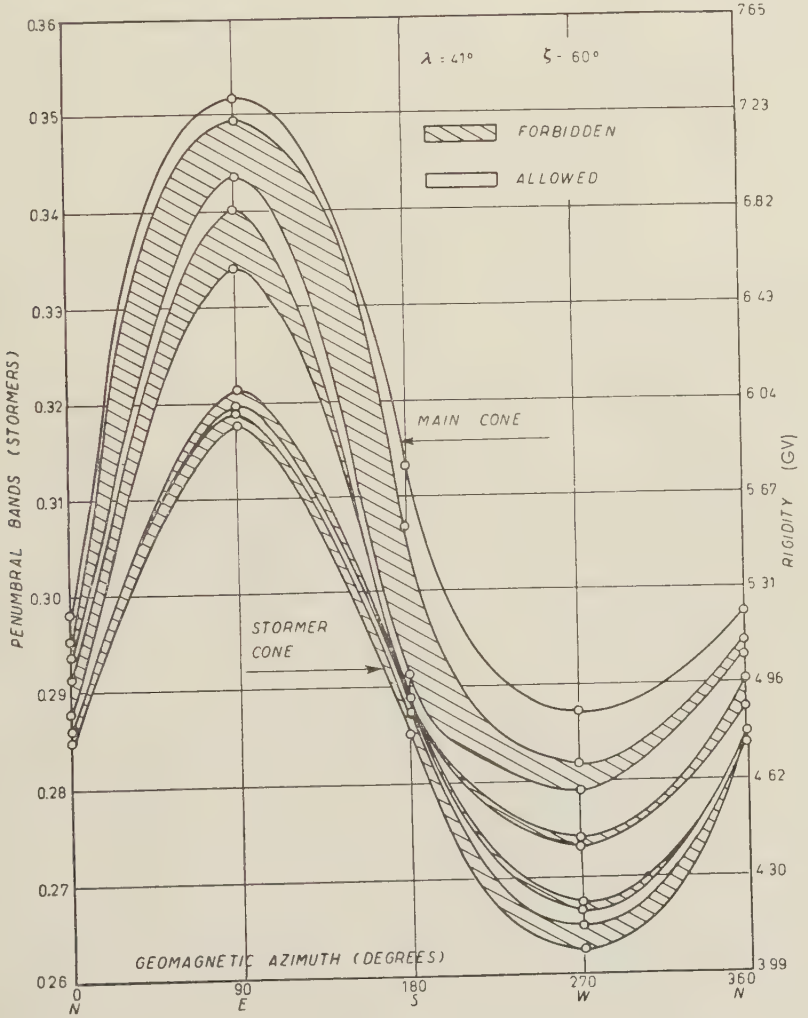

Fig. 4. – Penumbral bands for 60° zenith angle at $\lambda = 41°$.

The maximum error made in locating the boundary between two adjacent bands has been estimated and listed (except as indicated in the footnotes) in Tables I through XIII. The estimates are based on the size of $\Delta\gamma$ and the structure of the trajectories immediately preceding and succeeding the boundary trajectory.

2) It is extremely difficult to present a significant quantitative discussion of the accuracy of the boundary curves in Figs. 2 through 6 ([12]) because (except for the main cone and Størmer cut-offs) each curve was constructed from a few widely distant points. It is possible to give a significant quantitative estimate of the accuracy of effective cut-offs determined from the curves, but we will postpone discussing this until the next Section.

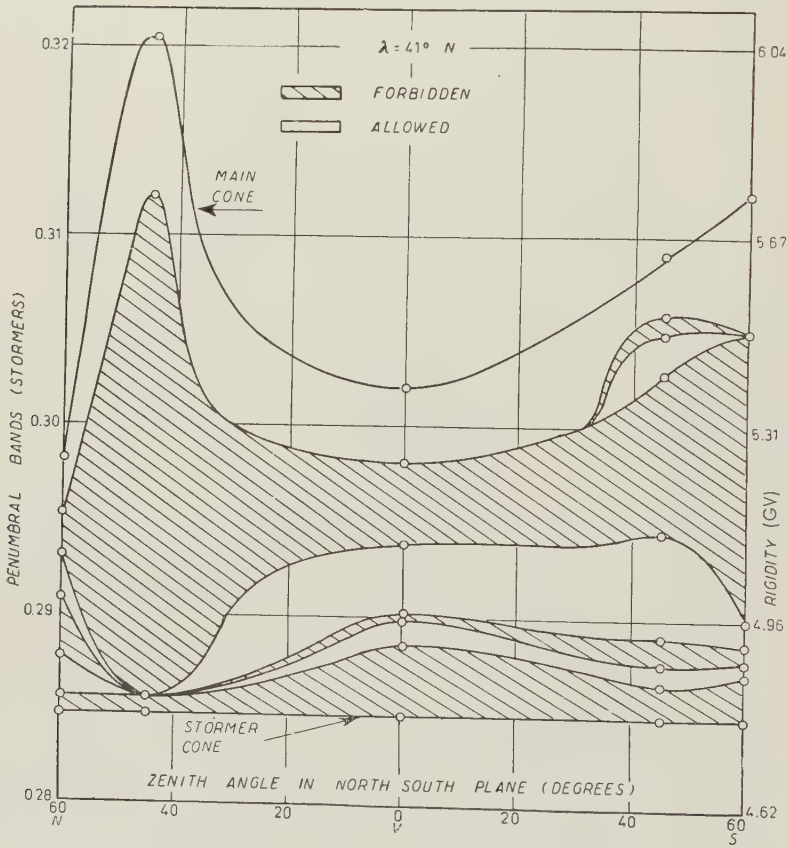

Fig. 5. – Penumbral bands in North-South plane at $\lambda = 41°$ N.

The curves of Figs. 2 through 6 may be read in terms of either Størmer units or rigidity. However, in discussing the purely mathematical accuracy of the present results, we find it convenient to discuss the curves with reference to Størmer units.

([12]) We refer here only to those allowed and forbidden regions along the curves lying between the calculated regions.

Let r_m denote the main cone cut-off in Stormer units. The curves representing plots of r_m are considered accurate to two or three significant figures. The justification of this estimate of accuracy is as follows. The calculated values of r_m are accurate to four significant figures. The vertical direction r_m determined by LEMAITRE and VALLARTA [2b] differ respectively from the present values at $\lambda = 30°$, $35°$, $41°$, $45°$ by the order — 0.1%, +2%, +0.7% 0%.

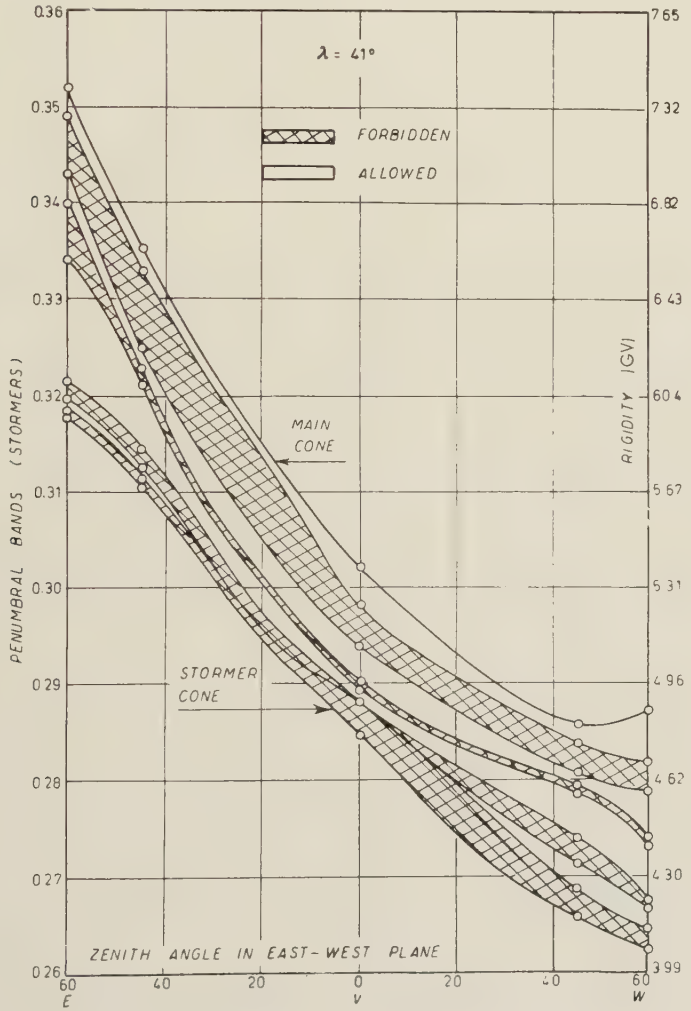

Fig. 6. – Penumbral bands in East-West plane at $\lambda = 41°$.

Therefore, intermediate values of r_m were taken from the curves of LEMAITRE and VALLARTA [2b], adjusted accordingly between $\lambda = 30°$ and $\lambda = 41°$, and used as guides in plotting the vertical direction r_m as a function of latitude to three significant figures.

The estimates of r_m made from Jory's 40° data are considered accurate to three significant figures. These estimates were extrapolated to $\lambda = 41°$ and used as guides in filling in the curves between the vertical direction and 45° zenith angle. Additional help along these lines came from Malmfors' curves ([9,13]). Therefore, we consider the r_m curves in the north-south and east-west planes at $\lambda = 41°$ to be accurate to at least two significant figures (and likely three).

There is no other work available at present which could be used as an aid in drawing the azimuthal variation of the r_m curves for zenith angles 45° and 60° at $\lambda = 41°$. Nevertheless, from qualitative consideration of how the distribution of force affects the structure of trajectories as one increases the zenith angle from the vertical direction (based largely on what is known from the calculated trajectories), and from consideration of the range of r_m involved, one can see that these curves must be accurate to at least two significant figures (quite possibly three).

If one uses the r_m and Størmer cut-off curves as guides, one can obtain a qualitatively correct (and at least roughly quantitatively correct) picture of the distribution of allowed and forbidden bands which consist of trajectories having the same structure.

The above remarks are valid despite the existence of the regions marked (*,*) on Tables I through XIII. The total size of these regions for a given observation direction and latitude is on the average about 10% of the spread between r_m and the Størmer cut-off. Therefore, for two reasons, it is useful to guess at the allowed or forbidden character of the bands on the basis of trajectory structure. First, one gets a qualitatively correct picture regardless of the actual relative size and location of the allowed and forbidden bands. Second (and more important), there are definitely both allowed and forbidden bands in the regions spanned by the triple star bands. Now suppose one calculates an integral directional intensity by integrating a differential spectrum over the allowed ranges of rigidity. If one calls the bands all allowed or all forbidden, on the average they will contribute an uncertainty of about 1% to the calculation of the integral intensity. By making the guesses, one can cut the uncertainty down to about 0.5% on the average; the effective cut-offs which we define in the next Section will then be that much more accurate.

3. – Determination of rigidity spectra from experimental data.

It is well known that Liouville's theorem implies that if the directional differential intensity of cosmic rays is isotropic at infinity, it will be constant and isotropic in all accesible regions of space whether a static magnetic field

([13]) We might add here that we used Malmfors' curves with confidence since in places of overlap, his results agree with ours to about 5%.

is present or not ([2a,14]). Thus, if we know the differential intensity spectrum we can find the total intensity at a given point on the earth and in a given direction there by integrating the differential spectrum over the corresponding ranges of allowed rigidities.

Conversely, if the directional intensities of any component of the primary cosmic ray beam are measured in a variety of locations and directions at the top of the earth's atmosphere then it is possible to determine the rigidity spectrum of this component over a corresponding range of magnetic rigidity. The procedure is as follows:

At any given location and in any given direction of observation, there are in general alternate allowed and forbidden bands of rigidity due to the complex nature of orbits in the geomagnetic field. Thus in principle it is not possible to specify a single value of cut-off rigidity. But *for a given spectrum* it may be convenient to list a single effective value of cut-off rigidity R_c which is defined such that the integral of the differential spectral function $j(R)$ from R_c to infinity is equal to the actual intensity as it would be properly calculated by piecewise integration over the several ranges of allowed rigidities. The numerical value of R_c as so calculated is a function of the spectral form except when the penumbra is completely black or except when the shadow cone places an absolute lower limit on the rigidity of arriving particles. However, we have found by a series of sample calculations that the effective cut-off rigidity typically varies by less than one percent for integral number-rigidity spectra of the form $R^{-\alpha}$ for values of α between 1.0 and 1.5.

Hence for most purposes in the interpretation of cosmic ray observations it is sufficient to list a single effective cut-off R_c for each location and direction of observation.

The middle curve of Fig. 1 is a plot of the vertical R_c *vs.* λ. Bouckaert ([3]) has shown that the penumbra is completely black in the vertical direction below $\lambda = 20°$. Further consideration indicates

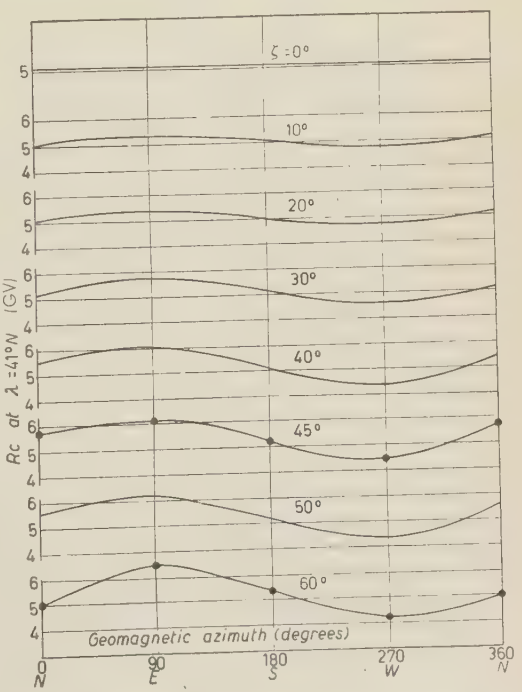

Fig. 7. - Effective cut-off rigidities at λ 41 N.

([14]) W. F. G. Swann: *Phys. Rev.*, **44**, 224 (1933).

TABLE XIV. – *Percentage of region between « main » and Størmer cut-offs which is allowed as determined from Tables I through XII* (*).

λ	ζ (**)	Percentage
30°	0	31%
35°	0	1%
41°	0	50%
45°	0	53%
50°	0	71%
41° North	45° North	22%
41° North	60° North	53%
41°	45° East	46%
41°	60° East	54%
41° North	45° South	48%
41° North	60° South	33%
41°	45° West	53%
41°	60° West	72%

(*) The above percentages were determined from the Størmer values given in Tables I through XIII; they were determined to the nearest percent. Except for a few cases, the percentages determined from the rigidities are the same as above. In the few cases, the percentages differ by about 1%.

(**) ζ is the zenith angle measured from the vertical.

TABLE XV. – *Effective cut-off rigidities* (*).

λ	ζ (**)	R_c (GV)
0°	0	14.76
10°	0	14.3
20°	0	13
30°	0	9.65
35°	0	7.60
41°	0	5.07
45°	0	3.98
50°	0	2.62
55°	0	1.6
41° North	45° North	5.77
41° North	60° North	4.98
41°	45° East	6.13
41°	60° East	6.47
41° North	45° South	5.20
41° North	60° South	5.40
41°	45° West	4.46
41°	60° West	4.26

(*) Except for the first three entries in the table which are main cone cut-offs, all entries have been calculated from those of Tables I through XIII.

(**) ζ is the zenith angle measured from the vertical.

that there is no appreciable amount of light in the penumbra in vertical directions until about $\lambda = 25°$. Therefore, in Fig. 1, we have set $R_c = R_m$ below $\lambda = 25°$. Above $\lambda = 50°$, the R_c curve in Fig. 7 represents an extrapolation with R_c essentially equal to the Størmer cut-off above $\lambda = 55°$.

Note that when R_c coincides with either R_m or R_s, it is independent of α. Moreover, from about $\lambda = 35°$ to about $\lambda = 50°$, the variation of R_c as one varies α from about 1.0 to about 1.5 is negligible up to three significant figures in R_c. Below $\lambda = 35°$, R_c varies in the third significant figure as α goes from 1 to 1.5. For example, in the vertical direction at $\lambda = 30°$, $R_c = 9.64$ GV when $\alpha = 1$ and $R_c = 9.60$ GV when $\alpha = 1.5$.

Because of the above mentioned insensitivity of R_c as a function of α at $\lambda = 41°$, it is worth-while to plot the azimuthal variation of R_c at that latitude for various zenith angles. Such curves are presented in Fig. 7. The curves of Fig. 7 are based on values given in Table XV and values calculated from the curves of Figs. 3 through 6.

In estimating the accuracy of the values of R_c determined from the tables and curves, several things should be noted.

1) We consider only the purely mathematical errors which arise from the calculations and curves alone. We neglect any error introduced in the trasformation from Størmer units to rigidity as a result of error either in the experimental value of the earth's dipole moment or the effective mean radius of the earth. The effective radius of the earth which we used corresponds to current balloon altitudes (30 km). If one took the above sources of error into account, they would increase the uncertainty in R_c by not more than 0.5%.

2) The reader should recall the discussion in Sect. 2 regarding the accuracy of the r_m curves and the qualitative correctness of the band structure curves.

With the above remarks in mind, we estimate that an upper limit to the uncertainty in R_c determined from Tables I through XIII is of the order 0.5 to 1%. For R_c determined from Fig. 2, we estimate an upper limit to the uncertainty of about 1 to 2%. For R_c determined from Figs. 3 through 6, we estimate an upper limit to the uncertainty of about 2 to 2.5%.

For the curves of Fig. 7 corresponding to zenith angles other than 45° and 60°, we estimate that an upper limit to the uncertainty in R_c for those points between the N, E, S, W azimuths is about 2 to 3%.

No attempt will be made to present our results in terms of kinetic energy/nucleon. However, one can easily obtain kinetic energy/nucleon from rigidity by means of the formula

$$\frac{E}{A} = \left(\frac{Z^2}{A^2} R^2 + (0.938)^2\right)^{\frac{1}{2}} - 0.938 \text{ GeV}/A \ , \tag{5}$$

where R is given in GV and 0.938 GeV is the rest energy of a proton.

On the basis of the above one can assign a cut-off rigidity to a measured value of the directional intensity of any component of the primary radiation and can determine the rigidity spectrum of that component by changing the observing conditions to vary the cut-off rigidity over the range available in the geomagnetic field (ideally from about 60 GV to zero).

4. - Schremp's shadow cone calculations and the Winckler-Anderson experiment.

WINCKLER *et al.* [15] have summarized in their Table II various measurements of the apparent total primary intensity in the vertical direction at several latitudes—their own measurements, those of Van Allen and Singer, and those from an analysis by Montgomery. These measurements may be fitted with an $R_c^{-1.02}$ spectrum. Recent work [16] favors an $R^{-1.5}$ spectrum. One may reasonably expect that if the spectrum is well fitted by $R^{-\alpha}$, α will be not far outside the range $1 \leqslant \alpha \leqslant 1.5$.

If the geomagnetic theory based on the earth's dipole field and Liouville's theorem is valid for cosmic rays, it is necessary that a rigidity spectrum as so determined should predict correctly the directional intensity under any condition for which R_c lies within the range $2.6 \leqslant R_c \leqslant 15$ GeV [17]. Subject to some uneasiness about footnote 17, experimental data for such a test are available from the work of WINCKLER and ANDERSON [7], who measured the azimuthal variation of total intensity at $\lambda = 40°$ for zenith angles of 60° and 90°.

The Winckler-Anderson measurements for 60° zenith angle exhibited strong disagreement with Schremp's shadow cone calculations [5]. It was the strength of this disagreement which led the author to check Schremp's work in the neighborhood of $\lambda = 40°$. As a result of this check, we find that large errors exist in Schremp's work.

Not one of the trajectories calculated at $\lambda = 41°$, 60° zenith angle, imposed a simple shadow cut-off. One may therefore conclude that there is no simple shadow cut-off for zenith angles less than or equal to 60° at $\lambda = 41°$; *i.e.* for each zenith angle, the banded structure of the penumbra exists and extends all the way from R_m to the Stormer cut-off. In fact, only the 60° N trajectories exhibited the structure required for simple shadow orbits and these indicate that in the latitude range from 40° to 45°, one does not encounter a simple

[15] J. R. WINCKLER, T. STIX, K. DWIGHT and R. SABIN: *Phys. Rev.*, **79**, 660 (1950).

[16] F. B. MCDONALD: *Phys. Rev.*, **104**, 1723 (1956); **107**, 1386 (1957); P. H. FOWLER and C. J. WADDINGTON: *Phil. Mag.*, **1**, 637 (1956).

[17] For detailed comparison with experimentally observed intensities there is the very stringent assumption that the « primary » intensity itself is being measured correctly and that there are no other contributions.

shadow cut-off until zenith angles of about 70° are reached. The author has checked one of the machine-calculated 60° N orbits against his own calculation of the same orbit and the two calculations agree to four significant figures.

Since the 60° N and 60° E group of trajectories at $\lambda = 41°$ included orbits corresponding to $\gamma = 0.8$ (well below γ_m) with $r_e = 0.356$ stormers for 60° N and $r_e = 0.432$ stormers for 60° E (both well above r_m), one expects that the above conclusions regarding the simple shadow cut-off at $\lambda = 41°$ should hold also at $\lambda = 40°$ (or at least that if a simple shadow cut-off does occur, it occurs at most very close to r_m). This expectation was confirmed by two trajectories calculated at $\lambda = 40°$. One was a 60° N trajectory corresponding to $r_e = 0.339$ stormers and the other was a 60° E trajectory corresponding to $r_e = 0.503$ stormers. Both trajectories are allowed with $r_e > r_m$ in both cases. This clearly contradicts Schremp's result that the simple shadow cut-off at $\lambda = 40°$ is 0.415 størmers for 60° N and 0.54 størmers for 60° E. The 60° E trajectory did not possess the structure required for simple shadow orbits, while the 60° N trajectory did; however, the relative minimum of r on the latter orbit misses the earth by 7.2% of an earth radius.

The present calculations are not the only ones which contradict Schremp's results. Since the present results were reported ([18]), Vallarta and his co-workers have also checked Schremp's results with numerical integration. They also find the same large errors in Schremp's work ([19]).

The original curves of Lemaitre and Vallarta also contradict Schremp's results. Their Figs. 5 and 6 of reference ([2b]), from which one may determine meridian plane r_m values as a function of latitude, indicate that the simple shadow cut-off does not occur in the meridian plane at $\lambda = 40°$ until zenith angles greater than 70° N are reached.

There is also concrete evidence of errors in Schremp's results in the neighbourhood of $\lambda = 30°$. One of Størmer's trajectories through the dipole ([13]) (corresponding to $\gamma = 0.943$) has a portion which may be used to determine a simple shadow cut-off at $\lambda = 30°.1$ for a zenith angle of about 60° and an azimuth (measured from the north) of about 33°. According to Schremp, the cut-off for this case occurs at about 0.53 stormers whereas Størmer's trajectory indicates that the cut-off should be about 0.424 stormers. Fig. 6 of reference ([2b]) also indicates disagreement with Schremp at $\lambda = 30°$. At $\lambda = 30°$, in the neighborhood of 60° N, Lemaitre and Vallarta report a cut-off of about 0.39 størmers ([20]).

([18]) M. Schwartz: *Bull. Amer. Phys. Soc.*,

([19]) M. S. Vallarta: private communication.

([20]) It should be noted that the points of Fig. 6 to which we are referring are the lowest points on the sections marked « earth's shadow ». These lowest points refer to trajectories which are simultaneously simple shadow and asymptotic orbits. There

The size of the errors involved in the above discussion results in doubt being cast upon the reliability of all of Schremp's curves Therefore, since the trajectories of both Schremp, and Lemaitre and Vallarta were calculated on the Bush differential analyser, the question of the reliability of the Lemaitre-Vallarta results is raised. However, on the basis of their own accuracy checks, and on the basis of comparison with both the author's and Størmer's results where overlap occurs, it is possible to say that the Lemaitre-Vallarta calculations are reliable within their stated accuracy (which decreases with increasing latitude and increasing zenith angle).

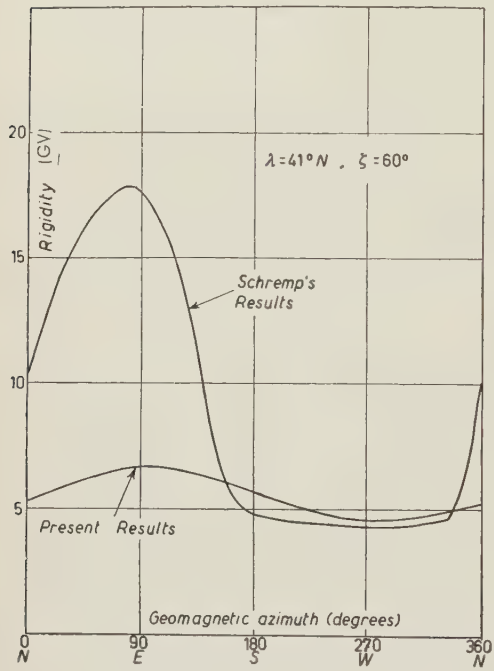

Fig. 8. – Comparison of Schremp's shadow plus Størmer cone at $\lambda = 40°$, 60° zenith angle, with present results as extrapolated to $\lambda = 40°$.

In Fig. 8 we present a graphical comparison between the present results and Schremp's. The large differences are manifest.

If we now use the present values for R_c to « predict » 60° zenith angle results, we find that the Winckler-Anderson measurements are consistent with any spectrum which lies between R_c^{-1} and $R_c^{-1.5}$. Thus we may conclude that any currently reasonable spectrum will be quite inconsistent with the Schremp shadow cone curves.

In Table XVI, we exhibit the comparison between the Winckler-Anderson measurements and geomagnetic theory based on the present calculations and on Schremp's. All intensities in the table are compared with the 60° W intensity which is normalized to one. The $\lambda = 40°$ predictions based on the present calculations were determined from an extrapolation based on considerations of the slope of the vertical R_c *vs.* λ curve and the variation of the 60° zenith angle Størmer cut-off as a function of latitude. The Winckler-Anderson entries are

is no indication in the Lemaitre-Vallarta text whether or not the other points on the « earth's shadow » sections are less than or equal to the actual cut-offs. If they are meant to be the actual cut-offs, then the « earth's shadow » sections (for all latitudes in Fig. 6) also disagree with Schremp's results.

mean values determined from their flights E and L. It appears from the table that the Winckler-Anderson azimuthal measurements are indeed consistent with geomagnetic theory as developed herein.

TABLE XVI. – *Comparison of observed and predicted values of azimuthal effects at* 60° *zenith angle at* $\lambda = 40°$.

Direction	Normalized total intensity				
	Present cut-offs		Schremp's cut-offs		Winckler-Anderson
	$\alpha = 1$	$\alpha = 1.5$	$\alpha = 1$	$\alpha = 1.5$	
60° N	0.88	0.83	0.45	0.30	$0.80 \pm .10$
60° E	0.70	0.59	0.27	0.14	$0.67 \pm .07$
60° S	0.83	0.75	0.83	0.75	$0.83 \pm .10$
60° W	1.00	1.00	1.00	1.00	$1.00 \pm .10$

A recent experiment performed by DANIELSON and FREIER at $\lambda = 42°$ also disagrees with Schremp's curves and appears to be consistent with the present work ([21]).

5. – Note on the north-south asymmetry at $\lambda = 41°$ N.

Let J_S refer to the total directional intensity for a given southerly zenith angle in the north-south plane. Let J_N refer to the total directional intensity for the same northerly zenith angle in the north-south plane. If one then measures the north-south asymmetry by the ratio, $2(J_S - J_N)/(J_S + J_N)$, the present calculations indicate that the asymmetry is of the order zero for zenith angles up to 30°. For zenith angles between 30° and 45°, the asymmetry increases until a maximum is reached around 45°. For zenith angles between 45° and 50°, the asymmetry decreases toward zero; it becomes negative somewhere between 50° and 60° zenith angle, whereupon it proceeds to decrease. The asymmetry will not continue to decrease all the way to 90° zenith however. Eventually, the simple shadow cut-off will set in at about 70° N and make the asymmetry positive once more.

([21]) R. E. DANIELSON and P. S. FREIER: *Phys. Rev.*, **109**, 151 (1958).

6. – Remarks.

In the present work we have assumed that as far as cosmic rays are concerned, the magnetic field of the earth may be adequately represented by a magnetic dipole field. We have made the further assumption that this dipole field is the predominant factor in determining the set of allowed and forbidden rigidities which would be observed in any given direction at any given point on the earth.

The first assumption is equivalent to assuming that the higher order multipole terms in the expansion for the earth's magnetic field contribute only small effects on cosmic ray orbits in comparison with the dipole term. Implicit in the second assumption is the assumption that magnetic fields produced by extra-terrestrial currents have negligible effects on cosmic ray orbits. However, recent experiments ([22]) measuring geomagnetic cut-off energies and the cosmic ray equator indicate that at least one if not both of the above assumptions are invalid. How the superposition of other fields with that of a dipole field will affect the results obtained in the present paper is a matter for future investigation.

* * *

It is a pleasure to express deep appreciation to Professor J. A. Van Allen for suggesting and encouraging this research, for his continued interest, support, and constructive discussions; to Professor E. C. Ray for strongly urging the author to undertake this research, for his interest, encouragement and discussion, and for acting as an invaluable guide to the original literature; to Mr. J. Kasper for a discussion of differential analysers; to Mr. R. F. Missert for some general discussions; to Dr. D. A. Flanders and his computing staff at Argonne National Laboratory for their splendid cooperation; and to the joint program of the Atomic Energy Commission and the Office of Naval Research.

Note added in proof.

It is immediately evident that Schremp's shadow cone curves ([5]) at the equator are in error since they are not all symmetrical with respect to the east-west plane (which coincides with the equatorial plane). Investigation strongly indicates the lack of a

([22]) J. A. Simpson, K. B. Fenton, J. Katzman and D. C. Rose: *Phys. Rev.*, **102**, 1648 (1956); P. H. Fowler and C. J. Waddington: *Phil. Mag.*, **1**, 637 (1956); C. J. Waddington: *Nuovo Cimento*, **3**, 930 (1956); P. H. Fowler, C. J. Waddington, P. S. Freier, J. Naugle and E. P. Ney: *Phil. Mag.*, **2**, 157 (1957); F. B. McDonald: *Phys. Rev.*, **107**, 1386 (1957); P. Rothwell and J. Quenby: preprint.

simple shadow cone in the neighborhood of the equator, but if it exists at the equator, it must have mirror symmetry with respect to the equatorial plane because of the mirror symmetry of the dipole field. Furthermore, since the present article was first written, Dr. J. KASPER (preprint) has completed shadow cone calculations which confirm that Schremp's curves are in error.

Since this paper was first submitted, a portion of the future investigation alluded to in the remarks of Section 6 has been completed. Dr. P. J. KELLOGG and the author have shown by orbit computation in the earth's dipole+quadrupole+octupole field that one can account for the cosmic ray equator experiments ([22]) without invoking the existence of extra-terrestrial currents. The quadrupole effect is generally small compared with the octupole effect, however, in some areas of the world it is comparable. Moreover, there are indications that in some areas of the world moments higher than the octupole moments are contributing to cosmic ray cut-offs.

SUPPLEMENTO AL VOLUME XI, SERIE X
DEL NUOVO CIMENTO

N. 1, 1959
1° Trimestre

Propagation of Radio Waves along an Inhomogeneous Surface.

E. L. FEINBERG

P. N. Lebedev Physical Institute
of the USSR Academy of Sciences - Moscow

(ricevuto il 23 Aprile 1958)

CONTENTS. — **1.** Introduction. – **2.** Basic ideas. – **3.** Fundamental integral equation. – **4.** Flat earth path composed of homogeneous segments. 1. The second segment. 2. The third segment. – **5.** Conclusion for flat earth. Generalization. – **6.** Spherical inhomogeneous earth surface. – **7.** Conclusion.

1. – Introduction.

The problem of radio-waves propagation along an electrically inhomogeneous surface (the ionospherical influences being neglected) is essential for a number of cases in radio communication, radio navigation, radio geodesy, etc., in particular in seashore countries. Here, for instance, the electrical conductivities of sea and land differ by a factor $10^2 \div 10^4$. Corresponding effects are not small, and qualitatively new phenomena appear, such as, for example, the theoretically predicted and experimentally proved *increase* of field amplitude for *increasing* distance between transmitter and receiver. However, due to the peculiar history of the general theory of radio-waves propagation, these problems were investigated and related phenomena discovered only after 1940.

The need of a theory of earth wave propagation arose about half a century ago. The problem was very akin to that of the optical diffraction. As a matter of fact, the only difference was that the source or (and) the observation point fell in the vicinity of a surface, dividing two media. However, the theory developed here along lines which were different in principle from those followed in optics.

In optics at first a very efficient approximate method has been adopted —that of Fresnel-Kirchhoff,—based on almost intuitive qualitative conceptions concerning the process of light propagation. It enabled one to investigate rather simply a variety of diffraction phenomena. Thus, diffraction essentially ceased to be a serious problem. It was only a few decades later that there appeared a single rigorous treatment of an electrodynamical problem formulated in a highly abstract form—the famous Sommerfeld solution for diffraction on an edge. This solution supported the validity of the approximate Fresnel-Kirchhoff method for the majority of important optical diffraction problems—for diffraction at small angles.

Contrary to that, in the problem of radio-wave propagation, there existed no elementary qualitative ideas concerning the process of propagation, which would enable to estimate, to grasp the situation in various conditions of propagation. An attempt was made at the very beginning to use an idea from optics and to represent the process as a gliding of a plane wave along the interface of two media (air and land). However, this led merely to mistakes, and the theory proceeded along quite a different way—that of constructing rigorous solutions for separate idealized problems: for an ideal perfectly homogeneous flat and spherical earth. Every new problem generated new serious difficulties. There were no qualitative, conceivable pictures and criteria, and mathematical mistakes in theoretical works could not be detected for quite a number of years. In practical situations it was hardly possible to decide whether particular deviations from the idealized theoretical scheme were essential or not.

It is very natural that the *inhomogeneous* earth problem was unsolved for many years even for the simplest highly idealized case, that of a flat earth divided by a straight line—by a « coast »—into two homogeneous parts: « land » and an infinitely conducting « sea ». In this « coastal refraction » problem no shore relief was taken into account. An attempt at a simplified treatment of this problem [18] led to a result which later was shown [19] to be wrong, even in sign.

By 1940 it was becoming more and more clear that the whole method of treating these problems needed a fresh approach. A simpler theoretical scheme, which could work in various conditions, was needed. Such a scheme, we believe, was given in 1940-44 in a series of works by Soviet investigators [1-10]. It enabled one to get very simply once more all previous results of the theory of propagation of an earth radio wave (homogeneous flat and spherical earth [2, 3, 1*b*]), and in the problem of coastal refraction, mentioned above, to come to some results although quite special, but important in principle [4, 1*c*]. Moreover, it resulted in a rather simple and general theory of propagation of radio waves along inhomogeneous surfaces [5-9, 1*d*] predicting new phenomena and lead to a general picture of the process of propagation, which has already been applied in practical radiophysics in the Soviet Union. It is

essential that all these results were obtained exactly in the same approximation, with the same accuracy as the results of the so-called « strict theories » developed previously for a homogeneous earth. The simplification is not paid for by the loss of accuracy.

These works were published almost exclusively in the USSR and only recently they begin to receive some development in other countries [20-22]. In 1957 an account of a particular result was published in this magazine [11]. Unfortunately, however, in ref. [11] the situation was represented as if the whole method would lead only to a new deduction of the well-known Sommerfeld-Weyl-Van der Pohl formula for a homogeneous flat earth. Actually, this was merely a kind of a test on a well-studied problem of a new method, giving various new results. The present paper reviews systematically the basic ideas and main results of the method.

2. – Basic ideas.

Classical works by Sommerfeld, Weyl, Van-der-Pohl, etc., for a homogeneous earth surface (as well as recent works by Clemmow [12] and Furutsu [13] on an inhomogeneous surface) proceed, in general, as follows. A problem is formulated and investigated rigorously, but at some stage—usually somewhere close to the end of the investigation—two circumstances are taken into account, without which no results of practical value could be obtained. These are: 1) the transmitter-receiver distance is large in comparison with the wave length; 2) the refractive index of the soil is large compared to unity (we leave aside the plane wave reflection formulas for which this section is inessential). Nobody paid special attention to the necessity of accounting for these peculiarities since they really take place in all practical cases of ground wave propagation.

The method described here is based first of all on taking into account these points from the very beginning.

First, instead of looking for the electric force E it is reasonable to write from the very beginning, for instance

$$E(\boldsymbol{r}) = A \frac{\exp[ikr]}{r} w(\boldsymbol{r}) , \tag{2.1}$$

$\boldsymbol{r}$ being the distance from the transmitter, $k = 2\pi/\lambda$, λ the wave length in vacuum, A a constant factor, while w is the attenuation function normalized by the condition $w(0) = 1$. It is exactly this attenuation factor $w(\boldsymbol{r})$ that should be found. Usually the field equations were written for $\boldsymbol{E}$, or for the Hertz vector $\boldsymbol{\Pi}$, and only after having found the solution w could be separated from it.

w always changes but little over a wavelength λ:

$$\left|\frac{\lambda}{w}\frac{\partial w}{\partial x}\right| \ll 1, \qquad \left|\frac{\lambda}{w}\frac{\partial w}{\partial y}\right| \ll 1, \tag{2.2}$$

(where x and y are co-ordinates in the surface plane). Therefore it seems convenient to separate rapid oscillations and to go over from the equations for E to the equation for w from the very beginning.

Second, following a proposal by M. A. Leontovič (for the first time applied in ref. [10], in full form published in ref. [1a]), it seems reasonable to take into account from the very beginning that

$$\varepsilon' = \varepsilon + \frac{4\pi i\sigma}{\omega} \gg 1, \tag{2.3}$$

(ε real dielectric permeability, σ conductivity of the soil, ω circular frequency; we put throughout the following time dependence in the form $\exp[-i\omega t]$). In this case it may be easily shown that the field underground decreases along the vertical z as $\exp[-ik\sqrt{\varepsilon'}z]$ and the approximate boundary condition for the vertical component E_z of E in the air on the earth surface $z=0$ may be written as (for the sake of simplicity, let the transmitter be here situated at $z=0$):

$$\frac{\partial E_z}{\partial z} = -\frac{ik}{\sqrt{\varepsilon'}}E_z. \qquad \text{for } z=0. \tag{2.4}$$

Later it was shown by the author [8, § 39] that instead of ε' we should write $\varepsilon'_{\text{eff}} = \varepsilon' + 1$,

$$\frac{\partial E_z}{\partial z} = -\frac{ik}{\sqrt{\varepsilon'+1}}E_z, \qquad \text{for } z=0, \tag{2.5}$$

in which case the inaccuracy is of the order of $|\varepsilon'|^{-2}$ and the eq. (2.5) may be used practically always, even for ultrashort waves (we leave aside all details, including proof of eqs. (2.4) and (2.5) and generalization for the case of transmitter above the earth, etc., since they are given in § 2 and 3 of ref. [11], which are essentially a somewhat abbreviated translation of § 19 from ref. [8]).

For inhomogeneous earth, when $\varepsilon' = \varepsilon'(x, y)$, the boundary condition is in general more complicated (see ref. [8, § 40]),

$$\frac{\partial E_z}{\partial z} = -\frac{ik}{\sqrt{\varepsilon'+1}}E_z - \frac{1}{2\varepsilon'}\left(E_x\frac{\partial \varepsilon'}{\partial x} + E_y\frac{\partial \varepsilon'}{\partial y}\right) \to$$
$$\to -ik\left\{\frac{1}{\sqrt{\varepsilon'+1}} + \frac{1}{k^2}(\boldsymbol{k}\ \mathrm{grad}\ln\sqrt{\varepsilon'})\right\}E_z, \tag{2.6}$$

(here we assume that propagation is along the x axis). It holds if $|\varepsilon'^{-1}\,\mathrm{grad}\,\varepsilon'| \ll k|\sqrt{\varepsilon'}|$, *i.e.*, if the soil properties vary in the x, y plane but slowly with respect to the « wave length within the soil » $\lambda/|\sqrt{\varepsilon'}| \ll \lambda$. If they vary only little even with respect to the wave length in air, λ, then we come back to eq. (2.5), which thus holds even for inhomogeneous surface, if

$$|\varepsilon'^{-1}\,\mathrm{grad}\,\varepsilon'| \ll k\,. \tag{2.7}$$

Due to eq. (2.5) we may solve the propagation problem restricting ourselves to the upper half space (after finding the field in the air, in particular at $z = 0$, we obtain the field underground $E_{1z}(x, y, z)$ by multiplying $E_z(x, y, 0)$ by $\varepsilon'^{-1}\exp[-ik\sqrt{\varepsilon'}z]$ (here ε'^{-1} comes from the boundary condition $E_z(x, y, 0) = -\varepsilon' E_{1z}(x, y, 0)$, while the exponential factor shows that the field in a given point underground is attached to the field in the respective point above it in the air and is « dragged » away by it). This simplifies the investigation considerably.

All these relations are approximately local. Therefore they hold even if the surface of the earth is not flat, *e.g.* if it is spherical. But the radii of curvature should be large compared to λ.

For w holds the same condition:

$$\frac{\partial w}{\partial z} = -\frac{ik}{\sqrt{\varepsilon' - 1}}\,w\,. \qquad \text{at } z = 0\,. \tag{2.5a}$$

Application of this boundary condition turned out to be quite successful. In Soviet radiophysics it was given the name of Leontovič.

The problem of determining w satisfying eq. (2.5*a*) may be reduced either to a differential or to an integral equation. It turns out that the first one is useful only for the already studied case of homogeneous earth [2, 3, 1*b*]. For inhomogeneous earth it is better to use the integral equation [4-6, 9, 1*c*, 1*d*], which implies the Huygens principle, when the secondary sources are distributed over the earth's surface. However, it can be solved directly only in the most simple case of « coastal refraction » [4] and even here it calls for the development of a special method [1*c*, 14].

A sufficiently general theory for inhomogeneous earth could be achieved only after introducing, besides the two above ideas (equation for w instead of E and approximate boundary condition), two others.

3) When using the integral equation in Huygens principle, we must integrate over the surface. Not the whole of this surface is equally essential. The main contribution comes from the first narrow elliptical Fresnel zone, transmitter and receiver being its foci. Therefore, we may introduce the conception of a *path of radiowaves* [5, 6*b*] (*caeteris paribus*, this is the first elliptic zone) and

the integral over surface may be transformed into an integral along a line—along the axis of the path. The problem is thus reduced to the problem of an integral equation with a single independent variable.

4) When constructing the integral equation from the differential field equations with the aid of Green's theorem, usually, as a Green function, the field of a point source in vacuum, $v_0 = r^{-1} \exp[ikr]$ is made use of. However, we may use instead of v_0 the field of the same source *in presence of a homogeneous surface* with some electrical parameter $\varepsilon' = \varepsilon'_0 = \text{const}$, *i.e.*, we may use a Green function $v = r^{-1} \exp[ikr] w_0$, w_0 being an attenuation function in presence of this fictitious, auxiliary surface. Assuming properly the value of this arbitrary parameter ε'_0 we can eliminate from the integrated expression the unknown function w. Thus we are left simply with quadratures of known functions instead of an integral equation. This is always possible if the path is composed of homogeneous segments [5, 6 1*d*].

On the basis of these ideas, a number of results was obtained which enabled one to give answers on various practical problems. Moreover, these results helped to form some general qualitative picture of the process of wave propagation, permitting sometimes to estimate the situation without detailed calculations. During the last two decades various authors proposed a number of empirical formulas to calculate the field over a mixed path. Comparing them with the results of the theory, we can estimate the accuracy of these formulas, to accept some of them and to reject others.

A rather detailed review of the theory and results for flat inhomogeneous earth is given in ref. [8]. In English many results were published in ref. [6] and reported in [15]; for the inhomogeneous spherical earth see ref. [9] and [16]. Below, as a rule, references are given to the first publication of a given result.

3. – Fundamental integral equation.

Consider at first a flat earth (plane $z = 0$). The source—a vertical dipole of properly chosen power—for simplicity's sake is supposed to be at $O(0, 0, 0)$. It produces an electric field with the vertical component E:

$$E = \frac{\exp[ikr]}{r} w(\boldsymbol{r}), \qquad r = \sqrt{x^2 + y^2 + z^2}. \tag{3.1}$$

Here $w(\boldsymbol{r})$ the attenuation function we are looking for, $w(0) = 1$. Let us introduce the field $v(\boldsymbol{r})$, which would be generated by the same source if the earth were electrically homogeneous with $\varepsilon' = \varepsilon'_0 = \text{const}$, ε'_0 being an arbitrary parameter:

$$v = \frac{\exp[ikr]}{r} w_0(\boldsymbol{r}). \tag{3.2}$$

Here $w_0(\boldsymbol{r})$ is the attenuation function for homogeneous earth with $\varepsilon' = \varepsilon_0'$. From the wave equations, satisfied in the air by both E and v:

$$(\nabla^2 + k^2)E = 0\,, \tag{3.3}$$

$$(\nabla^2 + k^2)v = 0\,, \tag{3.4}$$

we easily obtain for $z = 0$

$$E = v + \frac{1}{2\pi}\int\left(\frac{\partial E}{\partial n}v - \frac{\partial v}{\partial n}E\right)\mathrm{d}S\,, \tag{3.5}$$

where the integration is over the earth's surface, $\mathrm{d}S = \mathrm{d}x\,\mathrm{d}y$ and n is the outward normal. (For instance, let us form $v_+ = \frac{1}{2}(v(\boldsymbol{\rho}) + v(\boldsymbol{\rho}_1))$, $\boldsymbol{\rho}$ and $\boldsymbol{\rho}_1$ being vector radii from the variable point to the observation point $A(x, 0, z)$ and to its mirror image $(x, 0, -z)$ in $z = 0$ plane; multiplying eq. (3.3) by v_+, eq. (3.4), rewritten for v_+ by E and using Green's theorem we come to eq. (3.5)). Now we use eq. (2.5) for E and (2.5a) for v and get

$$w(\boldsymbol{r}) = w_0(\boldsymbol{r}) + \frac{ik}{2\pi}\int\left(\frac{1}{\sqrt{\varepsilon'+1}} - \frac{1}{\sqrt{\varepsilon_0'+1}}\right)\exp\left[ik(\varrho - r')\right]\frac{r'}{\varrho}\,w(\boldsymbol{r}')w_0(\boldsymbol{\rho})\,\mathrm{d}S\,. \tag{3.6}$$

Here $\boldsymbol{r}'$ is a radius vector from the source to the variable point x', y' $(r' = \sqrt{x'^2 + y'^2})$, $\boldsymbol{\rho}$ from (x', y') to the observation point $A(x, 0, z)$, $\varrho = \sqrt{(x - x')^2 + y'^2 + z^2}$. ε' may depend on x', y' (provided condition (2.7) is satisfied; otherwise the equation will be somewhat complicated, since eq. (2.6) should be used instead of (2.5). This complicated equation was applied, for example, to the treatment of the transition zone between sea and land [6c]).

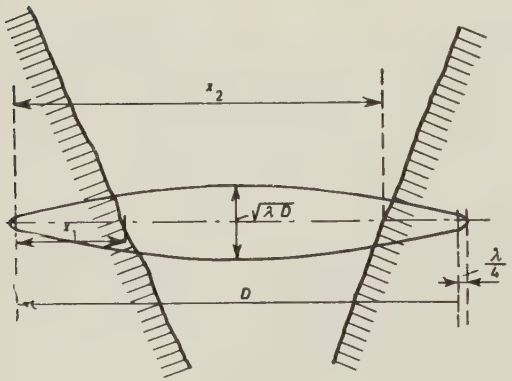

Fig. 1. – Schematical representation of the path of propagation. The transversal dimension is considerably exaggerated as compared to actual proportions.

Eq. (3.6) may be essentially simplified if we take into account that $\exp[ik(r' - \varrho)]$ is a comparatively rapidly oscillating function. For simplicity's sake we here put $z = 0$, *i.e.*, the observation point is also in the $z = 0$ plane. The most essential contribution, *caeteris paribus*, is given by the first Fresnel zone determined by (see Fig. 1)

$$k(r + \varrho - D) = \nu\pi\,, \qquad \nu = 0, 1, 2, \ldots. \tag{3.7}$$

where D is the distance between O and A. This zone is a narrow ellipse, having the width $\sim\sqrt{D/k}\ll D$. It protrudes behind O and A only little for a distance of the order of $\pi/2k\sim\lambda/4$. This is true, in fact, if, for instance, the boundary between different soils is not parallel and very near to the line OA, and if we are not specially interested in reflection from some obstacles outside the ellipsis, etc. (as a matter of fact, here we simply apply the method of stationary phase, see [6*b*, 1*d*]). It becomes clear that a change of the soil properties occurring behind the terminals of OA has but little influence (when it is necessary, it is taken into account, see below eq. (4.1*a*)). Therefore integration over co-ordinate y transversal to the path axis in eq. (3.6) can be performed by simply putting

$$r'\approx x'+\frac{y'^2}{2x'}\,,\qquad \varrho\approx x-x'+\frac{y'^2}{2(x-x')}\,,\qquad w(r')\approx w(x')\,, \tag{3.8}$$

while the integration along x' is to be performed from O up to D. Finally we come to the equation which is fundamental for treating various problems of interest.

$$w(D)=w_0(D)-i\sqrt{\frac{D}{\pi}}\int_0^D(\sqrt{s(x')}-\sqrt{s_0})\frac{\mathrm{d}x'}{\sqrt{x'(D-x')}}\,w(x')w_0(D-x')\,\mathrm{d}x'\,, \tag{3.9}$$

$$s=\frac{ik}{2(\varepsilon'+1)}\,,\qquad s_0=\frac{ik}{2(\varepsilon'_0+1)}\,.$$

The constant parameter s_0 (and, consequently, the attenuation function for homogeneneous path $w_0(x)$, corresponding to a given ε'_0) is to be chosen arbitrarily, according to the way of using the equation.

a) This equation, in the *case of homogeneous path*, may be used for a very simple deduction of the Sommerfeld–Weyl–Van-der-Pohl attenuation function for $z=0$:

$$w(r)\to y(sr)=1+2\sqrt{sr}\int_{\sqrt{sr}}^{i\infty}\exp\left[v^2-sr\right]\mathrm{d}v\,. \tag{3.10}$$

In fact, putting $s_0=0$, and therefore $w_0(x)=1$, we can either get a series for y by iteration, or by a standard procedure solve this Volterra equation [1*d*, appendix], or—and this is the most simple way of deducing the eq. (3.10)—we can rewrite eq. (3.9) for $s_0=0$, $s(x')=\mathrm{const}$ by substituting instead of the unknown function w another one:

$$W=\frac{w(D)-1}{\sqrt{sD}}\,. \tag{3.11}$$

After differentiation with respect to D we come to an elementary differential equation [8, § 27]

$$W'(x) + sW(x) + \sqrt{\frac{s}{x}} = 0, \tag{3.12}$$

which immediately leads to eq. (3.10).

No doubt, this treatment of the homogeneous earth is necessary only because it proves that the approximations done for obtaining eq. (3.9) remain within the frames of approximations which are usual for the Sommerfeld theory. The accuracy of our method is the same as in the classical theory of radiowaves propagation.

Other methods of deducing Sommerfeld's function (3.10) starting from the same principles, are to be found in ref. [2, 3, 1*b*], where the problem is reduced to a parabolic type equation for w, and in ref. [8, § 32], where a very simple deduction of some lemma, given by MALJUŽINETZ, is used (this last deduction may be found in § 4 of ref. [11]). All of them, of course, lead to identical results:

b) Now let us consider an *inhomogeneous earth* and, more specifically, the path, consisting of N homogeneous segments, having respectively $\varepsilon' = \varepsilon'_j$, $j = 1, 2, ..., N$. Let the terminals of the j-th segment be at x_j and x_{j+1}, $x_0 \equiv 0$, $x_{N+1} \equiv D$. We suppose that the change of ε' from j up to $j+1$ takes place within an interval which is small as compared to the segment's length (but large as compared to the wave length, see above remarks after eq. (2.6)). The w function has some peculiar form (Fig. 2). We describe by the function w_j its behaviour within the j-th segment. Eq. (3.9) assumes the form:

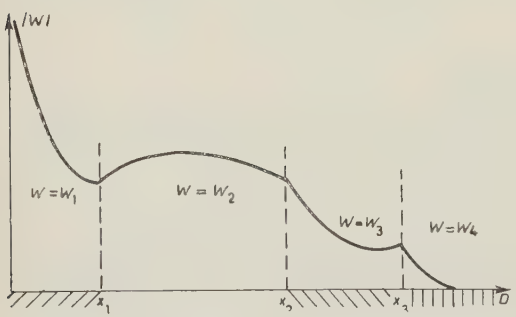

Fig. 2. – Behaviour of the attenuation function in case of an inhomogeneous path.

$$w(D) = w_0(D) - i\sqrt{\frac{D}{x}} \sum_{j=1}^{N} (\sqrt{s_j} - \sqrt{s_0}) \int_{x_j}^{x_{j+1}} \frac{w_j(x) w_0(D-x)}{\sqrt{x(D-x)}}\, dx\,. \tag{3.13}$$

c) Before solving this equation we would like to remark that it holds for a *spherical* earth surface as well [21, 9, 16], if by $w_0(x)$ we mean, instead of the attenuation function for the flat homogeneous earth $y(s_0 x)$, (3.10),

the attenuation function for the homogeneous spherical earth (see, for instance, [17] or [8]):

$$(3.14)\qquad w_0(D) = V(D; q_0) = \sqrt{i\pi\xi}\sum_{s=1}^{\infty}\frac{\exp[ixt_s]}{t_s - q^2} = \frac{1}{2}\sqrt{\frac{\xi}{i\pi}}\int_c \frac{\exp[i\xi t]\omega(t)}{\omega'(t) - q_0\omega(t)}\,dt\,,$$

$$\xi = \vartheta A\,, \qquad A = \sqrt[3]{\frac{1}{2}ka}\,, \qquad q_0 = \frac{iA}{\sqrt{\varepsilon_0' + 1}}\,, \qquad D = a\vartheta\,.$$

Here a is the earth's radius, ϑ the angular distance from source to transmitter, t_s the roots of equation $\omega'(t) = q_0\omega(t)$, $\omega(t)$ being an Airy function, and the constant factor is chosen in such a way that $V(0; q_0) = 1$. When differentiating at the earth's surface $z = 0$ along the normal to the sphere, z, the approximate boundary condition (2.5) holds, it may be rewritten as:

$$(3.15)\qquad \frac{\partial E_z}{\partial z} = -k\frac{q}{A}E_z\,, \qquad \frac{\partial V}{\partial z} = -k\frac{q_0}{A}V\,, \qquad q = \frac{iA}{\sqrt{\varepsilon' + 1}}\,;$$

x and D in (3.13) are to be taken along the large circle on the earth's surface.

For a spherical surface this equation is deduced exactly in the same way as for the flat one. Co-ordinate y in this case is taken along large circles, perpendicular to the large circle connecting O and A. An essential restriction is imposed by the condition that it should be $\vartheta_A = D/a \ll \pi/2$. Otherwise Fresnel zones cut-off on the sphere quite distinct essential regions and moreover various other distinctions take place. However, well before $\vartheta_A \sim \pi/2$ our problem becomes meaningless due to interference of the ionosphere.

4. – Flat earth path composed of homogeneous segments.

Eq. (3.13) immediately leads to a recurrent method.

At first, let us determine the attenuation function for the first segment, $j = 1$, $0 < D < x_1$, $w = w_1$. As far as we neglect the influence of other segments besides $j = 1$, this function is known. It is the attenuation function for a homogeneous flat earth (3.10) with $\varepsilon' = \varepsilon_1'$:

$$(4.1)\qquad w_1 = y(s_1 x)\,, \qquad s_1 = \frac{ik}{2(\varepsilon_1' + 1)}\,.$$

In the vicinity of the boundary of the second segment a small correction may arise, which is essential in the coastal refraction problem. It has the form of a wave reflected from the boundary of the second segment. For

instance, if the first segment is « sea » $s_1 = 0$, $y(s_1 x) = 1$, then instead of eq. (4.1) we have (ref. [6c], eq. (12.4)):

$$w = 1 + \sqrt{\frac{i}{2\pi(\varepsilon' + 1)}} \frac{D}{\sqrt{kD' x_A x_0}} \frac{\cos 2\theta}{2\cos^2\theta} \exp\left[ik(D' - D)\right]. \tag{4.1a}$$

Here θ is an « angle of reflection » from the coast line. For other designations see Fig. 3. A partial experimental check of this formula, particularly of the presence of the factor $\cos 2\theta$, giving zero for $\theta = \pi/4$, is supplied by experiment (23), analysed in ref. [1d, 6c].

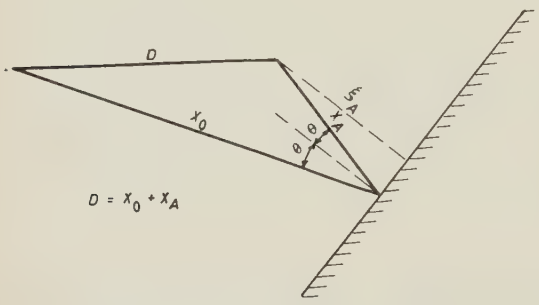

Fig. 3. – Reflection from a coast line.

Let us go now to the second segment, $j=2$, $x_1 < D < x_2$. Integration in eq. (3.13) is over $0 < x < x_1$, where instead of w we may substitute the function (4.1) just found, and over $x_1 < x < D$, where $w = w_2$ is unknown. However, we can dispose of the arbitrariness of the auxiliary parameter ε_0'. Let us put $\varepsilon_0' = \varepsilon_2'$, $s_0 = s_2$. In this case the integral over the segment $j = 2$ drops away and under $w_0(x)$ the homogeneous earth attenuation function (3.10) for $s_0 = s_2$ should be understood:

$$w_2(D) = y(s_2 D) + i\sqrt{\frac{D}{\pi}} (\sqrt{s_1} - \sqrt{s_2}) \int_0^{x_1} \frac{y(s_1 x) y(s_2(D-x))}{\sqrt{x(D-x)}} \, dx . \tag{4.2}$$

Thus $w_2(D)$ for $j = 2$ is given by integration of known functions. In particular, the coastal refraction problem $\left(s_2 = 0,\ y(s_2(D-x)) = 1\right)$ is solved explicitly.

For the segment $j = 3$ we find $w = w_3$ by choosing $s_0 = s_3$. Then equation (3.13) gives

$$w_3(D) = y(s_3 D) + i\sqrt{\frac{D}{\pi}} (\sqrt{s_1} - \sqrt{s_3}) \int_0^{x_1} \frac{y(s_1 x) y(s_3(D-x))}{\sqrt{x(D-x)}} \, dx + \tag{4.3}$$

$$+ i\sqrt{\frac{D}{\pi}} (\sqrt{s_2} - \sqrt{s_3}) \int_{x_1}^{x_2} \frac{w_2(x) y(s_3(D-x))}{\sqrt{x(D-x)}} \, dx .$$

Here $w_2(x)$ should be introduced from eq. (4.2). In such a way we can proceed further. In the general case we put $s_0 = s_N$ and obtain w_N in the form of quadratures containing w_j for $j \leqslant N-1$. The practical usefulness of the method depends on our ability to calculate quadratures. It turns out that in many cases they may be expressed analytically, either if some numerical distances are large (or, *vice versa*, small), or if some relative distances are large. Otherwise, numerical calculations are necessary. In calculations we often use an easily proved formula for the y-function (3.10):

$$\int_0^x \frac{y(sx')\,\mathrm{d}x'}{\sqrt{x'}} = i\sqrt{\frac{\pi}{s}}\left\{1 - \frac{i}{\sqrt{\pi s x}}\,(1 - y(sx))\right\}. \tag{4.4}$$

Moreover, asymptotical formulas are used

$$\text{for} \quad |\varrho| \ll 1, \qquad y(\varrho) \approx 1 - i\sqrt{\pi\varrho} - 2\varrho\,, \tag{4.5}$$

$$\text{for} \quad |\varrho| \gg 1, \qquad y(\varrho) \approx -\frac{1}{2\varrho}\,. \tag{4.6}$$

Elementary calculations give then the results quoted below. We shall use the term «sea» (in quotation marks) to designate a segment with $\varepsilon' = \infty$ (actually for real sea sometimes, *e.g.* for Ultra Short Waves, finiteness of ε' is taken into account). The term «land» (in quotation marks) designates the case of finite ε'.

4·1. *The second segment.* – Here, as everywhere below (besides eq. (4.1*a*)), we suppose that both the receiver's and the transmitter's distances to the boundaries between segments are large compared to a wave length.

a) If one of the segments is considerably shorter than the other, for instance, $x_1 \ll D$, then in eq. (4.2) $\sqrt{D - x} \approx D$ and application of eq. (4.4) gives immediately [7, 8]

$$w_2(D) = y(s_2 D)\left\{\sqrt{\frac{s_2}{s_1}} + \frac{\sqrt{s_1} - \sqrt{s_2}}{\sqrt{s_1}}\,\frac{i}{\sqrt{\pi s_1 x}}\,(1 - y(s_1 x_1))\right\}. \tag{4.7}$$

Let us consider special cases:

aa) If the longer segment is «sea», *i.e.*, if $\varepsilon_2' = \infty$, $s_2 = 0$; then

$$w_2(D) = \frac{i}{\sqrt{\pi}}\,\frac{1 - y(s_1 x_1)}{\sqrt{s_1 x_1}}\,\exp\left[-s_1 x_1\right]\left\{1 + \frac{2i}{\sqrt{\pi}}\int_0^{\sqrt{s_1 x_1}} \exp\left[r^2\right]\mathrm{d}r\right\} \qquad z(s_1 x_1). \tag{4.8}$$

This formula, which was obtained long ago [5, 6*c*], describes a most interesting case of coastal refraction. The function designated here as z plays an essential part in the theory. It is simply connected with Sommerfeld's formula and asymptotically equal to

$$w_2(D) = z(s_1x_1) \approx 1 + \frac{2i}{\sqrt{\pi}}\sqrt{s_1x_1}\,, \qquad |s_1x_1| \ll 1, \tag{4.9}$$

(the numerical distance passed over the «land» is small), and to

$$z(s_1x_1) \approx \frac{i}{\sqrt{\pi s_1x_1}}\,. \qquad \text{for } |s_1x_1| \gg 1. \tag{4.10}$$

The eq. (4.10) had been previously obtained by G. A. Grünberg [4]. Eq. (4.8) was simultaneously found by another method by V. A. Fock [14] and subsequently by Clemmow [12] and Furutsu [13]. The graph of the function z is shown in Fig. 4. It is tabulated in ref. [1*d*].

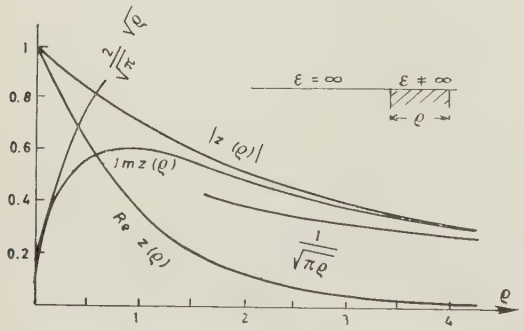

Fig. 4. Graphs of the attenuation function $z(\varrho)$. The curves give its modulus, real and imaginary parts and asymptotic formulas.

The important formula (4.10) shows that the influence of the coastal line on wave phase reduces itself to the constant phase shift when the distance increases. In such a way was obtained [4] the first proof of the fact that the influence of different segments of the path is not additive. The radio waves do not simply glide along the surface, accumulating distortions. This result was predicted qualitatively by L. I. Mandelstam on the basis of phase-velocity measurements performed by J. L. Alpert, V. V. Migulin and P. A. Ryasin. These experiments were interpreted exactly in this manner by T. L. Eckersly [24].

ab) If, on the contrary, the shorter segment is «sea» ($s_1 = 0$), then [5, 6*b*]

$$w_2 = y(s_2D)\left\{1 - \frac{2i}{\sqrt{\pi}}\sqrt{s_2x_1}\right\}, \tag{4.11}$$

$$w_2 \approx \frac{i}{\sqrt{\pi s_2D}}\sqrt{\frac{x_1}{D}}\,. \qquad \text{for } |s_2x_1| \gg 1. \tag{4.11a}$$

This equation, in particular, describes the recovery effect when a radiowave, after passing over a long land path, goes over to the sea surface. The field strength increases when the length of the highly conducting segment increases, this effect being more pronounced as the land is « worse » (*i.e.*, as s_2 is larger). This recovery in the vicinity of the boundary (when $x_1 \ll D$) is represented by a factor in brackets in eq. (4.11). When it exceeds unity considerably, then the approximate equation (4.11*a*) holds.

All these formulas do not contain the angle θ, which is formed by the path and the normal to the line, dividing two kinds of ground (to the coast). They are valid unless this angle is too close to $\pi/2$, *i.e.*, if the radiowave does not glide along the coast. More precisely, it must be

$$kx \cos^2 \theta \gg 1 , \tag{3.7}$$

where x is the smaller of the two distances from the shore, of the transmitter and of the receiver. The same inequality is supposed to hold in subsequent formulas as well. If the coast line is not straight but curved, then some of the formulas may be modified to some extent. However, if the coast-line within the essential zone (Fig. 1) deviates only little from a straight line, then there will be no modification.

ac) Let the numerical distance, at least for one (the shorter) segment be large, but s_1 and s_2 be arbitrary ($|s_1 x_1| \gg 1$).

aca) If $s_2 D$ is arbitrary, then

$$w_2 = y(s_2 D) \left\{ \sqrt{\frac{\bar{s}_2}{s_1}} + \frac{i}{\sqrt{\pi s_1 x_1}} \right\} . \tag{4.13}$$

acb) If, moreover, $|s_2 x_1| \gg 1$, then simply

$$w_2 = \sqrt{y(s_1 D) y(s_2 D)} = - \frac{1}{2\sqrt{s_1 s_2 D}} . \tag{4.14}$$

The last case shows that when all numerical distances are large, then the attenuation factor is a geometrical mean of those calculated for the corresponding homogeneous paths. This is obtained here for the case $x_1 \ll x_2$. However, due to symmetry, it holds also for $x_1 \gg x_2$. Therefore, it must also hold for any ratio of x_1 and x_2. This formula was also obtained, by T. L. Eckersley [24].

In Fig. 5 a w curve is shown for the case of a path composed of two segments with two s, both differing from zero: $s_1 = 2.0 \text{ km}^{-1}$ and $s_2 = 0.5 \text{ km}^{-1}$. In the

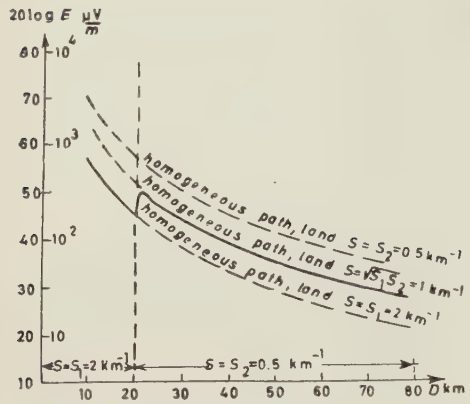

Fig. 5. – Attenuation function for a path, consisting of two segments with $s_1 = 2.0\,\mathrm{km}^{-1}$ and $s_2 = 0.5\,\mathrm{km}^{-1}$.

vicinity of the boundary we must use here the rather complicated formula (4.7). However, as the graph shows, it is already at a distance of the order of 2 km from the boundary, where the numerical distance travelled over the second soil is equal merely to $2s_2 = 1$, that the simple formula (4.14) becomes valid. Therefore, here and, as a rule, everywhere below, the requirements of the type $|s_j(x - x_{j-1})| \gg 1$ mean simply $\gtrsim 1$.

Above formulas were given for the case of one of the segments being comparatively short. Let us now go over to other cases:

b) Arbitrary ratio of lengths of the segment, but one of the segments is « sea », while for the other the numerical distance is large. Let, *e.g.* be $s_1 = 0$, $|s_2(D - x_1)| \gg 1$. Then putting in eq. (4.2) $y(s_1 x) = 1$, $y(s_2(D - x)) \approx -1/2s_2(D - x)$ we come to a very simple quadrature. The reciprocity theorem gives a corresponding case, $|s_1 x_1| \gg 1$, $s_2 = 0$ [5, 6*b*]:

$$w_2 = -\frac{1}{2s_1 D}\left\{1 - \frac{2i}{\sqrt{\pi}}\left| \frac{D}{x_1} s_1(D - x_1)\right\}\right. . \tag{4.15}$$

If, moreover, $|s_1(D - x_1)| \gg 1$, then we come to the eq. (4.11*a*) (with soils 1 and 2 interchanged).

As an example of application of these formulas we give Fig. 6 where it is shown how the modulus of the attenuation function $|w|$ changes if an initially homogeneous land path with numerical distance $R = sD$ (it is supposed to be real) is filled, step by step, by a « sea » ($s = 0$), starting from one terminal. The curves, for R ranging from $R = 20$ up to $R = 200$,

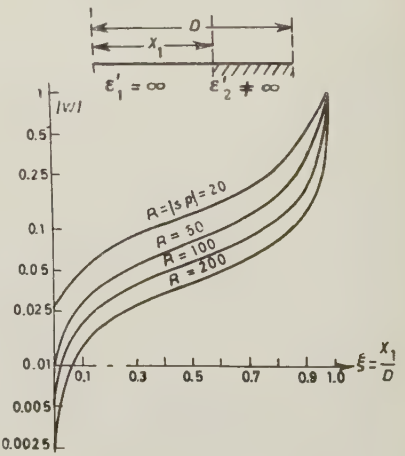

Fig. 6. – Dependence of the attenuation function on the degree of filling up of a path by an infinitely conducting ground (« sea ») for paths, having initially numerical distances ranging from 20 up to 200.

show that $|w|$ only suffers essential modification when the well conducting segment is addead near the first or the second terminal of the path. This circumstance alone demonstrates the important part played by the end portions of the path and unimportance of the ground properties in the middle of the path. It is exactly this conclusion, together with eqs. (4.23), (4.23*a*) and (4.23*b*), given below, that allowed to make the following statement [8*b*] (p. 5): « This formula, ..., suggests the possibilities of increasing the service area for a ground ray, which arise from a suitable disposition of transmitter and receiver. In certain conditions it would offer considerable advantages to move the transmitter a little further away, if the adjoining region of the effective path would as a result turn out highly conducting (for instance, to move it to the opposite shore of the gulf, etc.) ».

Up to the time of publication of Millington's measurements this prediction of the recovery effect could be experimentally supported only by qualitative indications (see [1*d*, p. 150]). Later the Millington measurements [25*b*, *c*] supported the existence of this effect in complete quantitative agreement with the formulas given above.

c) Coastal refraction. All the formulas quoted above give amplitudes as well as phases of the field strength. In particular, they secured a basis on which the theory of coastal refraction was obtained, *i.e.*, the angle α was found as a function of covered distance, α being declination of the wave normal from its initial direction after traversing the coastal line. Here we must take into account that on the shore the disturbance of propagation may arise not only from electrical inhomogeneity of the land, but from the shore relief as well. Correspondingly we must distinguish between the « land coastal error » α_L and the « relief coastal error » α_R. A theory for α_R was developed under the assumption that the slope is not steep [6*c*, 1*d*].

As has already been mentioned above (this will be seen also from the formulas given below), the coastal refraction occurs only within small distances from the coast line, where the difference from the « undisturbed » field is very small. Here a formula for the attenuation factor may be obtained, valid for arbitrary distances of the transmitter, x_0, and the receiver, x_1, from the coast line [5, 6*c*, 1*d*]. Namely,

$$w_2 = 1 + \frac{i}{2}\sqrt{\pi s D}\left[1 + \frac{2}{\pi}\arcsin\frac{x_A - x_0}{x_A + x_0}\right]. \tag{4.16}$$

In particular,

$$w_2 = 1 + \frac{i}{\sqrt{\pi}}\sqrt{sD}\arcsin\sqrt{\frac{4x_A x_0}{D^2}}, \qquad \text{if } x_A \leqslant x_0; \tag{4.16a}$$

$$w_2 = 1 + i\sqrt{\pi s D} - \frac{i}{\sqrt{\pi}}\sqrt{sD}\arcsin\sqrt{\frac{4x_A x_0}{D^2}}, \qquad \text{if } x_A \geqslant x_0, \tag{4.16b}$$

(in former designations, $x_0 = x_1$, $x_A = D - x_1$, $s = s_2$).

Herefrom, performing the corresponding differentiation [5, 6*c*, 1*d*] one may obtain explicit formulas for coastal refraction,

$$\alpha_L = -\frac{\operatorname{tg}\theta\sqrt{\cos\theta}}{\sqrt{2\pi\,|\,(\varepsilon'+1)\,|\,k\xi_A}}\sin\left(\frac{\pi}{4}+\frac{\chi}{2}\right)\sqrt{1-\frac{\xi_A}{D\cos\theta}}\,, \tag{4.17}$$

$$\alpha_L \approx -1.1\,\frac{\operatorname{tg}\theta\sqrt{\cos\theta}}{\sqrt{\sigma_0\,\xi_{A\,\mathrm{km}}}}\sqrt{1-\frac{\xi_A}{D\cos\theta}}\ \text{degrees}\,. \qquad \left(\chi\approx\frac{\pi}{2}\right). \tag{4.17a}$$

Here $\chi = \operatorname{arctg} 4\pi\sigma/(\varepsilon+1)\omega$, $\sigma_0 = 10^{-7}\sigma$ e.s.u., $\xi_{A\,\mathrm{km}}$ is the distance, expressed in kilometres, of the receiver, assumed to be situated on the land, from the coast line (taken along the perpendicular to the coast).

For certain cases this dependence is demonstrated in the Fig. 7. Negative sign shows that when passing over from sea to land the wave normal

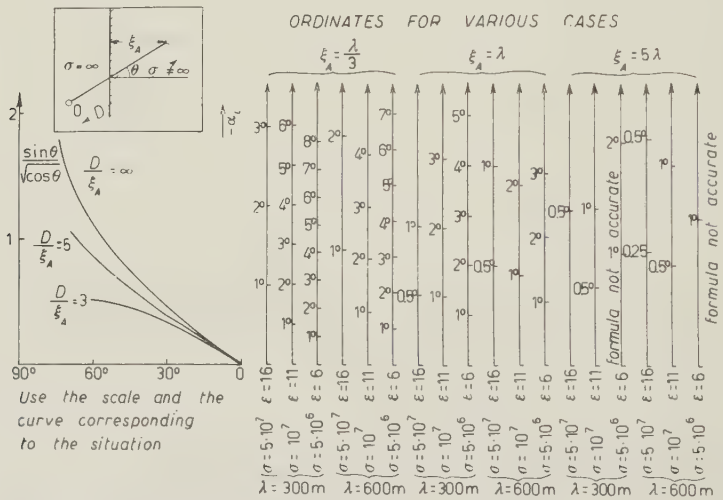

Fig. 7. – A nomogram for determining « coastal refraction ».

approaches the perpendicular of the coast line. This, as is well known, corresponds to the experiment (analysis of the experiments published prior to this theory was given in references [6] and especially [1*d*]). If the receiver is on the sea, while the transmitter is on the land (and is nearer to the coast line than the receiver), *i.e.*, if the r.d.f. is performed from a ship, then the sign is changed and the factor $(1-\xi_A/(D\cos\theta))^{\frac{1}{2}}$ is substituted by a small factor $(\xi_0/(D\cos\theta))^{\frac{1}{2}}$, where ξ_0 is the distance from the transmitter on the land to the coast line. In this case the error in r.d.f. decreases considerably, if $x_0 \ll D$. For a number of other cases (not abrupt transition from sea to land: the receiver within the transition zone or outside of it) an additional investigation was performed, starting from eq. (2.6), which does not necessarily assume

an abrupt change of the properties of the ground. Resulting formulas for α_L are given in references [6c, 1d], where the formulas for the «relief coastal error» α_R are given as well. If we are dealing with a wave passing not from the sea to the land, but between two lands, characterized by s_1 and s_2, then, for instance if they both are real, in the r.h.s. of the eq. (4.17) an additional factor $1-(s_2/s_1)^{\frac{1}{2}} \approx 1-(\sigma_1/\sigma_2)^{\frac{1}{2}}$ must be introduced. Recently similar results were obtained using another method by Furutsu [13a], who also gave a number of tables and graphs. In all cases for which the results are comparable, they coincide with those given above.

4·2. *The third segment.* – The most general formula of all obtained in this case is for the case when:

a) All numerical distances are large and one of the end segments is relatively short, say $x_1 \ll D$. Then [8]

$$(4.18)\quad w_3(D) = -\frac{1}{2\sqrt{s_1 s_3 D}}\left\{1-\frac{i}{\sqrt{\pi}}\frac{\sqrt{s_2}-\sqrt{s_3}}{\sqrt{s_2 s_3 D}}\left[\frac{D-2x_1}{\sqrt{x_1(D-x_1)}}-\frac{D-2(D-x_2)}{\sqrt{x_2(D-x_2)}}\right]\right\}.$$

In practice quite often the second term in parenthesis is small. Then we come to the geometrical mean formula:

$$(4.19)\qquad w_3(D) = -\frac{1}{2\sqrt{s_1 s_3 D}} = \sqrt{y(s_1 D)\, y(s_3 D)}\,.$$

The influence of the intermediate segment falls away.

Another rather widely applicable case is that of

b) All numerical distances being large, the electrical properties at the end segments coincide. Then again eq. (4.18) holds (x_1 should not necessarily be small as compared to D), where we may put $s_1 = s_3$:

$$(4.20)\quad w_3(D) = -\frac{1}{2s_1 D}\left\{1-\frac{i}{\sqrt{\pi}}\frac{\sqrt{s_2}-\sqrt{s_1}}{\sqrt{s_1 s_2 D}}\left[\frac{D-2x_1}{\sqrt{x_1(D-x_1)}}+\frac{D-2(D-x_2)}{\sqrt{x_2(D-x_2)}}\right]\right\}.$$

Now, let

c) The end segments be «sea», $s_1 = s_3 = 0$. This is the case «sea»–«land»–«sea» [6b]. With a single assumption that $|s_2(x_2-x_1)| \gg 1$ (for the intermediate segment the numerical distance is large) we have:

$$(4.21)\quad w_3(D) = -\frac{1}{2s_2 D}+\frac{i}{\sqrt{\pi s_2 D}}\left(\sqrt{\frac{x_1}{D-x_1}}+\sqrt{\frac{D-x_2}{x_2}}\right)+$$
$$+\frac{1}{2}\left\{1-\frac{2}{\pi}\arcsin\frac{(x_2-x_1)D-x_1(D-x_2)}{x_2(D-x_1)}\right\}.$$

cα) If moreover the end segments are relatively short, $x_1 \ll D, D - x_2 \ll D$, then

$$w_3(D) = -\frac{1}{2s_2 D} + \frac{i}{\sqrt{\pi s_2 D}}\left(\sqrt{\frac{x_1}{D}} + \sqrt{\frac{D-x_2}{D}}\right) + \frac{2}{\pi}\sqrt{\frac{x_1(D-x_2)}{D^2}}. \tag{4.22}$$

When, in addition, the numerical distances for the end segments, as calculated with respect to the properties of the intermediate one, are large, $|s_2 x_1| \gg 1$, $|s_2(D-x_2)| \gg 1$, then

$$w_3 = \frac{2}{\pi}\sqrt{\frac{x_1(D-x_2)}{D^2}}, \tag{4.23}$$

and for $x_1 = D - x_2 = x_0$ [6*b*]

$$w_3 = \frac{2}{\pi}\frac{x_0}{D}. \tag{4.23a}$$

If the path does not contain these relatively short well conducting segments, the attenuation factor is $w_1 = (-2s_2 D)^{-1}$. Thus the presence of « good », « starting » and « landing » areas leads to the increase of the field expressed by a factor

$$\left|\frac{w_3}{w_1}\right| = \frac{1}{\pi}|s_2 x_0| \gg 1. \tag{4.23b}$$

d) The case « land »–« sea »–« land », with large numerical distances, $|s_1 x_1| \gg 1$, $|s_1(D-x_2)| \gg 1$, $s_1 = s_3$ Here [6*b*, 8]

$$w_3(D) = -\frac{i}{2\sqrt{\pi}}\frac{1}{(s_1 D)^{\frac{3}{2}}}\left[\frac{D-2x_1}{\sqrt{x_1(D-x_1)}} - \frac{D-2x_2}{\sqrt{x_2(D-x_2)}}\right] - \\ - \frac{1}{\pi s_1\sqrt{x_1 D}}\sqrt{\frac{x_2-x_1}{D-x_2}} - \frac{1}{\pi s_1 D}\arcsin\sqrt{\frac{x_1(D-x_2)}{x_2(D-x_1)}}. \tag{4.24}$$

e) The case « land »–« sea »–« land » with relatively short end segments ($x_1 \ll D$, $D - x_2 \ll D$, $s_1 = s_3$):

$$w_3 = z(s_1 x_1)\, z(s_1(D-x_2)), \tag{4.25}$$

where z is a function expressible through the Sommerfeld function, see eqs. (4.8) and (4.9) and Fig. 4. In the case of two segments, « land »–« sea », with the « land » segment being short, we have $w_2 = z(s_1 x_1)$. When two such segments are on both ends of the path, then the attenuation function is a product of two such factors.

If the numerical distances for end segments are large, then, similarly to what follows from eq. (4.24), we get, using eq. (4.9):

$$w_3 = -\frac{1}{\pi s_1 \sqrt{x_1(D-x_2)}}. \tag{4.26}$$

While if these numerical distances are small, then

$$w_3 = 1 + \frac{2i}{\sqrt{\pi}}\left(\sqrt{s_1 x_1} + \sqrt{s_1(D-x_2)}\right). \tag{4.27}$$

As an example of these formulas we give, first of all, the Fig. 8 [1*d*, 8], which shows most clearly the predominance of the part played by end segments. Here two curves show how the attenuation function changes if an initially overall « sea » path of a definite length D is filled up with a « land ». The « land » is assumed to have such properties that when the whole path is filled the numerical distance equals $sD = 100$. The graph shows that if the filling up begins from the end points, then even the short badly conducting

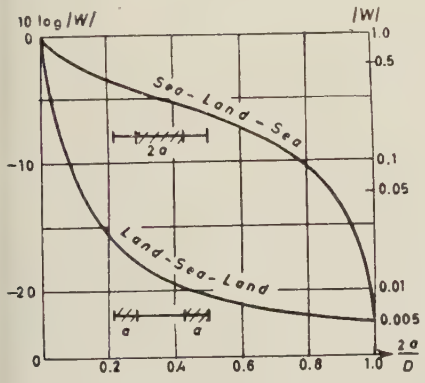

Fig. 8. – Influence of the properties of « starting » and « landing » areas for flat earth: attenuation functions for cases « land-sea-land » and « sea-land-sea » when filling up $\xi = 2a/D$ by « land » is the same. Total length of path D corresponds for $\xi = 1$ to a numerical distance $sD = 100$.

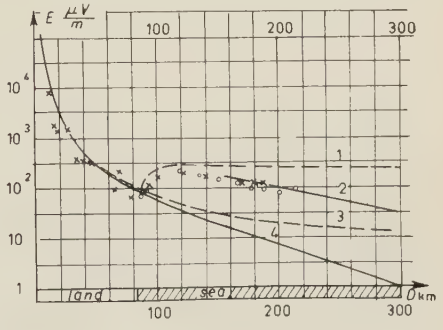

Fig. 9. – A comparison of theoretical predictions with experimental data by MILLINGTON for $\lambda = 96$ m. Curves correspond to theoretical eqs. (4.15) (curve 1 for flat earth) and (6.6) (curve 2, for spherical earth), and for homogeneous earth theory: flat (curve 3) and spherical (curve 4).

segments cause an abrupt decrease of the field. If, on the contrary, the segments adjacent to the end points remain well conducting, then a considerable part of the path must be filled up before the field decreases essentially.

In Fig. 9 the Millington measurements [25] at $\lambda = 96$ m are shown and four curves are drawn: 1) the one representing the eq .(4.15) for a flat earth;

2) the curve corresponding to eq. (6.6) for an inhomogeneous spherical earth (see below); 3) an usual homogeneous flat earth curve; 4) the same for spherical homogeneous earth. Thus, here the sphericity of the earth makes itself felt and this is the reason why the eq. (4.15) gives an error up to about 8 decibels.

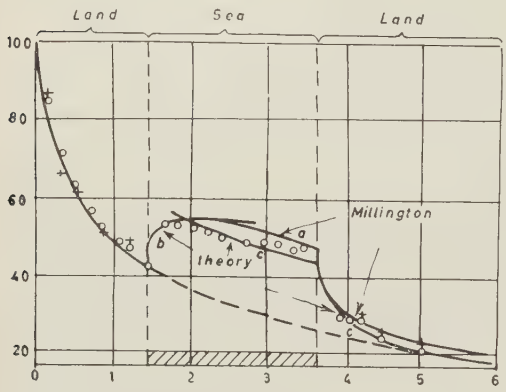

Fig. 10. – A comparison of theory with experimental data for $\lambda = 3.9$ m. Curves are drawn according to theoretical eqs. (4.14), (4.15) and (4.20) and according to Millington's semiempirical method.

Fig. 10 demonstrates the Millington measurements at $\lambda = 3.9$ m and contains: *a*) the curves drawn by Millington himself according to his semiempirical method; *b*) the theoretical curves obtained taking into account that $s_2 \neq 0$ (eqs. (4.14) and (4.20)). This case is especially interesting. Indeed, the starting assumption of the theory is that $|\varepsilon'| \gg 1$. Here s_1 is not real, $\varepsilon_1' = 16 + 2.3i$, $s_1 = (7.2 + 49.3i)$ (kilometres)$^{-1}$. For the sea $s_2 = (0.85 + 0.07i)$ (km)$^{-1}$. At the end of the second segment, when $x \approx 3.7$ km, $|s_2 x| \approx 3$ and we may use the geometrical mean formula (4.14). The difference with the Millington curve [25] seems strange, since in this case the Millington method must give an exact theoretical value [15]. On the third segment in the vicinity of the boundary, the difference with Millington curve possibly may arise as an effect of the second term in brackets in eq. (4.20). More recently H. Bremmer [20] solved eq. (3.13), taken for $s_0 = 0$, by means of a Laplace transformation, for the path composed of two and of three homogeneous segments. His solutions coincide with the results quoted above.

5. – Conclusion for flat earth. Generalization.

The most important qualitative conclusion from the above theory is that the influence of particular segments of the path on wave propagation is not simply accumulated. Eq. (4.17) shows that, as was proved already by Grünberg [4], a distortion of the wave normal caused by traversing a coastal line, disappears when the distance from this line increases. Fig. 8 demonstrates that a badly conducting segment reduces the field only if it appears near a terminal of the path. Bad properties of the soil are rather unimportant if they pertain to the middle of the path. The predominant part is played by

« starting » and « landing » areas (of course, all this is true if the numerical distances are large). Propagation of a ground wave does not resemble a wave gliding along the surface and decaying in the course of propagation. Most clearly this is shown by the « recovery effect », predicted by eq. (4.15) and experimentally proved by Millington's measurements. In the essential part radiowaves propagate via space rather high above the earth surface, where the absorption in the soil does not make itself felt and $w \approx 1$. However, as will be seen below, for observation points far beyond the horizon, this conclusion should be essentially modified.

Many practical semiempirical formulas, or rather recipes, were proposed for calculating the field over mixed paths. Almost all of them assume some kind of averaging (over the path) of the ground properties or of the attenuation function. It is clear now that these last methods could not be correct. In particular they fail to be able to give recovery effect. However, this does not pertain to the method proposed by Millington [25]. We can estimate its accuracy by comparing its prescriptions with the above theoretical results. Such a detailed comparison [15] shows that although the analytical expressions following from the Millington method sometimes have nothing in common with the theoretical ones — for instance, instead of eq. (4.21) this method gives

$$w_{3M} = \sqrt{\frac{y(s_2 x_2)\; y(s_2(D-x_1))}{y(s_2 x_1)\; y(s_2(D-x_2))}},$$

nevertheless, the numerical results (and often even the analytical expressions) turn out to be remarkably close to the results of the theory. Inaccuracy in amplitude usually does not exceed ~ 4 db; a figure which, in phase, in some cases is not large: in the vicinity of the boundary between two segments it is of the order of 20% of the complete phase shift, but sometimes it can be much larger. More subtle phenomena (*e.g.*, the one described by eq. (4.1*a*)) can not be treated by this method at all.

Generalization of the above results is possible along two lines.

First of all, we can consider observation point A at $z \neq 0$. The field at $z = 0$ being known, we can obtain a field at $z \neq 0$ by the Green theorem, after integrating over the earth's surface. In the general case the integral cannot be evaluated analytically. In the case of two segments it reduces exactly to the one, found by Clemmow [12], using more traditional methods.

Some qualitative features for the $z \neq 0$ case are nevertheless worth mentioning. In the case of $z = 0$ the method of stationary phase, applied to the integral equation of the Huygens principle, leads to the conception of an effective path of radiowaves, as represented by the first Fresnel zone (Sect. 3, especially Fig. 1 and eq. (3.7)).

If a transmitter is situated at some point $z_0 \geqslant 0$, a receiver at $z_A \geqslant 0$, then we may construct on these two points taken as foci a set of confocal ellipsoids, $\nu = 1, 2, \ldots$, according to the same eq. (3.7). The part of the earth surface which is most important for the process of wave propagation is the one which is cut off by an ellipsoid with the smallest possible ν. For $z_0 = z_A = 0$ this is $\nu = 1$. For $kz_0 \gg 1$, $kz_A \gg 1$ the first ellipsoid touching the earth will have $\nu \gg 1$. The most important part of the earth surface will be represented by a relatively small ellipse in the vicinity of a mirror reflection point. It can be shown [8 § 35], that if

$$k(z_0 + z_A) \gg |\sqrt{\varepsilon' + 1}|,$$

then the simple Fresnel reflection formulas hold for a plane wave.

Especially interesting is the case of $z_0 = 0$, $z_A \neq 0$, when the most important portion of the earth's surface is cut off by the ellipsoid $\nu = 1$ and has the form of an elongated ellipse, encircling the transmitter. If the receiver is situated so high that this ellipse is very small and within it the field of the transmitter does not attenuate appreciably (the numerical distance corresponding to the larger axis of the ellipse is small), then in the receiver point the situation is the same as if we had a perfectly conducting earth, $\varepsilon' = \infty$, *i.e.*, in the point A we have $w = 1$. If we have an inhomogeneous surface, consisting of many segments with $\varepsilon' = \varepsilon'_j$, $j = 1, 2, \ldots$, and if the receiver is placed above some distant segment, $j > 1$, a peculiar situation may arise for sufficiently large z_A, when the most important part of the earth surface is completely within the first segment. In this case the attenuation function will be given approximately by the homogeneous earth attenuation function y calculated for $\varepsilon' = \varepsilon'_1$.

Similar considerations are useful for spherical earth as well. For further details see ref. [8].

Secondly, we can consider uneven surface. However, this is possible only if the average declination ζ_0 of the surface from some averaging plane and the average angle γ_0, formed by the surface with the plane, are not too large:

$$\sqrt{k\gamma_0\zeta_0} \ll 1. \tag{5.1}$$

For this case a theory was developed [1*d*, 6*a*]. We shall mention here only some of its results.

The method consists in this: the boundary condition (2.5), written for the actual surface $z = \zeta(x, y)$, is developed in series of ζ and is thus transferred to an auxiliary plane $z = 0$. Therefore we again have to investigate the field in the upper half-space $z > 0$, while the boundary condition now contains a

term, describing the relief:

$$(5.2)\quad \frac{\partial E_z}{\partial z} = -\frac{ik}{\sqrt{\varepsilon'+1}}\left[1+\frac{1}{k^2}(\boldsymbol{k}\ \mathrm{grad}\ln\sqrt{\varepsilon'})\right]E_z+\frac{\partial}{\partial x}\left(\frac{\partial\zeta}{\partial x}E_z+\zeta\frac{\partial E_x}{\partial z}\right)+$$
$$+\frac{\partial}{\partial y}\left(\frac{\partial\zeta}{\partial y}E_z+\zeta\frac{\partial E_y}{\partial z}\right),\quad \text{at } z=0,$$

and we come to a correspondingly modified integral equation. It was used in two ways [6*c*, 1*d*].

On one side, small perturbations were investigated. *E.g.* for a not steep slope of the coast the error in radio direction finding, which is due to it, α_R, was found. It is to be added to the error due to the difference in conductivities of sea and land, α_L, (4.17). In accordance with the physical picture of propagation, sketched above, α_R vanishes at large distances from the slope.

On the other side a statistical treatment was given for the attenuation function at $z=0$ over a randomly corrugated surface. It was shown that this average attenuation function coincides with the Sommerfeld function $y(s_{\mathrm{corr}}D)$, for a certain effective dielectric permeability $\varepsilon'_{\mathrm{corr}}$, which differs from the actual ε'. For an infinitely conducting soil, if we put $\varepsilon'=\infty$,

$$\varepsilon'_{\mathrm{corr}} = [(A+iB)^2 k\zeta_0\gamma_0^3]^{-1}, \qquad \text{for } \sqrt{\gamma_0} < \sqrt{k\zeta_0} \ll \frac{1}{\sqrt{\gamma_0}},$$
$$\varepsilon'_{\mathrm{corr}} = (-Ck^2\zeta_0^2\gamma_0^2)^{-1}, \qquad \text{for } k\zeta_0 \ll \gamma_0 \ll 1.$$

Here A, B, C are real constants of the order of unity, ζ_0/γ_0 and ζ_0 some average horizontal and vertical dimensions of a single hump.

Sometimes this gives a very peculiar dependence of the attenuation function from distance (note, that in this case the attenuation of the field at $z=0$ leads to an increase of the field at $z>0$, since for $\varepsilon'=\infty$ the corrugation gives scattering of electromagnetic waves into the upper space, instead of absorbing them in the soil for $\varepsilon'\neq\infty$).

6. – Spherical inhomogeneous earth surface.

Propagation of ground radio waves over a spherical earth surface along a path, consisting of homogeneous segments has been recently investigated by Furutsu [13*b*]. He used a method which permitted to get a solution of the problem. However, it seems to be too complicated. The same results can be obtained in the same simple manner as for flat earth, starting from the same integral equation (3.13)–(3.15). Godzinsky [21], who pointed out that

this equation holds for spherical surface as well, has used it as a basis for a special numerical calculation procedure. At the same time, we can [9, 16] use *exactly* the same method as for flat earth, and come to the analytical solution of Furutsu.

First of all we rewrite eq. (3.13) for a sphere using as the independent variable the arc of a large circle ϑ:

$$(6.1)\qquad w_N(\vartheta_A) = V(\vartheta_A; q_0) + \sqrt{\frac{iA\vartheta_A}{\pi}} \sum_{j=1}^{N} (q_j - q_0) \int_{\vartheta_{j-1}}^{\vartheta_j} \frac{w(\vartheta) V(\vartheta_A - \vartheta; q_0)}{\sqrt{\vartheta(\vartheta_A - \vartheta)}}\, \mathrm{d}\vartheta\,.$$

Here ϑ_{j-1}, ϑ_j denote terminals (in radians of arc of large circle) of the j-th segment ($\vartheta_0 = 0$, $\vartheta_N = \vartheta_A$), and q_j a parameter, characterizing its properties. Let us put $q_0 = q_N$:

$$(6.2)\qquad w_N(\vartheta_A) = V(\vartheta_A; q_N) + \sqrt{\frac{i}{\pi} A\vartheta_A} \sum_{j=1}^{N-1} (q_j - q_N) \int_{\vartheta_{j-1}}^{\vartheta_j} \frac{w_j(\vartheta) V(\vartheta_A - \vartheta; q_N)}{\sqrt{\vartheta(\vartheta_A - \vartheta)}}\, \mathrm{d}\vartheta\,.$$

Thus the unknown attenuation function for the N-th segment is expressed through quadratures of attenuation functions for the preceding $N-1$ segments.

Let us obtain the attenuation function $w_2(\Delta\vartheta_1, \Delta\vartheta_2; q_1, q_2)$ for a path consisting of two homogeneous segments, $N = 2$, having lengths measured respectively by $\Delta\vartheta_1 = \vartheta_1$ and $\Delta\vartheta_2 = \vartheta_A - \vartheta_1$ and characterized by parameters $q = q_1$ and $q = q_2$. Over the first segment the attenuation function w_1 is known. It is equal to $V(\vartheta; q_1)$. In eq. (6.2) the sum contains now only one term, $j = 1$, in which $w(\vartheta) = w_1(\vartheta)$:

$$(6.3)\qquad w_2(\Delta\vartheta_1, \Delta\vartheta_2; q_1, q_2) =$$
$$= V(\vartheta_A; q_2) + \sqrt{\frac{i}{\pi} A\vartheta_A}(q_1 - q_2) \int_0^{\vartheta_1} V(\vartheta; q_1) V(\vartheta_A - \vartheta; q_2) \frac{\mathrm{d}\vartheta}{\sqrt{\vartheta(\vartheta_A - \vartheta)}}\,.$$

We substitute V from (3.14) in the form of a series and integrate over ϑ. This gives:

$$(6.4)\qquad w_2(\Delta\vartheta_1, \Delta\vartheta_2; q_1, q_2) = V(\vartheta_A; q_2) +$$
$$+ \sqrt{i\pi A\vartheta_A}(q_1 - q_2) \sum_{k,l} \frac{\exp\left[iA(\Delta\vartheta_1 \cdot t_k(q_1) + \Delta\vartheta_2 \cdot t(q_2))\right]}{(t_k(q_1) - q_1^2)(t_l(q_2) - q_2^2)(t_k(q_1) - t(q_2))} -$$
$$- \sqrt{i\pi A\vartheta_A}(q_1 - q_2) \sum_{k,l} \frac{\exp\left[iA\vartheta_A t_l(q_2)\right]}{(t_k(q_1) - q_1^2)(t_l(q_2) - q_2^2)(t_k(q_1) - t_l(q_2))}\,.$$

In the last term at the r.h.s. the sum over k can be calculated if we use the identity:

$$\frac{\omega(t)}{\omega'(t)-q_1\omega(t)} = \sum_k \frac{1}{t_k-q_1^2}\cdot\frac{1}{t-t_k}\,. \tag{6.5}$$

It follows, *e.g.*, from the fact that if we multiply both sides of eq. (6.5) by an *arbitrary* function $f(t)$ and integrate along a contour C encircling all poles $t=t_k$ we obtain an equality. Indeed, if we develop $f(t)$ in functions e^{ixt}, the neach term of this development gives an equality (see eq. (3.14)). Therefore it holds for $f(t)$ as well.

Taking now into account that $\omega'(t_l)=q_2\omega(t_l)$ we get:

$$\sum_k \frac{1}{t_k-q_1^2}\frac{1}{t_k-t_l} = -\frac{\omega(t_l)}{\omega'(t_l)-q_1\omega(t_l)} = \frac{1}{q_1-q_2}\,. \tag{6.5a}$$

Substituting this formula into the last term of eq. (6.4) we see that it cancels the term $V(\vartheta_A;\, q_2)$ (see (3.14)) and come finally to the equation:

$$w_2(\Delta\vartheta_1, \Delta\vartheta_2;\, q_1, q_2) = \tag{6.6}$$
$$= \sqrt{i\pi A\vartheta_A}(q_1-q_2)\sum_{k,l=1}^{\infty}\frac{\exp\left[iA(\Delta\vartheta_1\cdot t_k(q_1)+\Delta\vartheta_2\cdot t_l(q_2))\right]}{(t_k(q_1)-q_1^2)(t_l(q_2)-q_2^2)(t_k(q_1)-t_l(q_2))}\,,$$

i.e., to the FURUTSU result [13*b*].

In the extreme case of very large distances, when in every sum a single first term may be kept (*i.e.*, every segment penetrates beyond the horizon, $A\,\Delta\vartheta_1 \gtrsim 1$, $A\,\Delta\vartheta_2 \gtrsim 1$), we have

$$w_2(\Delta\vartheta_1, \Delta\vartheta_2;\, q_1, q_2) = \sqrt{i\pi A\vartheta_A}\,\frac{q_1-q_2}{t_1(q_1)-t_1(q_2)}\,\frac{\exp\left[iA(t_1(q_1)\Delta\vartheta_1+t_1(q_2)\Delta\vartheta_2)\right]}{(t_1(q_1)-q_1^2)(t_1(q_2)-q_2^2)}\,. \tag{6.7}$$

After introducing attenuation functions for each segment taken separately, $w_1(\Delta\vartheta_1;\, q_1)$, $w_1(\Delta\vartheta_2;\, q_2)$, eq. (6.7) may be rewritten as follows:

$$w_2 = \sqrt{\frac{\vartheta_A}{A\vartheta_1(\vartheta_A-\vartheta_1)}}\,\frac{q_1-q_2}{t_1(q_1)-t_1(q_2)}\,w_1(\Delta\vartheta_1;\, q_1)w_1(\Delta\vartheta_2;\, q_2)\,. \tag{6.8}$$

Often first and second fractional factors are comparatively less important. Then, as we see, attenuation of the field has a character of a step by step decay. The field decreases exponentially at the beginning over the first segment, then—over the second one. This accumulation of attenuation shows the fundamental difference between the processes of propagation over a spherical surface and a flat one; between the observation within the horizon and that behind it.

In a similar way we can obtain quite simply the formula for three seg-

ments, w_3. Putting in eq. (6.2) $N=3$, we get

$$w_3 = V(\vartheta_A; q_3) + \sqrt{\frac{i}{\pi} A\vartheta_A}\,(q_1 - q_3)\int_0^{\vartheta_1} \frac{V(\vartheta; q_1)V(\vartheta_A - \vartheta; q_3)}{\sqrt{\vartheta(\vartheta_A - \vartheta)}}\,\mathrm{d}\vartheta + \\ + \sqrt{\frac{i}{\pi} A\vartheta_A}\,(q_2 - q_3)\int_{\vartheta_1}^{\vartheta_2} \frac{w_2(\vartheta)V(\vartheta_A - \vartheta; q_3)}{\sqrt{\vartheta(\vartheta_A - \vartheta)}}\,\mathrm{d}\vartheta\,.$$

Substituting V from eq. (3.14), w_2 from eq. (6.6) and performing an elementary integration over ϑ we obtain three terms. Two of them contain threefold summation, one of them containing the sum (cf. eq. (6.5a)):

$$\sum_l \frac{1}{(t_l(q_2) - q_2^2)(t_k(q_1) - t_l(q_2))(t_l(q_2) - t_m(q_3))} = \\ = \frac{1}{t_k(q_1) - t_m(q_3)}\left\{\sum_l \frac{1}{(t_l(q_2) - q_2^2)(t_l(q_2) - t_m(q_3))} - \sum_l \frac{1}{(t_l(q_2) - q_2^2)(t_l(q_2) - t_k(q_1))}\right\} = \\ = \frac{1}{t_k(q_1) - t_m(q_3)}\left\{\frac{1}{q_2 - q_3} - \frac{1}{q_2 - q_1}\right\} = \frac{q_1 - q_3}{(q_1 - q_2)(q_2 - q_3)(t_k(q_1) - t_m(q_3))}\,,$$

where $t_m(q_3)$ is a root of the equation $\omega'(t_m) = q_3\omega(t_m)$. After taking into account this formula, two of three terms cancel each other and we are left with

$$(6.9)\quad w_3(\Delta\vartheta_1, \Delta\vartheta_2, \Delta\vartheta_3; q_1, q_2, q_3) = \sqrt{i\pi A\vartheta_A}\,(q_1 - q_2)(q_2 - q_3)\cdot \\ \cdot \sum_{k,l,m=1}^{\infty} \frac{\exp\left[iA(\Delta\vartheta_1 \cdot t_k(q_1) + \Delta\vartheta_2 \cdot t_l(q_2) + \Delta\vartheta_3 \cdot t_m(q_3))\right]}{(t_k(q_1) - q_1^2)(t_l(q_2) - q_2^2)(t_m(q_3) - q_3^2)(t_k(q_1) - t_l(q_2))(t_l(q_2) - t_m(q_3))}\,;$$

($\Delta\vartheta_1 = \vartheta_1$, $\Delta\vartheta_2 = \vartheta_2 - \vartheta_1$, $\Delta\vartheta_3 = \vartheta_A - \vartheta_2$ are the angular dimensions of the three segments).

This also coincides with the results of ref. [13b]. It is obvious how the formula may be generalized for $N > 3$.

Let us consider eq. (6.9) for the case of terminal segments having identical properties, $q_1 = q_3$ and investigate the influence of the middle segment, $q = q_2$. If observation is far beyond the horizon, $A\vartheta_A > 1$, while the width and position of the middle segment satisfy moreover the conditions $A\,\Delta\vartheta_1 > 1$, $A\,\Delta\vartheta_3 > 1$, then in the sums over k and m we may keep only the first terms and eq. (6.9) is:

$$(6.10)\quad w_3(\Delta\vartheta_1, \Delta\vartheta_2, \Delta\vartheta_3; q_1, q_2, q_1) = \\ = \sqrt{i\pi A\vartheta_A}\,\frac{\exp\left[iA\vartheta_A t_1(q_1)\right]}{[t_1(q_1) - q_1^2]^2}\,(q_1 - q_2)^2 \sum_{l=1}^{\infty} \frac{\exp\left[iA\,\Delta\vartheta_2(t_l(q_2) - t_1(q_1))\right]}{[t_l(q_2) - q_2^2][t_l(q_2) - t_1(q_1)]^2} = \\ = V(\vartheta_A; q_1) \sum_{l=1}^{\infty} \frac{\exp\left[iA\,\Delta\vartheta_2(t_l(q_2) - t_1(q_1))\right]}{[t_l(q_2) - q_2^2][t_l(q_2) - t_1(q_1)]^2} \cdot \frac{(q_1 - q_2)^2}{t_1(q_1) - q_1^2}\,.$$

Thus, a strip having different properties, if placed in the middle part of a homogeneous long path affects the field (for a completely homogeneous path we would have $V(\vartheta_A; q_1)$). However, its influence is determined solely by its width and properties, and does not depend on its position on the path. The perturbation of amplitude and phase, produced by this strip, is transferred to the observation point unmodified wherever it would be placed. This regularity differs fundamentally from the one in the case of flat earth, where one of the most characteristic features was that the field was independent of the properties of intermediate segments. In the extreme case there holds the « geometrical mean » formula (4.19), the propagation is determined completely by the properties of « starting » and « landing » areas; while if observing behind the horizon, the situation is quite different.

This does not mean, of course, that the electrical properties of the end segments do not play an important role. Let us consider, for instance, the case when *all* segments are sufficiently long, $A\Delta\vartheta_j \gtrsim 1$, $j = 1, 2, 3$, and we can keep the first term alone:

$$(6.11)\qquad w_3(\Delta\vartheta_1, \Delta\vartheta_2, \Delta\vartheta_3; q_1, q_2, q_1) = \sqrt{i\pi A\vartheta_A}\,\frac{\exp\left[iA\left((\Delta\vartheta_1+\Delta\vartheta_3)t_1(q_1)+\Delta\vartheta_2\cdot t_1(q_2)\right)\right]}{(t_1(q_1)-q_1^2)^2\,(t_1(q_2)-q_2^2)\,(t_1(q_2)-t_1(q_1))^2}.$$

Let us take two related cases differing only in that the soil which in the first case is adjacent to the terminals of the path, in the second case is in the middle, and *vice versa*. For convenience we may assume again the cases of « land-sea-land » (LSL, case « *a* ») and of « sea-land-sea » (SLS, case « *b* »). Similarly to the case of the flat earth we compare them for equal filling up of the path by a given soil (Fig. 8). Namely, let us for case « *a* » have segments $\Delta\vartheta_1^{(a)}$, $\Delta\vartheta_2^{(a)}$ and $\Delta\vartheta_3^{(a)}$ with $q_1^{(a)} = q_3^{(a)} = q_L$, $q_2^{(a)} = q_S$, while in case « *b* » $\Delta\vartheta_1^{(b)} + \Delta\vartheta_3^{(b)} = \Delta\vartheta_2^{(a)}$, $\Delta\vartheta_2^{(b)} = \Delta\vartheta_1^{(a)} + \Delta\vartheta_3^{(a)}$ and $q_1^{(b)} = q_3^{(b)} = q_2^{(a)} = q_S$, $q_2^{(b)} = q_1^{(a)} = q_3^{(a)} = q_L$. It follows from eq. (6.11) that the ratio of the attenuation functions for the two cases is:

$$(6.12)\qquad \frac{w_3^{(a)}}{w_3^{(b)}} = \frac{t_1(q_S)-q_S^2}{t_1(q_L)-q_L^2}.$$

Therefore, in contradistinction to the flat earth case, it does not depend either on the situation of the band $\Delta\vartheta_2$, or on the degree of filling up of the path. However, the field depends rather essentially on the properties of the soil adjacent to the terminals. Thus, *e.g.*, if for land $\sigma_L = 9\cdot 10^7$ CGSE, for sea $\sigma_S = 4\cdot 10^{10}$ CGSE, we have for $\lambda = 300$ m

$$q_L \approx 7.4\sqrt{i}, \qquad q_S \approx 0.35\sqrt{i}, \qquad A \approx 58.5.$$

The corresponding value of t_1 may be calculated approximately, *e.g.*, from the asymptotic expansions:

$$t_1(q_S) = t_1(0) + \frac{q_S}{t_1(0)} + \ldots \approx 0.82 + 0.84i\,,$$

$$t_1(q_L) = t_1(\infty) + \frac{1}{q_L} + \ldots \approx 1.27 + 1.92i\,.$$

Herefrom follows:

$$\frac{w_3^{LSL}}{w_3^{SLS}} \approx 0.26 \exp\left[0.45 \cdot \pi i\right]. \tag{6.12a}$$

Fig. 11 and 12 show for $\lambda = 100$ m and $\lambda = 300$ m respectively in semi-logarithmic scale w_3^{LSL} and w_3^{SLS} versus the degree of filling up of the path by « land », *i.e.*, versus $\xi = (\Delta\vartheta_1^{(a)} + \Delta\vartheta_3^{(a)})/\vartheta_A = \Delta\vartheta_2^{(b)}/\vartheta_A$. For the length of the path we assume $\vartheta_A = A/8 \approx 0.137$. This corresponds approximately to $a\vartheta_A = D \approx 900$ km. Since eq. (6.11) may be applied only if $A\Delta\vartheta_j > 1$, the curves are calculated only for $\frac{1}{4} < \xi < \frac{3}{4}$. For other ξ's they show possible extrapolation. On the same figures similar curves are drawn according to the respective formulas for inhomogeneous flat earth (which here, for $D = 900$ km, $\lambda = 100$ and 300 m, are of course incorrect). It can be seen from the figure (and from Fig. 8) that although in the spherical case the ground properties, generally speaking, are essential (for instance, for $\lambda = 300$ m variation of ξ from 0 up to 1 induces a 32 db decrease of the field), the particular type of distribution of a given soil over the path is in no way as important as in the flat case. Indeed, if in the middle of a path is placed a well conducting segment, then, as is shown by the lower curve of the upper pair of curves in Fig. 12, in the flat case it has no effect even if it covers a half of the path (for $\xi = 0.5$, we have almost the same value $20 \lg |w| \approx \approx -38$ db as for $\xi = 1$). On the contrary, in the similar case for a sphere, we have

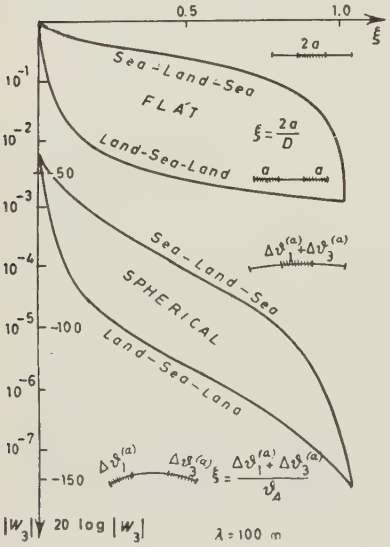

Fig. 11. – Influence of the properties of « starting » and « landing » areas according to the theory for flat earth (upper pair of curves; for such large distances the flat earth theory is incorrect) and for spherical earth (lower pair of curves): attenuation functions for cases « sea-land-sea » and « land-sea-land » for various degrees of filling up by land $\xi = (\Delta\vartheta_1^{(b)} + \Delta\vartheta_3^{(b)})/\vartheta_A = \Delta\vartheta_2^{(a)}/\vartheta_A$. For sea here a finite value of σ is assumed: $\sigma_S = 4 \cdot 10^{10}$. For land $\sigma = \sigma_L = 9 \cdot 10^7$; $\lambda = 100$ m.

for $\xi = 0.5$, a field which is 20 db larger than in the case of the path completely filled up by land (for $\xi = 1$, $20 \lg |w| = -92$ db, $\xi = 0.5$, -72 db).

Thus, although for spherical earth the « starting » and « landing » areas for radio waves, if the observation point is far beyond the horizon, affects the signal to a considerable extent (the curves of the lower pair are separated from each other approximately by (14÷18) db), at variance with flat earth it is here in general much more reasonable to consider the propagation of ground waves as gliding along the earth surface with accumulation of attenuation.

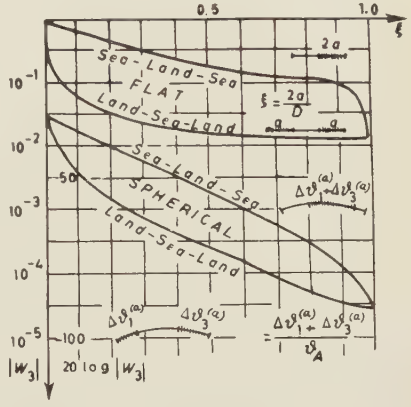

Fig. 12. – The same as Fig. 11, but for $\lambda = 300$ m.

For comparison of the theory with experiment see in Fig. 9 for $\lambda = 96$ m and in Fig. 13 for $\lambda = 250$ m.

Similarly to the case of flat earth, all formulas do not contain the angle θ, formed by the perpendicular to the line separating two adjacent segments and the axis of the path. Its influence is small and may be investigated along the same lines as for a flat path. It may be shown, for instance [9], that

$$\frac{w_2^{(\theta)} - w_2^{(0)}}{w_2^{(0)}} = \frac{[t_1(q_1) - t_1(q_2)]^2}{2A} \operatorname{tg}^2\theta \cdot \frac{\vartheta_1(\vartheta_A - \vartheta_1)}{\vartheta_A}. \tag{6.13}$$

Since $A \gg 1$, this ratio is quite small. The perturbation of the field means an equally small perturbation of the direction of propagation (« coastal refraction »), in addition to the one which takes place in the vicinity of the line separating two segments (see eq. (4.17)). It is interesting to note that, in agreement with the above-mentioned, also this additional perturbation can be accumulated (more detailed account see in ref. [9]).

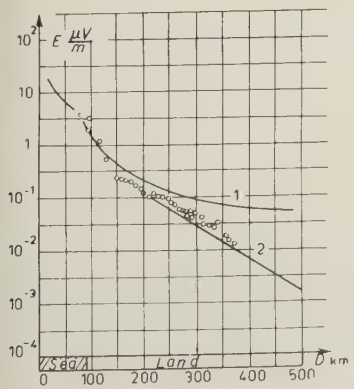

Fig. 13. – A comparison of the theory with experiment [26] for $\lambda = 250$ m. The path consists of two segments. Upper curve according to eq. (4.17) for flat earth, lower one-according to eq. (6.7) for spherical earth.

Eqs. (6.6) and (6.9) may be simply generalized for the case of a receiver which is above the earth at the height z_A while the transmitter is in z_0. For this case it is only necessary to introduce into the sums the height factors. In the series in (6.6) we should introduce

$$\frac{\omega(t_k(q_1) - bz_0)}{\omega(t_k(q_1))} \quad \text{and} \quad \frac{\omega(t\,(q_2) - bz_A)}{\omega(t_l(q_2))},$$

while in (6.9)

$$\frac{\omega(t_k(q_1) - bz_0)}{\omega(t_k(q_1))} \quad \text{and} \quad \frac{\omega(t_m(q_3) - bz_A)}{\omega(t_m(q_3))},$$

where $b = 2A^2/a$. It is exactly in such a generalized form that these series have been obtained by FURUTSU [13*b*], However, we shall not investigate these formulas here.

7. – Conclusion.

As is shown above, the fundamental integral equation (3.9) for a field at the earth's surface gives an useful and convenient basis for treating propagation of radiowaves both for flat and for spherical earth, for homogeneous or inhomogeneous surfaces. If it is necessary, it may be easily generalized for the case of the presence of not too steep corrugations (Sect. **5**), or for a comparatively rapidly changing conductivity (eq. (2.6); recently a particular combination of inhomogeneity and corrugation for spherical earth on the basis of this equation has been treated in ref. [22]); or for the receiver not at the, earth's surface. Simple formulas for special cases, obtained in Sect. **4**, do not of course, give all possible situations. Generally speaking, the quadratures involved should be numerically tabulated (this was performed by CLEMMOW [12] and FURUTSU [13]). However, the deduction of expressions containing these quadratures seems to be most simply effected by the above method, which practically eliminates the problem of solving integral equations.

REFERENCES

[1] *Investigation of Propagation of Radiowaves*, edited by B. A. VVEDENSKY, a symposium; published by the Academy of Sciences of the USSR, Moscow, 1948 (in Russian). *a*) M. A. LEONTOVIČ, pp. 5-12; *b*) M. A. LEONTOVIČ and V. A. FOCK, pp. 13-39; V. A. FOCK, pp. 40-68; *c*) G. A. GRÜNBERG and V. A. FOCK, pp. 69-96; *d*) E. L. FEINBERG, pp. 97-215.

[2] M. A. Leontovič: *Izv. Akad. Nauk SSSR* (*Bull. of the USSR Acad. of Sci.*), physical series, **8**, 16 (1944) (in Russian).
[3] M. A. Leontovič and V. A. Fock: *Journ. of Phys.*, **10**, 13 (1946).
[4] G. A. Grünberg: *Journ. of Phys.*, **6**, 185 (1942); *Phys. Rev.*, **63**, 185 (1943).
[5] E. L. Feinberg: *Izv. Akad. Nauk SSSR* (*Bull. of the USSR Acad. of Sci.*) physical series, **7**, 168 (1943) (in Russian).
[6] E. L. Feinberg: *Journ. of Phys.*, *a*) **8**, 317 (1944); *b*) **9**, 1 (1945); *c*) **10**, 410 (1946).
[7] E. L. Feinberg: *Radiotekhnika*, **5** (No. 4), 3 (1950) (in Russian).
[8] J. L. Alpert, V. L. Ginzburg and E. L. Feinberg: *Propagation of Radiowaves*, a monograph, pp. 1-883 (Moscow, 1953), (in Russian).
[9] E. L. Feinberg and Yu. K. Kalinin: *All-Union scientific session in memory of A. S. Popov* (Moscow, May, 1957); *Radiotehnika i Elektronika*, **3**, 1122 (1958) (in Russian),
[10] J. L. Alpert: *Journ. Techn. Phys* (*USSR*), **10**, 1358 (1940).
[11] G. Boudouris: *Suppl. Nuovo Cimento*, **7**, 71 (1957).
[12] P. C. Clemmow: *Phil. Trans. Roy. Soc.*, A **246**, 1 (1953); *Nature*, **165**, 107 (1950).
[13] K. Furutsu: *Journ. Radio Res. Laboratories* (*Japan*), *a*) **2**, No. 7, 1 (1955); **2**, No. 9, 239 (1955); *b*) **2**, No. 10, 345 (1955).
[14] V. A. Fock: *Matematichesky Sbornik*, No. 1-2, 3 (1944) (in Russian).
[15] E. L. Feinberg: *VIIIth Plenary Assembly of ICCR, Warsaw*, 1956 (Doc. 563-E).
[16] E. L. Feinberg: *XIIth General Assembly of URSI, Boulder, USA*, 1957 (No. 84/Comm II).
[17] H. Bremmer: *Terrestrial Radiowaves*.
[18] T. L. Eckersley: *Radio Rev.*, No. 1, 421 (1920); *Jahrb. d. drahtl. Tel. u. Tel.*, **18**, 349 (1920).
[19] R. Smith-Rose: *Nature*, **116**, 426 (1925).
[20] H. Bremmer: *Physica*, **20**, 441 (1954).
[21] A paper presented to the *VIIIth Plenary Assembly of ICCR, Warsaw*, 1956, by People's Republic of Poland on « Extension of Feinberg's Theory etc. » (Question No. 6, Study Group N. IV).
[22] J. R. Wait: *Canad. Journ. of Res.*, **36**, 9 (1958).
[23] J. L. Alpert and B. Gorošankin: *Journ. of Phys.*, **9**, 115 (1945).
[24] T. L. Eckersley: *Atti del Congresso Internazionale per il Cinquantenario della Scoperta Marconiana della Radio*, Roma, 1947.
[25] G. Millington: *a*) *PIEE*, **96**, 53 (1949); *b*) *Nature*, **163**, 128 (1949); **164**, 114 (1949).
[26] H. L. Kirke: *PIRE*, **37**, 489 (1949).

SUPPLEMENTO AL VOLUME XI, SERIE X
DEL NUOVO CIMENTO

N. 1, 1959
1° Trimestre

Le sorgenti di energia nelle stelle.

A. MASANI

Osservatorio Astronomico di Brera
Istituto di Fisica dell'Università - Genova

(ricevuto il 20 Maggio 1958)

Un rapido calcolo basato sulla misura della costante solare consente di ottenere l'energia L irraggiata dal Sole in ogni secondo. Si ricava $L = 3.73 \cdot 10^{33}$ erg/s che, tradotta in massa equivalente, si può esprimere come $4.1 \cdot 10^{7}$ quintali/s.

Se ci si riferisce alle altre stelle questi valori vanno moltiplicati per fattori che possono variare fra 10^{-2} e 10^{5}.

Per renderci conto se debbono essere ritenuti grandi o piccoli alla scala astronomica, occorre conoscere la sorgente energetica dalla quale L origina e quindi valutare per quanto tempo la stella può irraggiare a un tasso del genere e dedurre la sua vita presumibile.

1. – L'energia gravitazionale.

Nasce così il problema di ricercare la fonte energetica delle stelle. La prima idea è che esse si contraggano: che l'energia potenziale riscaldi la stella la quale a sua volta irraggi il flusso energetico L.

Per valutare l'energia potenziale Ω di una massa avente distribuzione della densità a simmetria sferica non resta che valutare il lavoro fatto per portare in quella configurazione una quantità di materia M, supposta origina-

riamente « diffusa » all'infinito. Sarà:

$$\Omega = -G \int_0^M \frac{M(r)\,\mathrm{d}M(r)}{r} ,$$

G = costante di gravità;
$M(r)$ = massa della sfera di raggio r del modello considerato.

Introducendo le equazioni dell'equilibrio idrostatico cui si suppone soggetta la massa stellare si ottiene:

$$\Omega = -\int_0^M \frac{M(r)\,\mathrm{d}M(r)}{r} = -\frac{3}{5-n}\,G\,\frac{M^2}{R} , \qquad R = \text{raggio della stella,}$$

dove n è l'indice politropico. Nel caso particolare e molto frequente di

$$n = \frac{3}{2} , \quad \Omega = -\frac{6}{7}\,G\,\frac{M^2}{R} .$$

L'energia termica invece sarà:

$$U = C_v \int_0^M T\,\mathrm{d}M(r) ,$$

C_v = calore specifico a volume costante;
T = temperatura.

Tenendo conto dell'equazione di stato dei gas perfetti (al cui caso limitiamo per ora le nostre considerazioni) si ottiene:

$$U = -\frac{\Omega}{3(\gamma-1)} , \qquad \gamma = \text{rapporto dei calori specifici}$$

cioè, per $\gamma = \frac{5}{3}$, $U = -\Omega/2$.

Se supponiamo dunque che la stella irraggi per un processo termico alimentato dalla contrazione gravitazionale sarà (per $\gamma = \frac{5}{3}$)

$$L = -\frac{\mathrm{d}(U+\Omega)}{\mathrm{d}t} = -\frac{3}{4}\,G\,\frac{M^2}{R}\cdot\frac{1}{R}\,\frac{\mathrm{d}R}{\mathrm{d}t} .$$

Applicando questa formula al Sole si ottiene un valore del tempo scala $((1/R)(dR/dt))^{-1}$ dell'ordine di $2.5 \cdot 10^7$ anni, che è inferiore almeno di due ordini di grandezza all'età della Terra.

Tempi scala inammissibilmente brevi si otterrebbero per le stelle più luminose del Sole e non ancora plausibili per quelle meno luminose rappresentate un po' a destra del Sole nella sequenza principale del diagramma H-R (Fig. 1).

Da questo punto di vista la luminosità delle stelle è enorme. La fase gravitazionale, che pure deve regolare la stella nei primi stadi della sua evoluzione, deve presto essere sostituita da un'altra nella quale la contrazione si arresta per l'equilibrio raggiunto fra la energia gravitazionale e quella termica e nella quale questa ultima rimane costante, venendo continuamente rifornita da quella sorgente opportuna (capace di alimentarla) nella stessa misura in cui la stella disperde energia nello spazio.

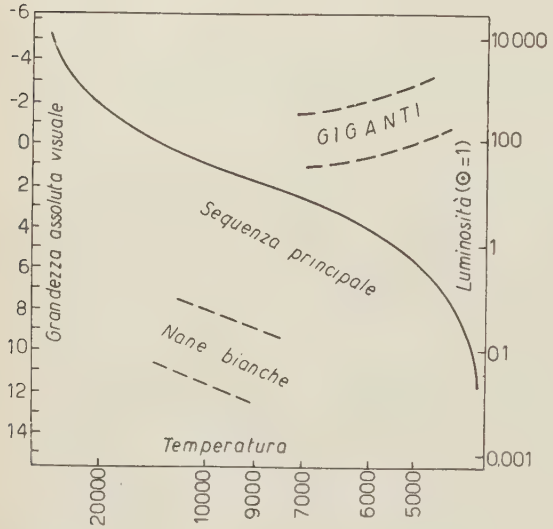

Fig. 1. – Diagramma Hertzsprung-Russell per le stelle di popolazione 1.

Avremo occasione di citare il caso di due ammassi le cui stelle debbono pensarsi per la maggior parte alimentate dalla energia gravitazionale. Per quanto precede esse non potranno essere considerate in lenta evoluzione ma in rapida evoluzione.

Tralasciando per il momento questo caso, consideriamo quelle stelle le quali sono poste, dall'arresto della contrazione, in uno stato di equilibrio secolare in cui le temperature, densità, pressioni ecc. rimangono praticamente inalterate a meno che tale arresto sia dovuto a una causa diversa da quella dell'intervento di una nuova fonte energetica che mantiene l'equilibrio energetico fra energia termica e gravitazionale. Tale causa potrebbe essere costituita dalla degenerazione elettronica ad esempio. In tal caso l'irraggiamento della stella potrebbe essere alimentato dal raffreddamento della massa stellare.

L'energia termica interna è come si è detto (*)

$$U = -\frac{\Omega}{3(\gamma-1)} = -\frac{\Omega}{2} \cong 0.43\, G\frac{M^2}{R}\,,$$

che per una massa solare o un raggio dell'ordine di qualche unità di 10^{10} cm, assume il valore di circa 10^{50} erg.

(*) In condizioni di sola degenerazione elettronica le formule precedenti mantengono la loro validità e il loro significato; basta usare per γ un valore compreso fra $\frac{4}{3}$ e $\frac{5}{3}$ a seconda del grado di degenerazione.

Rispetto a questo valore le stelle meno luminose non pongono esclusioni di principio, dal punto di vista del tempo scala, per una tale interpretazione della luminosità, neppure se il loro numero (vedi in particolare le ricerche sulle nane bianche aventi un grado di degenerazione elettronica assai alto) è elevato, superiore al $(3 \div 4)\%$ dell'intera popolazione stellare.

Affinchè un tipo di sorgente di energia possa essere ritenuto possibile, occorre che dia per la stella non solo un tempo scala accettabile ma che soddisfi anche alla seguente condizione: considerando una stella in equilibrio termodinamico e meccanico è possibile costruire dei modelli stellari i quali hanno le funzioni $T = T(r)$ e $\varrho = \varrho(r)$ (T = temperatura, ϱ = densità, r = distanza dal centro). Detta ε la quantità di energia prodotta per grammo e per secondo, ad ogni tipo di sorgente di energia corrisponderà un certo $\varepsilon = \varepsilon(T, \varrho)$.

Nel caso gravitazionale si dimostra facilmente che

$$\varepsilon = \varepsilon_0 T\,, \qquad \text{con} \qquad \varepsilon_0 = \frac{3\gamma - 4}{\gamma - 1} \frac{K}{\mu H} \frac{1}{R} \frac{\mathrm{d}R}{\mathrm{d}t}$$

(K = costante di Boltzmann, H = peso dell'atomo di idrogeno, μ = peso molecolare medio).

Il tipo di sorgente che alimenta la stella dovrà essere tale che la luminosità calcolata con la formula

$$L = \int_0^R 4\pi \varrho \varepsilon(T, \varrho) r^2 \mathrm{d}r$$

coincide con la luminosità effettiva della stella per la quale il modello è stato fatto.

Tralasciando la discussione, che riprenderemo in seguito, delle stelle di piccola luminosità per le quali la condizione del tempo scala è soddisfatta considerando la luminosità dovuta al raffreddamento della massa stellare, riferiamoci alle stelle di tipo solare e a quelle più brillanti per le quali una sorgente di energia di tale tipo darebbe un tempo scala inammissibilmente breve.

2. – L'energia termonucleare.

Se si scrivono le equazioni di equilibrio di un loro modello si giunge a calcolare, per l'interno, temperature e densità assai elevate, dell'ordine rispettivamente di $(13 \div 20) \cdot 10^6$ gradi e $(80 \div 150)$ g/cm^3. Tali temperature corrispondono ad energie cinetiche di pochi keV, assai basse rispetto a quelle cui sono abituati gli studiosi di particelle elementari, ma non così basse da precludere

la possibilità che vi siano protoni di energia sufficiente da poter statisticamente superare la barriera di potenziale di certi nuclei, e dar luogo a reazioni nucleari esotermiche in numero tale da giustificare la luminosità di queste stelle.

È appunto in questa direzione che si sono indirizzati BETHE e CRITCHFIELD [1], BETHE [2], SALPETER [3], FOWLER [4] ed altri.

La materia racchiusa in un ambiente le cui condizioni fisiche di temperatura e densità sono quelle ora ricordate, si trova allo stato di gas perfetto, con i nuclei atomici dotati di diverse energie cinetiche corrispondenti a una distribuzione maxwelliana delle velocità. Si tratta allora di calcolare il numero N, per grammo e per secondo, di incontri capaci di dar luogo a una reazione nucleare.

Il problema si risolve tenendo presente che la probabilità secondo cui avviene un certo tipo di reazione nucleare fra due particelle, dipende da tre fattori: *a*) dalla probabilità di incontro delle due particelle; *b*) dalla probabilità che una particella penetri attraverso la barriera di potenziale dell'altra; *c*) dalla probabilità che, una volta penetrata, la particella sia catturata o comunque modifichi la struttura interna del nucleo.

Per una esposizione dettagliata di tali questioni rimandiamo ai testi citati in fondo alla bibliografia. Adesso ci basta dire che se si considera un ambiente costituito da nuclei di due tipi 1 e 2 (distinti o uguali), il numero N di reazioni nucleari che avvengono per grammo e per secondo, è dato da una espressione di questo tipo:

$$N = \varrho x_1 x_2 f(A_1 A_2 Z_1 Z_2 T) \,, \tag{1}$$

dove ϱ indica la densità, x_1 e x_2 le percentuali in peso dei nuclei 1 e 2, e f una funzione dei pesi atomici A, delle cariche elettriche Z e della temperatura.

Se con N_2 si indica il numero di nuclei di tipo 2 per cm^3 e con M_2 la loro massa, l'espressione $N/N_2 = (M_2/x_2)N$ dà la probabilità per secondo che un nucleo prefissato di tipo 2 interagisca con un nucleo qualsiasi di tipo 1, e il suo inverso la vita media del nucleo 2 per la reazione considerata nelle condizioni fisiche ammesse.

Se nel campo di energia delle particelle urtanti ve ne è una E_1 coincidente con quella di un livello eccitato del nucleo derivante dalla reazione, allora la probabilità che dopo la penetrazione tale nucleo si formi e la reazione considerata abbia luogo assume un valore molto alto (risonanza) e fa sì che in un inter-

---

[1] H. A. BETHE e C. L. CRITCHFIELD: *Phys. Rev.*, **54**, 118 (1938).
[2] H. A. BETHE: *Phys. Rev.*, **55**, 434 (1939); *Ap. Journ.*, **92**, 118 (1940).
[3] E. E. SALPETER: *Phys. Rev.*, **88**, 547 (1952).
[4] W. A. FOWLER: *V^e colloque international d'Astrophysique* (Liège, 1954), p. 88.

vallo di energie di larghezza Γ intorno all'energia E_1 la curva: numero di reazioni utili — energia assume un massimo. Naturalmente sono molto importanti le energie E_1 che cadono nelle vicinanze del massimo che si ha in assenza di risonanza poichè allora il numero delle reazioni utili risulta notevolmente maggiore.

Una accurata trattazione teorica di tali reazioni e una esposizione dettagliata della sua applicazione al caso astrofisico si trova in [5].

Limitatamente al caso non risonante si constata che N è maggiore per i nuclei leggeri mentre è trascurabile per i nuclei pesanti. Se il peso atomico dei nuclei di tipo 2 supera 18 e quello dei nuclei di tipo 1 è 1, per densità dell'ordine di 100 e per temperature di $15 \cdot 10^6$ gradi la vita media non è inferiore a 10^{12} anni; la reazione avviene in misura trascurabile.

La fonte di energia per reazioni termonucleari, se c'è, deve essere ricercata nelle reazioni nucleari tra nuclei leggeri. Cominciamo colla più semplice possibilità: quella del protone la quale, secondo i dati più recenti, può così essere illustrata:

Reazione	Vita media (alla temperatura di $13 \cdot 10^6$ gradi e densità di 100 g/cm^3)
$^1H(p, \beta^+ \nu)^2D$	$14 \cdot 10^9$ anni
$^2D(p, \gamma)^3He$	5.7 s
$^3He(^3He, 2p)^4He$	10^6 anni

Si può essere tentati di continuare il processo di formazione di elementi seguendo, almeno per i nuclei leggeri, le reazioni dell'^4He con i nuclei presenti: ^1H, ^2D, ^3He. Ma tali reazioni conducono alla formazione di Li, Be, B i quali, reagendo a loro volta con i protoni presenti, danno luogo ad un nucleo composto che si disintegra di nuovo in particelle ^4He.

Sembrerebbe di dover constatare l'impossibilità di formare elementi più pesanti del ^4He, e di vedere nella catena di reazioni sopra illustrata la sintesi di quattro protoni in un nucleo di He l'unica possibile sorgente dell'energia stellare. Non solo ma anche la riprova che nell'interno delle stelle gli elementi leggeri: ^2D, ^3He, Li, Be, B, ecc. non possono esistere perchè se esistessero verrebbero in breve tempo disintegrati e consumati.

Nel 1939 il Bethe fece rilevare che, se per ipotesi ammettiamo nell'interno delle stelle la presenza di una certa percentuale originaria sia pure piccola (e ad ogni modo dell'ordine di quella osservata negli spettri stellari) di nuclei

(5) S. Hayakawa, C. Hayashi, M. Imoto and K. Kikuchi: *Progr. Theor. Phys.*, **16**, 507 (1956).

di carbonio e di azoto, è possibile mettere in evidenza una nuova sorgente di energia nucleare basandosi sulla proprietà di tali nuclei secondo la quale una loro interazione coi protoni comporta una reazione che non è una disintegrazione, bensì una emissione di un quanto γ mentre il protone catturato è trattenuto (quindi una trasformazione in un nucleo più pesante). Si arriva a formare per successiva cattura del protone e emissioni β^+, γ il nucleo ^{15}N il quale catturando un H dà luogo a un nucleo instabile disintegrandosi in una particella ^4He e un nucleo ^{12}C. Così il ciclo può ricominciare e il carbonio e l'azoto, mantenendosi in proporzioni inalterate nel tempo, agiscono come da intermediari, da « catalizzatori » in un processo che, anche questa volta, si può riassumere in una sintesi di quattro protoni in un nucleo di He.

Per la formula (1) risulta inoltre che i nuclei C e N non sono così « pesanti » da rendere troppo rari gli urti con penetrazione dei protoni e che anzi in questo modo, per temperature leggermente maggiori di quelle alle quali la catena protone protone diviene sensibile (ma sempre dell'ordine di quelle plausibili nell'interno stellare secondo le indicazioni delle integrazioni dei modelli stellari), si può disporre di una sorgente energetica ancora più efficace della prima.

Secondo i dati più recenti il ciclo di Bethe si può esprimere nella seguente forma:

Reazione	Vita media ($T = 13 \cdot 10^6$ gradi; $= 100$ g/cm^3
$^{12}C(p, \gamma)^{13}N$	$1.3 \cdot 10^7$ anni
$^{13}N(\beta^+ \nu)^{13}C$	7 min
$^{13}C(p, \gamma)^{14}N$	$2.7 \cdot 10^6$ anni
$^{14}N(p, \gamma)^{15}O$	$3.2 \cdot 10^8$ anni
$^{15}O(\beta^+ \nu)^{15}N$	82 s
$^{15}N(p, \alpha)^{12}C$	$1.1 \cdot 10^5$ anni

La temperatura e la densità scelte per il calcolo della vita media sono ancora quelle usate per la reazione p-p cioè dell'ordine della temperatura centrale e della densità centrale del sole.

In tal modo si è potuto individuare le due principali fonti di energia termonucleare che operano nell'interno delle stelle qualora si ammetta, per la seconda, una certa percentuale originaria di C e di N.

Indicando con α e con β rispettivamente le energie prodotte nei due cicli e con N il numero delle reazioni che avvengono per grammo e per secondo, definito dalla relazione (1) e calcolato per la reazione più lenta, si ha che l'energia prodotta per grammo e per secondo è:

$$\varepsilon_{pp} = \alpha N_{pp}, \qquad \text{(processo del primo tipo)}$$

$$\varepsilon_{CN} = \beta N_{CN}, \qquad \text{(processo del secondo tipo)}$$

Sostituendo a N_{pp} e N_{CN} il corrispondente valore calcolato dalla (1), e anzi approssimando la funzione f a un'espressione del tipo $f = hT^n$ ($h = \cos t$) (col che risulta: $\eta = -\frac{2}{3} + (1417/T^{\frac{1}{3}})[A_1A_2Z_1^2Z_2^2/(A_1 + A_2)]^{\frac{1}{3}}$) si ottiene, nell'intorno di $T = 13 \cdot 10^6$ °K:

$$\varepsilon_{pp} = K_{pp}\varrho T^{4.1} \text{ erg g}^{-1}\text{ s}^{-1}, \qquad K_{pp} = 0{,}28\, x_H,$$

$$\varepsilon_{CN} = K_{CN}\varrho T^{20.3} \text{ erg g}^{-1}\text{ s}^{-1}, \qquad K_{CN} = 1{,}66\, x_H x_{CN},$$

(T in unità $13 \cdot 10^6$ gradi).

Quando nel nucleo stellare c'è una certa percentuale di He occorre tener presente che la reazione $^3\text{He}(\alpha, \gamma)^7\text{Be}$ può competere efficacemente con la $^3\text{He}(^3\text{He}, 2\text{p})^4\text{He}$ poichè la sua sezione d'urto è più elevata di quanto si è ritenuto finora secondo le recenti misure di Holmgren e Johnston [6]. Hanno luogo allora le due seguenti reazioni:

$$^3\text{He}(\alpha, \gamma)^7\text{Be}(e^-, \nu)^7\text{Li}(\text{p}, \alpha)^4\text{He},$$

oppure

$$^7\text{Be}(\text{p}, \gamma)^8\text{B}(\beta^+\nu)^8\text{Be}(\alpha)^4\text{He},$$

con le quali la catena p-p si chiude.

Queste reazioni divengono importanti, secondo Fowler [7], per temperature superiori a $1.3 \cdot 10^7$ gradi e comportano una produzione di energia maggiorata del fattore

$$\Phi(\alpha) = 1 - \alpha + \alpha\left(1 + \frac{2}{\alpha}\right)^{\frac{1}{2}}$$

dove

$$\alpha \cong 5 \cdot 10^{18}\left(\frac{x_{He}}{4x_H}\right)^2 \exp\left[-100\, T^{-\frac{1}{3}}\right], \qquad T \text{ in unità } 10^6 \text{ gradi},$$

rispetto a quella che si ha quando la catena p-p è chiusa dalla reazione $^3\text{He}(^3\text{He}, 2\text{p})^4\text{He}$.

Una tale precisazione sposta, nel diagramma H-R, di circa mezza grandezza a sinistra la zona di delimitazione le stelle alimentate dalla catena p-p e quelle alimentate dal ciclo del C-N di cui diremo meglio in seguito. Non vengono alterate invece le considerazioni relative all'evoluzione di stelle in formazione per mancanza di una sufficiente percentuale di ^4He.

[6] H. D. Holmgren R. L. Johnston *Bull. Am. Phys. Soc.*, II, **3**, 26 (1958).
[7] W. A. Fowler: *Ap. Journ.*, **127**, 551 (1958).

Purtroppo quanto precede non è esente da qualche incertezza. Bisogna infatti aggiungere che esistono alcuni dubbi sulla reazione.

$$^1\mathrm{H(p,\ \beta^+\gamma)^2D}\ ,$$

che è più lenta di tutte quelle della prima catena.

Non sono state ancora eseguite misure sperimentali dirette per verificare i risultati teorici, a causa della sezione d'urto troppo piccola.

Dai risultati teorici si ha che la precedente reazione, che rappresenta il decadimento β dell'^{2}H, può avvenire o secondo la regola di selezione:

$$I - I' = 0\ ,$$

I = spin dello stato iniziale in unità h;
I' = spin dello stato finale;
oppure secondo la seguente

$$I - I' = \pm 1 - 0\ .$$

La prima è la regola di selezione di Fermi per transizioni prime permesse, la seconda quella di Gamow-Teller. Ora la produzione di energia è diversa naturalmente a seconda che vale l'una o l'altra; più precisamente i valori numerici che abbiamo portato nelle formule di produzione di energia di tutta la catena, si riferiscono al caso che le regole di selezione valide siano quelle di Gamow-Teller, ma si deve aggiungere che dal punto di vista teorico non c'è ragione di escludere quelle di Fermi. In quest'ultimo caso la produzione di energia sarebbe molto minore, a tal punto che si dovrebbe escludere la reazione p-p quale sorgente importante nella produzione di energia delle stelle di tipo solare e a temperatura centrale più bassa.

Non sembra che questo sia il caso perchè si è riusciti a costruire modelli stellari aventi caratteristiche bene adattabili a queste stelle con la reazione p-p, modelli che non potrebbero essere costruiti naturalmente col ciclo del C-N poichè la temperatura centrale non risulta sufficientemente alta.

Si può allora considerare la possibilità astrofisica di rappresentare le stelle di sopra con la reazione p-p come una riprova del fatto che nella reazione in discussione sono proprio le regole di selezione di Gamow-Teller e non quelle di Fermi, ad essere valide.

Anche a proposito del ciclo del C-N esiste una incertezza derivante dal fatto che non siamo sicuri della vita media della reazione $^{14}\mathrm{N(p,\gamma)^{15}O}$. Non si può escludere, anche se sembra improbabile, che esista qualche livello di risonanza alle basse energie in giuoco fra le particelle nell'interno delle stelle. Se un tale livello esistesse nell'intervallo $10 \div 50$ keV allora queste reazioni avverrebbero molto più velocemente e la vita media di tutto il ciclo diverrebbe quella del $^{12}\mathrm{C(p,\gamma)^{13}N}$ che è la più lenta dopo quella dell'$^{14}\mathrm{N(p,\gamma)^{15}O}$ e per la quale non sembra vi siano particolari livelli di risonanza che alterino la vita media indicata.

Per questo motivo il FOWLER [4] prima e BOSMAN-CRESPIN, FOWLER e HUMBLET [8] poi hanno preferito tabulare l'energia prodotta tanto nel caso che la reazione più lenta sia la $^{14}N(p, \gamma)^{15}O$ quanto nel caso invece che sia la $^{12}C(p, \gamma)^{13}N$.

Ne riportiamo i risultati in Fig. 2 nella quale è riprodotta anche la curva della generazione di energia dovuta alla catena p-p nell'ipotesi che valgano le regole si selezione di Gamow-Teller. In ordinate è compreso un fattore f che tiene conto del fatto che gli elettroni ancora legati ai nuclei pesanti modificano, con la loro carica negativa, la barriera di potenziale dei nuclei stessi. Di esso a tutt'oggi si hanno solo dei valori orientativi che non possono dirsi abbastanza soddisfacenti; tuttavia il suo valore non è molto diverso dall'unità.

Si vede allora molto chiaramente che alle basse temperature prevalgono le reazioni della catena p-p mentre alle temperature maggiori prevale il ciclo ^{12}C.

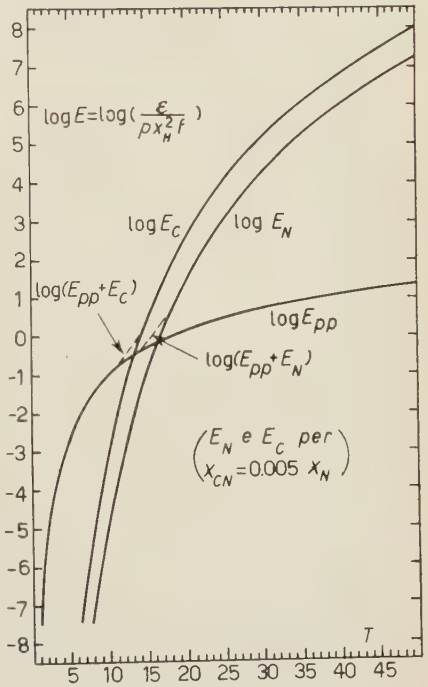

Fig. 2.

Recentemente SALPETER [9], FOWLER, BURBIDGE e BURBIDGE [10], MARION e FOWLER [11], CAMERON [12] hanno mostrato che anche il Neon potrebbe dar luogo a un ciclo secondo il seguente schema:

$$^{20}Ne(p, \gamma)^{21}Na$$
$$^{21}Na(\beta^+\nu)\,^{21}Ne$$
$$^{21}Ne(p, \gamma)^{22}Na$$
$$^{22}Na(\beta^+\nu)\,^{22}Ne$$
$$^{22}Ne(p, \gamma)^{23}Na$$
$$^{23}Na(p, \alpha)^{20}Ne \qquad \text{oppure} \qquad ^{23}Na(p, \gamma)^{24}Mg\ .$$

(8) D. BOSMAN-CRESPIN, W. A. FOWLER e J. HUMBLET: *Bull. Soc. Roy. des Sc. de Liége* (1954), p. 327.
(9) E. E. SALPETER: *Phys. Rev.*, **97**, 1237 (1955).
(10) W. A. FOWLER, G. R. BURBIDGE e E. M. BURBIDGE: *Ap. Journ.*, **122**, 271 (1955).
(11) J. B. MARION e W. A. FOWLER: *Ap. Journ.*, **125**, 221 (1957).
(12) A. G. W. CAMERON: *Stellar evolution.*, CRL-41 (Chalk River, Ontario, 1957).

È difficile valutarne esattamente l'importanza per la mancanza di precise informazioni intorno alla prima e terza reazione che sono le più lente (circa nella stessa misura). Stando ai dati più recenti, discussi nuovamente dal Cameron, sembra che tale ciclo sia importante, ma non ci sarebbe da meravigliare se, in seguito a informazioni ulteriori, si dovesse pervenire a una diversa conclusione.

C'è ancora da osservare, col Cameron, che l'ultima reazione del ciclo del Carbonio è 10^4 volte più probabile della seguente: $^{15}N(p, \gamma)^{16}O$, la quale spezzerebbe il ciclo e convertirebbe il ^{12}C in ^{16}O. Tale reazione deve però essere presa in esame nelle stelle di basso contenuto di metalli (popolazione 2) perchè il numero di cicli necessari per esaurire l'H è, per ogni atomo di carbonio o di azoto, molto superiore (proprio circa 10^4) a quello impiegato dalle stelle di popolazione 1 (circa 550). Può allora accadere che nelle prime questa reazione contribuisca ad alterare il rapporto $^{16}O/^{12}C$ arricchendo la stella di ^{16}O a spese del ^{12}C. Se ciò si verifica, in luogo delle prime tre reazioni si deve considerare le seguenti:

$$^{16}O(p, \gamma)^{17}F\,,$$

$$^{17}F(\beta^+\nu)\ ^{17}O\,,$$

$$^{17}O(p, \alpha)^{14}N\,,$$

che stabiliscono un ciclo di reazioni le quali convertono ancora H in He, e nelle quali l'^{16}O si sostituisce al ^{12}C nella funzione di catalizzatore. La reazione $^{16}O(p, \gamma)^{17}F$ è più lenta della $^{14}N(p, \gamma)^{15}O$ per un fattore circa $10^3 \div 10^4$ (nell'intervallo di temperatura compreso fra 20 e $60 \cdot 10^6$ gradi) e perciò nelle stelle di popolazione 2 l'O svolge probabilmente un ruolo molto importante.

Occupiamoci adesso di vedere se, facendo ricorso alla catena p-p e al ciclo C-N, è possibile calcolare la luminosità delle stelle nell'ordine di grandezza osservato.

Per questo occorre fare riferimento ai modelli relativi a varie stelle del diagramma di Russell e controllare, come si è già detto, se le caratteristiche fisiche calcolate coincidono con quelle osservate.

3. – Stelle di piccola luminosità.

Considerando modelli stellari che tengono conto che nella zona più esterna di queste stelle il materiale si trova in equilibrio convettivo, Osterbroek [13] mostra che è possibile ricostruire i punti rappresentativi delle stelle

[13] D. E. Osterbroek: *Ap. Journ.*, **118**, 529 (1953).

situate a destra del sole, nel ramo della sequenza principale del diagramma di Russell, supponendo che la reazione p-p si sviluppi in base alle condizioni fisiche di pressione e temperatura caratteristiche della zona centrale.

I modelli di Osterbroek non si adattano ai dati osservativi delle stelle di tipo spettrale più avanzato (M4 V e oltre) della sequenza principale, ma il LIMBER [14] dopo un'analisi critica di questi dati e considerando modelli costituiti da un'atmosfera in equilibrio radiativo, da una zona di ionizzazione dell'H e dell'He in equilibrio convettivo e infine dal corpo della stella nel quale l'H e l'He sono completamente ionizzati e l'equilibrio convettivo è anche adiabatico, trova un buon accordo fra i dati di osservazione e i modelli alimentati dalla reazione p-p.

Un altro lavoro assai interessante di P. NAUR [15] mostra anche l'influenza che la legge di opacità può avere sulla struttura dei modelli stellari alimentati dalla reazione p-p, confermandola quale sorgente di energia per le stelle di bassa luminosità.

4. – Il Sole.

Poichè per il sole i dati di osservazione sono molto precisi è possibile costruire modelli nei quali si può tener conto di effetti che per altre stelle ha meno senso considerare.

Il Sole si può considerare una stella fra le più luminose della classe prima considerata di stelle a piccola luminosità. Il suo modello grosso modo quindi si adatta alla serie di modelli calcolati da Osterbroek. Tuttavia per tener conto di un lavoro di KELLER e MEGEROTT [16] sul coefficiente di assorbimento, e del fatto pel quale col passare del tempo ($5 \cdot 10^9$ anni) nella zona radiativa interna il contenuto di idrogeno deve diminuire, verso il centro, per effetto della variabile velocità di trasformazione in elio alle diverse condizioni locali di temperatura e densità, SCHWARZSCHILD-HOWARD-HÄRM [17] hanno calcolato una serie di modelli simili a quelli di Osterbroek fra i quali assai bene si adatta ai dati osservati quello avente una temperatura centrale di $1.5 \cdot 10^7$ gradi e una densità di 130 gm/cm^3.

Poichè i modelli di questi autori sono stati calcolati assumendo per la formula della produzione di energia quella relativa alla reazione p-p mentre alla temperatura e densità ricavata anche il ciclo del C-N diviene importante, WEYMANN [18] ha calcolato una nuova serie di modelli, in tutto analoghi a quelli

[14] D. N. LIMBER: *Ap. Journ.*, **127**, 363 e 387 (1958).
[15] P. NAUR: *Dan. Mat. Fys. Medd.*, **30**, no. 16 (1956).
[16] G. KELLER e E. R. MEYEROTT: *Ap. Journ.*, **122**, 32 (1955).
[17] M. SCHWARZSCHILD, R. HOWARD e R. HÄRM: *Ap. Journ.*, **125**, 233 (1957).
[18] R. WEYMANN: *Ap. Journ.*, **126**, 208 (1957).

precedenti, salvo nella produzione di energia per la quale tiene conto, oltre che della reazione p-p, anche di quella del ciclo del C-N. Trova così che il miglioramento è di scarsa importanza pratica per il fatto che la zona in cui questo diviene sensibile è limitata a una ristrettissima zona centrale. Ciò dà fiducia che questi modelli inquadrano assai bene il Sole nella sua costituzione interna.

5. – Stelle ad alta luminosità della sequenza principale.

Sono assai bene comprese dai modelli che conducono a temperature centrali superiori a $1.5 \cdot 10^7$ gradi e che derivano la loro sorgente di energia dal ciclo del C-N. Quelle dei primissimi tipi spettrali (O-B 1,2) si trovano prevalentemente raggruppate in associazioni con caratteristiche sufficientemente ben determinate da poter concludere che esse si espandono e si disgregano in breve tempo. D'altra parte l'alta luminosità caratteristica delle stelle di cui parliamo è un indice sicuro della loro giovine età poichè l'H, che consumano in così grande quantità, non può rifornirle energeticamente che per un tempo assai limitato (ciclo C-N).

Pertanto mentre l'associazione si disgrega sia per un effetto di « evaporazione » sia per quello che le grandi nubi di materia interstellare provocano sui suoi membri, questi ultimi « invecchiano », di modo che si ha ragione di ritenere ([19]) che tali cluster e associazioni mentre rappresentano una sede di particolare attività tutt'ora efficiente della formazione delle stelle, svolgono probabilmente anche un ruolo rilevante nel « rifornire » il campo generale della galassia di stelle le quali, quando diventano membri di questo campo, non sono più giovanissime e hanno percorso il processo evolutivo caratteristico della loro massa e della loro età.

A tutt'oggi non sono stati studiati i processi evolutivi di tali stelle in tutto il loro svolgimento; tuttavia i modelli di Teyler ([20]), Kuswaha ([21]), Schwarzschild e Härm ([22]) indicano che la luminosità va aumentando col tempo mentre la temperatura effettiva diminuisce; assumono cioè lo stato di stella gigante. Studi di tal genere possono dirsi assai avanzati per stelle di massa leggermente superiore a quella del Sole (e ne parleremo a proposito delle stelle giganti), ma non per quelle di massa considerevolmente superiore.

Per adesso ci interessa riferire che gli studi procedono alacremente ed è probabile che quando saranno compiuti si potrà chiarire, oltre ad altri problemi delle stelle molto luminose, la natura e la fase evolutiva di quelle superluminose

---

([19]) J. H. Oort: *Ric. Astr.*, **5**, 63 (1958).
([20]) R. J. Teyler: *Ap. Journ.*, **120**, 336 (1954).
([21]) R. S. Kushwaha: *Ap. Journ.*, **125**, 242 (1957).
([22]) M. Schwarzschild e R. Härm: *Ap. Journ.*, **128**, 348 (1958).

che, per quanto rare, esistono tuttavia nella nostra galassia, hanno grandezza bolometrica assoluta -8, -9, -10 e perfino -11.8 ([23]) con tipi spettrali prevalentemente O e B.

6. – Le nane bianche.

Sono stelle di piccola luminosità e di elevata temperatura effettiva; hanno perciò un raggio assai piccolo. Le masse non sono ben note e solo in qualche caso è stato possibile determinarle indipendentemente dalla teoria della loro costituzione interna. Assumendo valori dell'ordine della massa solare ne è derivata una densità media estremamente elevata.

Come è noto per ogni valore della densità esiste una temperatura limite al di sotto della quale la degenerazione elettronica è notevole. Quando ciò accade la pressione esercitata dagli elettroni è molto importante rispetto a quella del gas perfetto dei nuclei; in molti casi è addirittura predominante e nell'equazione di stato la temperatura svolge un ruolo secondario; anzi, per elevati gradi di degenerazione, è addirittura trascurabile e tutto si svolge come avessimo a che fare con un gas di soli elettroni allo zero assoluto.

Nello studio della costituzione interna delle nane bianche occorre vedere se quel limite viene superato oppure no.

I modelli delle loro atmosfere, nelle quali la degenerazione è molto piccola e la temperatura svolge il suo ruolo normale nell'equazione di stato dei gas perfetti, calcolati assumendo la gravità corrispondente alla massa e al raggio ritenuti più probabili e con temperature effettive quali si valutano attualmente, mostrando che la densità sale così rapidamente da comportare degenerazione elettronica nonostante la temperatura dell'ordine di milioni di gradi. Da questo punto fino al centro perciò occorre introdurre l'equazione di stato del gas degenere mentre la temperatura, in virtù dell'elevata conduzione termica, può essere considerata costante e uguale al valore prima trovato.

Con una atmosfera di puro H si calcola che la temperatura dell'interno della stella è dell'ordine di $(6 \div 7) \cdot 10^7$ gradi ([24]). A questa temperatura la reazione p-p è ancora assai energetica e la luminosità dedotta con l'ultima formula scritta risulterebbe molto maggiore di quella osservata. La conclusione cui si giunge è pertanto la seguente: o nel loro interno non c'è H, salvo in una zona sottile nella quale avviene la produzione di energia (di importo naturalmente assai piccolo per la limitatezza della zona utile), oppure l'H c'è ma valgono le regole di selezione di Fermi per cui la produzione di energia della reazione p-p è ridotta praticamente a zero date le basse temperature.

([23]) A. D. Code e T. E. Houck: *P.S.A.P.*, 261 (1958).
([24]) E. Schatzman: Contr. I.A.P., serie B, no. 89 (1951).

La prima tesi è stata sostenuta da SCHATZMAN ([25]) il quale ha mostrato anche che l'H, sotto il forte campo gravitazionale, deve separarsi dagli elementi più pesanti e portarsi in una zona superficiale, per una specie di effetto di stratificazione assai noto. In questo caso occorre giustificare l'abbondanza di elementi pesanti la cui origine rimane molto oscura.

La seconda tesi è stata sostenuta da MESTEL ([26]) ma senza altra giustificazione che quella di eliminare una difficoltà altrimenti insormontabile. In tal caso la stella potrebbe derivare la sua luminosità dal raffreddamento della massa stellare, l'energia termica essendo sufficiente ad alimentarla per un tempo scala compatibile col loro numero.

L'autore di queste pagine ([27]) ha osservato che mettendosi da un punto di vista evolutivo e tenendo conto della incompressibilità della materia fin dal momento della sua degenerazione incipiente, è possibile valutare, per masse stellari inferiori a $\frac{1}{4} M_{\odot}$, un valore della temperatura centrale assai bassa, inferiore al limite oltre il quale la reazione p-p diviene sensibile pur mantenendo valide le regole di selezione di Gamow-Teller, che oggi vanno acquistando un sempre maggior interesse. Anche in tal caso naturalmente occorre appellarsi al raffreddamento della stella quale possibile e probabile fonte della bassa luminosità.

Occorre aggiungere che i dati di osservazione di questo tipo di stelle tanto importante sono assai incerti per cui è difficile affidarsi a una teoria piuttosto che a un'altra.

La loro massa, che è uno dei dati più importanti, è, come si è detto, la meno conosciuta. Su circa 250 nane bianche questo dato è noto, con precisione assai scarsa, per tre o quattro di esse (per una, Sirio B, si è ottenuta una massa $0{,}96\ M_{\odot}$, per le altre dell'ordine di $0.5\ M_{\odot}$). Anche le loro caratteristiche spettrali non sono note in maniera soddisfacente. P. COUTEAU ([28]) studiando la teoria delle fotosfere di tali stelle, sottolinea che esse sono costituite di idrogeno quasi puro e arriva alla conclusione che le temperature superficiali dovrebbero essere almeno di un ordine di grandezza superiori a quelle generalmente ammesse (circa 300 000 gradi) per comprendere alcune caratteristiche spettrali osservate. Se così fosse, la luminosità di queste stelle sarebbe elevata, il massimo dello spettro cadendo nel lontano ultravioletto.

È difficile dare un giudizio sulla accettabilità di tale risultato e specialmente sulla possibilità di adattarlo a certi dati osservativi di indice di colore ([29]).

Tuttavia dopo quanto precede vorremmo richiamare l'attenzione sulla importanza che ha la conoscenza delle regole di selezione nella prima reazione

([25]) E. SCHATZMAN: *Le spectre des naines blanches* (Copenhagen, 1949).
([26]) L. MESTEL: *M. N.*, **112**, 583 (1952).
([27]) A. MASANI: *Mem. S.A.I.*, **27**, 517 (1956).
([28]) P. COUTEAU: *Ann. Astroph. Suppl.*, no. 3 (1957).
([29]) W. J. LUYTEN: *Ap. Journ.*, **116**, 283 (1952).

della catena p-p per decidere non solo quale è la sorgente di energia delle stelle a bassa luminosità, ma anche la loro composizione chimica interna; se cioè possono essere costituite di idrogeno oppure se nel loro interno ci sono solo elementi pesanti. Tale questione si inserisce allora nel problema più generale dell'evoluzione stellare.

Se valessero le regole di selezione di Fermi non si potrebbe pensare alla catena p-p neppure per le stelle più fredde del Sole appartenenti alla sequenza principale. Tali stelle verrebbero a costituire una enigma energetico non potendoci rivolgere al ciclo C-N che a queste temperature è inefficace. A meno di non pensare contemporaneamente alla presenza di un livello di risonanza per la 4° reazione del ciclo che sposti sulla prima l'ufficio di reazione pilota (nel tempo). Allora il ciclo diverrebbe più energetico e potrebbe essere esteso a tutto il ramo della sequenza principale.

È bene ricordare in appoggio a tale tesi che la sequenza principale non mostra due pendenze diverse col loro punto di incontro nelle stelle del tipo solare, come dovrebbe essere teoricamente se quelle a destra (del Sole) fossero alimentate dalla reazione p-p e quelle a sinistra dal ciclo C-N. Ma si deve aggiungere anche che dal punto di vista teorico la diversità della pendenza dovrebbe essere piccola, e quindi potrebbe risultare mascherata dagli errori di osservazione per la verità assai notevoli.

Se ci si riferisce ai diagrammi colore grandezza di ammassi di popolazione I è difficile mettere in evidenza la diversità di pendenza cercata poichè sono scarsi i dati osservativi, specie dalla parte delle basse luminosità, e non consentono un sicuro tracciamento della linea media. Fa eccezione l'ammasso aperto delle Hyadi ([30]) il quale mostra un leggero ma netto cambiamento di pendenza proprio nella zona solare (un pò a destra del Sole) e dell'importo che ci si può attendere teoricamente.

Esso è tuttavia dubbio se ci riferiamo al diagramma H-R anche solo relativo alle stelle vicine ([31]).

La via migliore di risolvere la questione è naturalmente quella di eseguire misure dirette per vedere se un tale livello di risonanza esiste oppure no. Perciò con molto interesse si deve attendere il risultato dell'esperienza che il Fowler ([32]) sta conducendo a questo scopo.

Esse potranno indirettamente gettare luce anche sulla dibattuta questione delle regole di selezione nella prima reazione della catena p-p perchè, se negativa, le stelle a destra del Sole della sequenza principale potranno essere assunte quale riprova astrofisica della validità delle regole di selezione di Gamow-Teller; se positiva invece la questione rimarrà aperta.

([30]) H. L. Johnson e C. F. Knuckles: *Ap. Journ.*, **122**, 209 (1955).
([31]) H. L. Johnson e W. W. Morgan: *Ap. Journ.*, **117**, 313 (1953).
([32]) W. A. Fowler: *P.S.A.P.*, **68**, 505 (1956).

7. – Le stelle giganti.

Venendo a parlare delle fonti energetiche delle stelle giganti e supergiganti si va incontro a due gravi difficoltà: da una parte i modelli stellari aventi un grande raggio danno una temperatura centrale piccola, dall'altra le stelle giganti hanno una luminosità molto alta. Un modello stellare che voglia adattarsi a una stella gigante, comporta una distribuzione di temperature cui corrisponde una produzione di energia termonucleare in generale molto minore di quella irraggiata dalla stella.

Nel 1947 HAYASCHI ([33]) e nel 1949 HOYLE e LITTLETON ([34]) e HAYASCHI ([35]) osservarono che era possibile superare le difficoltà considerando la stella suddivisa in due parti; una esterna e una interna, quest'ultima con peso molecolare medio più alto della prima.

Poichè ciò era fisicamente possibile solo come effetto della conversione in He di una opportuna quantità di H, con questa osservazione ci si metteva da un punto di vista evolutivo e si considerava la stella gigante sufficientemente vecchia da rendere ragione appunto di tale diversità.

Altri autori confermarono in seguito questa osservazione calcolando con maggiore precisione e con maggiore cura dei dettagli modelli di giganti rosse: LI HEN e SCHWARZSCHILD ([36]), C. M. e H. BONDI ([37]), OKE e SCHWARZSCHILD ([38]), GARDINER ([39]), ROY ([40]). Il problema sembrava avviato a soluzione quando un importante tentativo di DUMEZIL-CURIEN ([41]) riportò la questione in discussione. DUMEZIL-CURIEN calcolò un modello stellare di gigante rossa tenendo conto del fatto che dal nucleo centrale convettivo non si passa a una zona esterna interamente in equilibrio radiativo ma a una regione esterna anch'essa divisa in due zone quella più prossima alla superficie, assai estesa, risultando in equilibrio convettivo. (La parte più superficiale era inoltre trattata seguendo la teoria dei modelli di atmosfere stellari).

Questa precisazione assai importante e necessaria ha però condotto a temperature centrali troppo basse ($6.8 \cdot 10^6$ °K) insufficienti ad alimentare energeticamente la stella. In questo lavoro non sono stati considerati certi valori, ben plausibili, di alcuni parametri arbitrari quali ad esempio quelli cui è legata

---

([33]) C. HAYASCHI: *Progr. Theor. Phys.*, **2**, 127 (1947).
([34]) F. HOYLE e R. A. LITTLETON: *M. N.*, **109**, 614 (1949).
([35]) C. HAYASCHI: *Phys. Rev.*, **75**, 1619 (1949).
([36]) LI HEN e M. SCHWARZSCHILD: *M. N.*, **109**, 631 (1949).
([37]) C. M. BONDI e H. BONDI: *M. N.*, **110**, 287 (1950).
([38]) J. B. OKE e M. SCHWARZSCHILD: *Ap. Journ.*, **116**, 317 (1952).
([39]) J. G. GARDINER: *M. N.*, **111**, 102 (1951).
([40]) A. E. ROY: *M. N.*, **112**, 484 (1952).
([41]) P. DUMEZIL-CURIEN: *Ann. d'Astroph.*, **17**, 197 (1954).

l'estensione della zona convettiva superficiale e perciò rimane aperta la possibilità di risolvere in maniera soddisfacente e definitiva anche questa importante questione.

Anzi HOYLE e SCHWARZSCHILD [42] in uno studio sulle stelle giganti di popolazione 2 di cui diremo subito, rivolgono brevemente l'attenzione sul fatto che i modelli delle prime possono adattarsi alle seconde col solo cambiamento del contenuto di elementi pesanti (il rapporto metalli/H è circa 10^{-4} nelle stelle di popolazione 1, e circa $7 \cdot 10^{-6}$ in quelle di popolazione 2). Vedremo però che è difficile pensare che i due gruppi di stelle differiscono semplicemente per tale contenuto e hanno una struttura interna assai simile.

Fra i meriti più importanti della scoperta del meccanismo pel quale l'energia termonucleare si produce nell'interno delle stelle si deve sottolineare quello che ha permesso di affiancare alla così detta teoria α, β, γ della formazione degli elementi, una seconda teoria a lunga scala dei tempi che insieme sembra dia ragione dei diagrammi colore grandezza degli ammassi globulari e di precisare una visione evoluzionistica nella quale le popolazioni stellari 1 e 2 hanno preso un posto assai ben definito.

È chiaro infatti che se nell'interno delle stelle della sequenza principale l'H si trasforma in He, l'H andrà impoverendosi mentre l'He diverrà sempre più abbondante. Il peso molecolare medio del nucleo aumenterà mentre, in assenza di mescolamento fra interno ed esterno, il peso molecolare medio di quest'ultima zona rimarrà costante e uguale a quello « originario ».

Si può allora calcolare una successione di modelli a peso molecolare medio interno diverso ma con lo stesso peso molecolare medio esterno e la stessa massa. Ciascuno rappresenterà una stella in successive fasi di evoluzione intervallate dal tempo (facilmente calcolabile in base alla luminosità) necessario perchè la massa centrale cambi il peso molecolare medio nella misura voluta.

I risultati di questi calcoli eseguiti oltre che dagli autori ricordati, da SCHÖNBERG e CHANDRASEKHAR [43], SANDAGE e SCHWARZSCHILD [44], hanno dimostrato che i raggi di tali modelli crescono con l'aumentare del rapporto μ_i/μ_e (μ = peso molecolare medio; i = interno, e = esterno) cresce anche la luminosità mentre la temperatura effettiva che ne risulta rimane praticamente costante, eccetto ai più alti valori del rapporto μ_i/μ_e nei quali tende a diminuire notevolmente. Ma in questa fase di evoluzione il nucleo centrale contiene ben poco idrogeno e le sorgenti di energia vengono a mancare. La stella allora va incontro a uno stato che può essere schematizzato da un nucleo isotermo (per mancanza di quella fonte energetica che stabilisce un gradiente termico) in fase di contrazione gravitazionale circondato da una zona (shell) ad alta temperatura,

---

([42]) F. HOYLE e M. SCHWARZSCHILD: *Ap. Journ. Suppl.*, **2**, 1 (1955).
([53]) M. SCHÖNBERG e S. CHANDRASEKHAR: *Ap. Journ.*, **96**, 161 (1942).
([44]) A. R. SANDAGE e M. SCHWARZSCHILD: *Ap. Journ.*, **116**, 475 (1952).

contenente H e capace di alimentare energeticamente la stella tramite il ciclo del C-N.

Questi concetti hanno trovato una significativa applicazione nell'interpretazione dei diagrammi H-R di stelle di popolazione 2 (Fig. 3) tanto che oggi, dopo i lavori di SANDAGE e SCHWARZSCHILD e specialmente dopo quelli di HOYLE e SCHWARZSCHILD ([45,42]) e HAYASHI ([46]) possiamo dire di avere delle idee assai chiare intorno alla evoluzione stellare di tali aggruppamenti di stelle.

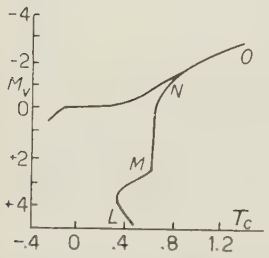

Fig. 3. - Diagramma di Hertzsprung-Russell per le stelle di popolazione 2.

Poichè si ha ragione di ritenere (SANDAGE ([47,48])) che le stelle più luminose di questi ammassi non hanno una massa maggiore di (1.1 ÷ 1.2) volte la massa del Sole, HOYLE e SCHWARZSCHILD hanno seguito la fase evolutiva di una tale stella dopo che il nucleo è divenuto isotermo e costituito interamente di He. Mano a mano che la shell (a $20 \cdot 10^6$ °K) brucia H il nucleo di He cresce mentre il punto rappresentativo si sposta verso M. In M il nucleo contiene il 20% della massa ed ha un raggio molto grande.

A questo punto le condizioni al contorno superficiale non possono essere più semplicemente quelle valide in prima approssimazione per le stelle nane e cioè:

$$T \to 0\,, \qquad \varrho \to 0\,, \qquad \text{per } r \to R$$

bensì le seguenti:

$$T \to T_{\text{eff}} \qquad \varrho \to \frac{\mu H G M}{K R^2} \qquad \text{per } r \to R.$$

La necessità di introdurre alla superficie tali condizioni fisiche più precise già suggerita da HOYLE e LITTLETON ([34]), rispettata da GARDINER ([39]) e DUMEZIL-CURIEN ([41]), comporta, nei modelli degli autori, l'introduzione di importanti correnti di convezione superficiali.

Queste condizioni al contorno si presentano come condizioni critiche nel senso che è ad esse e alle correnti convettive che ne derivano che si deve se la traccia evolutiva cambia, in M, e segue la direzione M-N-O. In M la massa del nucleo è circa 0.33 volte la massa totale mentre in O è circa 0.50.

([45]) F. HOYLE e M. SCHWARZSCHILD: *Ap. Journ.*, **121**, 776 (1955).
([46]) C. HAYASHI: *Progr. Theor. Phys.*, **17**, 737 (1957).
([47]) A. R. SANDAGE: *V^e coll. Int. d'Astr.* (Liège, 1954), p. 255.
([48]) A. R. SANDAGE: *Ap. Journ.*, **126**, 326 (1957).

Le condizioni di temperatura e densità centrali che si hanno per una stella il cui punto rappresentativo si trova oltre la zona L di figura, sono tali da dover tener presente la degenerazione elettronica ma nell'ultimo tratto M-O, mano a mano che il nucleo assume una massa maggiore, la degenerazione (di grado mai molto elevato) consente un processo di contrazione che toglie l'isotermicità al nucleo e che alla fine prende il sopravvento sulla stessa degenerazione. In O la temperatura della shell risulta di $(4 \div 5) \cdot 10^7$ K° mentre al centro $T_c = 1.2 \cdot 10^8$ °K ($\varrho_c \cong 10^4$); la zona esterna, in equilibrio convettivo, occupa circa il 90% del raggio.

Hoyle e Schwarzschild hanno trattato la zona degenere trascurando il contributo, in verità non trascurabile, dei nuclei (non degeneri) alla pressione; inoltre hanno raccordato in maniera non esatta la regione radiativa e quella convettiva. A eliminare tali approssimazioni ha provveduto C. Hayashi ([16]), ma le principali conclusioni di prima sostanzialmente non cambiano. L'autore ha fatto notare inoltre che il ramo delle giganti può essere assai bene spiegato anche se l'inviluppo è composto di H puro e la sorgente energetica deriva dalla reazione p-p che avviene nella zona attigua al nucleo centrale di He. In tal caso anzi è molto importante tener conto della pressione ionica nel nucleo isotermo degenere e il tenerne conto fa sì che il punto rappresentativo del diagramma H-R di stelle di popolazione 2 si trova nella metà del ramo orizzontale superiore.

È interessante chiedersi cosa accade di una stella che si trova nello stato finale del processo evolutivo descritto.

A temperature dell'ordine di 10^8 °K le energie cinetiche delle particelle sono tali da poter superare, con sensibile probabilità, la loro barriera di potenziale e si può innescare la seguente reazione termonucleare:

$$^4\mathrm{He} + {}^4\mathrm{He} + 95\ \mathrm{keV} \rightleftarrows (^8\mathrm{Be}) ,$$

$$(^8\mathrm{Be}) + {}^4\mathrm{He} \rightarrow {}^{12}\mathrm{C} + \gamma + 7.37\ \mathrm{MeV} .$$

Il ^{8}Be è instabile per disintegrazione in 2 ^{4}He con una vita media dell'ordine di 10^{-18} s, ma poichè per la sua formazione si richiede l'energia di 95 KeV, paragonabile all'energia termica corrispondente alla temperatura di 10^8 gradi, una piccola frazione di materiale stellare (circa $1/10^{11}$ per $\varrho = 10^3$) si trova sotto forma di ^{8}Be in stato di equilibrio dinamico e consente la formazione del ^{12}C.

Intorno a queste temperature si possono innescare anche le seguenti due reazioni:

$$^{12}\mathrm{C} + {}^4\mathrm{He} \rightarrow {}^{16}\mathrm{O} + \gamma + 7.15\ \mathrm{MeV} ,$$

$$^{16}\mathrm{O} + {}^4\mathrm{He} \rightarrow {}^{20}\mathrm{Ne} + \gamma + 4.75\ \mathrm{MeV} .$$

La prima di queste tre reazioni è stata discussa da Öpik [49] e da Salpeter [50] i quali hanno così richiamato l'attenzione su un tipo di sorgente di energia nucleare che, mentre interviene ad alimentare le stelle in un certo punto della fase gravitazionale, apre la porta alla teoria della formazione degli elementi, alla quale già Hoyle [51] aveva dato un valido contributo, ma per la cui comprensione l'estremamente breve vita media del ^{8}Be (e del ^{5}Li) sembrava un ostacolo insormontabile.

Salpeter ha calcolato l'energia prodotta nella prima delle tre reazioni, intorno alla temperatura di $2\cdot10^8$ °K, e nella sua breve nota [50] riporta, senza i dettagli del calcolo, una espressione la quale però risulta maggiorata di un fattore $10^3 \div 10^4$ probabilmente a causa del fatto, secondo Öpik [52], che l'Autore non deve avere tenuto conto della probabilità di penetrazione.

L'espressione precisa della produzione di energia per la reazione in parola è rimasta incerta fino a poco tempo fa, ma poichè non si sapeva se esiste nel ^{12}C uno stato eccitato di energia corrispondente a quelle stellari, Salpeter lo aveva ammesso mentre Öpik non lo considerava, mancandone l'evidenza sperimentale. La questione era molto importante poichè i due punti di vista comportano un fattore dell'ordine di $10^9 \div 10^{10}$: va rilevato tuttavia che data l'alta sensibilità rispetto a $T(\sim T^{18})$ l'incertezza si rifletteva in definitiva nella valutazione precisa di T alla quale la produzione di energia diviene importante: $2\cdot10^8$ °K se il livello eccitato esiste, $(3 \div 4)\cdot10^8$ °K se non esiste.

Nel 1955 Ajzenberg e Lauritzen [53] hanno studiato i livelli eccitati di bassa energia del ^{12}C e ne hanno individuato uno a 7.65 MeV; nel 1956 il Fowler [32] aveva già rilevato che esso poteva servire quale livello di risonanza termonucleare nella reazione di cui si parla. Contemporaneamente Obi e collaboratori [54] hanno valutato le formule di quelle reazioni tenendo conto di quel livello e più precisamente ancora Hayakawa, Hayashi, Imoto, Kikuchi hanno dato un'espressione più accurata e precisa [5] di ε relativa a tutte e tre le reazioni di sopra, che è la seguente

$$\varepsilon = \frac{1.64\cdot10^{11-(1\cdot75/T)}}{T^3}\,\varrho^2 f x_{\mathrm{He}}^3 \text{ erg g}^{-1}\text{ s}^{-1}.$$

f = fattore dell'ordine dell'unità, T in unità 10^8 °K.

Essa risulta maggiore di un fattore 10^6 rispetto a quella data da Salpeter (per $T = 2\cdot10^8$ °K, $\varrho = 2.5\cdot10^4$) e la sua importanza diviene sensibile anche a temperature di $1\cdot10^8$ °K. Il grafico di Fig. 4 ne indica l'andamento in fun-

---

[49] J. E. Öpik: *Proc. Roy. Irish. Acad.*, A **54**, no. 4 (1951).

[50] E. E. Salpeter: *Ap. Journ.*, **115**, 326 (1952).

[51] F. Hoyle: *M. N.*, **106**, 343 (1946).

[52] J. E. Öpik: *V^e coll. Int. d'Astr.* (Liège, 1954), p. 131.

[53] F. Ajzenberg e T. Lauritsen: *Rev. Mod. Phys.*, **27**, 77 (1955).

[54] K. Nakagawa, T. Ohmura, H. Takebe e S. Obi: *Progr. Theor. Phys.*, **16**, 389 (1956).

zione di T; è interessante confrontarlo con quello di Fig. 2 per dedurne che il ciclo del carbonio è più energetico di questo processo, anche alle temperature minori, pur senza tener conto di un eventuale livello di risonanza alle bassissime energie.

È bene aggiungere che gli autori si sono valsi dei recenti livelli di eccitazione trovati nel ^{16}O, ^{20}Ne, in prossimità dell'energia corrispondente alla somma delle masse delle particelle interagenti. È risultato infatti che anche nel ^{20}Ne esiste un livello di eccitazione di poco superiore a tali energie e che agisce quindi come un livello di risonanza.

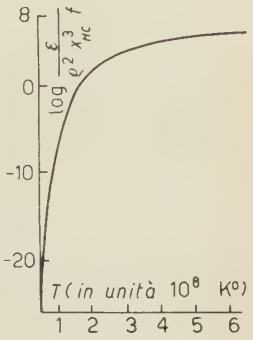

Fig. 4.

Nel ^{16}O questa situazione non esiste poichè il livello di eccitazione più vicino a tale somma ha un'energia inferiore, mentre quello superiore ne ha una troppo alta. Tuttavia il livello inferiore rende efficace l'urto non risonante a causa della notevole probabilità di dintegrazione. Riportiamo in Fig. 5 gli schemi dei livelli del ^{12}C, ^{16}O, ^{20}Ne, situati in prossimità delle energie interessanti l'urto, data la loro importanza nelle reazioni termonucleari che dovrebbero innescarsi nelle stelle a nucleo centrale estremamente caldo.

Da quanto precede risulta chiaro che lo studio delle fonti energetiche stellari ha portato come conseguenza quello dell'evoluzione delle stelle e della formazione degli elementi. È essenziale pertanto, al fine di una precisa comprensione dell'energetica stellare, porre attenzione ai seguenti lineamenti riguardanti il processo evolutivo di una stella in rapporto all'intervento di questa o quella fonte di energia.

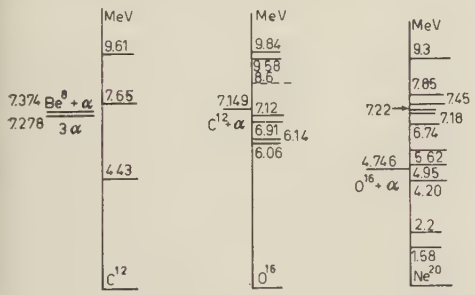

Fig. 5.

La teoria della costituzione interna delle stelle, studiata nell'aspetto evolutivo, ha preso in considerazione il fatto che col tempo varia il peso molecolare medio interno dovuto alla continua trasformazione dell'H in He. Con riferimento a una data stella, la temperatura centrale è considerata costante durante questa fase poichè si prova che per il tempo necessario alla trasformazione in He del contenuto di H interno essa non cambia apprezzabilmente (Roy [10]). È chiaro allora che per questa via una stella alimentata dalla catena p-p non può, nel seguito, essere alimentata dal ciclo del C-N. Le stelle alimentate da questo ciclo debbono raggiungere lo stato termonucleare condensandosi dalla materia interstellare superando la fase p-p direttamente, ancora in fase gravitazionale.

8. – La fase gravitazionale.

Per studiare la fase di innesco delle reazioni nucleari di cui si è detto (p-p, C-N, ^{12}C ^{16}O ^{20}Ne) riferiamoci a un importante lavoro del LEVÉE ([55]) il quale ha considerato una serie di modelli che derivano la loro energia dalla contrazione gravitazionale. Quei modelli sono validi fino al momento in cui la temperatura centrale, continuamente crescente per effetto della contrazione, diviene tale da produrre reazioni termonucleari in misura sufficiente da dare energia paragonabile a quella irraggiata per effetto della contrazione gravitazionale. Quando ciò accade la stella cessa di contrarsi e si modella su uno schema di equilibrio alimentato da sorgenti termonucleari. Ora l'energia irraggiata in fase di contrazione è data, secondo LEVÉE, da:

$$L = 9.92 \cdot 10^{24} \frac{\mu^{7.5} M^{5.5}}{K_0 R^{0.5}}$$

(L, M, R in unità solari; K_0 = fattore dell'espressione che dà il coefficiente di assorbimento $K = K_0 \varrho T^{-3.5}$).

Posto genericamente:

$$\varrho = \varrho_0 f(x) , \qquad T = T_0 \varphi(x) , \qquad \varepsilon = \varepsilon_0 \varrho^\delta T^\eta ,$$

dove

$$\varrho_0 = \frac{M}{4\pi R^3} , \qquad T_0 = \frac{\mu H G}{K} \frac{M}{R} , \qquad x = \frac{r}{R} ,$$

avremo nella fase che ci interessa:

$$L = \frac{1}{L_\odot} \int_0^R 4\pi \varrho r^2 \varepsilon \, \mathrm{d}r = \frac{\varepsilon_0}{(4\pi)^\delta} \left(\frac{\mu H G}{K} \right)^\eta M_\odot^{\eta+\delta+1} R_\odot^{-\eta-3\delta} M^{\eta+\delta+1} R^{-\eta-3\delta} \cdot$$

$$\cdot \int_0^1 x^2 f^{\delta+1}(x) \varphi^\eta(x) \, \mathrm{d}x = 9.92 \cdot 10^{24} \frac{\mu^{7.5} M^{5.5}}{K_0 R^{0.5}}$$

(L, M, R in unità solari).

Di qui si ha subito il raggio relativo alla fase di passaggio:

$$R^{\eta+2.5} = \frac{(2.24 \cdot 10^7)^\eta K_0 \varepsilon_0 I(\eta) \mu^{\eta-7.5} M^{\eta-3.5}}{4.25 \cdot 10^{25}}$$

(abbiamo indicato con $I(\eta)$ il valore dell'integrale) e quindi la temperatura

([55]) R. D. LEVÉE: *Ap. Journ.*, **117**, 200 (1956).

centrale relativa a questa fase:

$$T_c = 1.95 \cdot 10^7 \mu \frac{M}{R} ,$$

dove R è dato dalla precedente espressione. È importante tener presente l'espressione di Levée dell'inverso del tempo scala della contrazione

$$\frac{1}{R}\frac{\mathrm{d}R}{\mathrm{d}t} = 5.98 \cdot 10^{-8} \cdot \frac{LR}{M^2}\frac{1-\gamma}{3\gamma - 4} \text{ anni}^{-1} = -\frac{3.98 \cdot 10^{17}}{K_0} \mu^{7.5} M^{3.5} R^{0.5} \qquad \left(\gamma = \frac{5}{3}\right).$$

Per valutare l'integrale $I(\eta)$ basta tener presente che le funzioni $f(x)$ e $\varphi(x)$ possono essere assunte uguali a quelle di Levée le quali d'altronde sono assai vicine alle analoghe funzioni del modello standard (cosa facilmente giustificabile se teniamo presente la relativa funzione che ha la distribuzione delle sorgenti energetiche agli effetti della costituzione della stella). Scelto $\delta = 1$ abbiamo eseguito l'integrazione nel caso $\eta = 4$, $\eta = 5$, $\eta = 18$ ottenendo rispettivamente i seguenti risultati: $I(\eta) = 15,\ 7.5,\ 0.15$.

Il corrispondente valore di ε_0 si ricava subito servendoci dei dati numerici di Bosman Crespin, Fowler, Humblet ([8]), Si trova così che una massa solare segna il limite di separazione fra quelle che, condensandosi, vengono alimentate dalla reazione p-p e quelle che vengono alimentate dalla reazione C-N.

Naturalmente per le prime occorre che la massa non sia inferiore al limite già detto ([27]) poichè in tal caso la stella manifesta i fenomeni della degenerazione elettronica. Ad ogni modo masse superiori a quel limite ma inferiori a quella del Sole, date le basse temperature involte e la conseguentemente lunga vita media della reazione p-p confrontata col tempo scala della stella in fase contrazionale, producono, prima di passare alla fase termonucleare, una quantità di He trascurabile.

Questa conclusione rimane approssimativamente valida anche se consideriamo che prima della fase p-p la stella, in contrazione gravitazionale, passa per le fasi in cui vengono distrutti i nuclei leggeri ^{2}D, ^{3}He, litio, berilio, boro. I primi, tramite le reazioni:

$$^2\mathrm{D(p, \gamma)^3He} , \qquad ^2\mathrm{D(d, n)^3He} , \qquad ^2\mathrm{D(d, p)^3H} ,$$

le quali anche in base alla abbondanza notevole del ^{2}D rispetto all'H (10^{-4} in peso nei meteoriti e sulla terra), possono essere assai energetiche e rappresentare una fonte di energia comparabile a quella gravitazionale per un periodo di tempo non del tutto trascurabile, a temperature centrali dell'ordine di 0.5 $(1 \div 2) \cdot 10^6$ °K rispettivamente per masse minori, uguali, maggiori di quella solare.

La rispettiva importanza di queste reazioni dipende dal rapporto $x_{\mathrm{D}}/x_{\mathrm{H}}$

e naturalmente dalla temperatura e dalla densità. Nelle stelle meno calde prevale la prima, nelle altre sono quasi ugualmente importanti.

È interessante considerare la seconda reazione che produce neutroni di circa 2.5 MeV. Poichè il mezzo in cui si vengono a trovare è costituito prevalentemente di H e poichè a queste energie la sezione d'urto per diffusione H-n è maggiore di quella per assorbimento, tali neutroni vengono termalizzati. In queste condizioni la sezione d'urto dell'H per assorbimento non è ancora alta (~ 5 milibar) ma, sempre per la sua preponderanza rispetto agli altri elementi, l'H catturerà un numero notevole di neutroni formando ^{2}D. La reazione ^{3}He(n, p)^{3}H che ha una sezione d'urto assai alta (~ 80 bar) può costituire un importante fattore di eliminazione dei neutroni solo se il ^{3}He supera, in concentrazione di massa, l'H per un fattore 10^{-4}.

Il ^{3}H decade in ^{3}He con una vita media dell'ordine di 12 anni.

A temperature non superiori a $4 \cdot 10^6$ K° le seguenti reazioni:

$$^6\mathrm{Li}(\mathrm{p}, \alpha)^3\mathrm{He}\,, \qquad ^7\mathrm{Li}(\mathrm{p}, \alpha)^4\mathrm{He}\,,$$

$$^9\mathrm{Be}(\mathrm{p}, \mathrm{d})^8\mathrm{Be}(2\alpha)\,, \qquad ^9\mathrm{Be}(\mathrm{p}, \alpha)^6\mathrm{Li}\,,$$

$$^{10}\mathrm{B}(\mathrm{p}, \alpha)^7\mathrm{Be}\,, \qquad ^7\mathrm{Be}(\mathrm{e}, \nu)^7\mathrm{Li}\,, \qquad ^{11}\mathrm{B}(\mathrm{p}, \alpha)^8\mathrm{Be}(2\alpha)\,,$$

distruggono litio, berilio, boro e non costituiscono una importante fonte di energia termonucleare a causa della scarsità di tali elementi nell'interno stellare.

L'^{4}He è stabile fino a temperature molto alte come si è visto e il ^{3}He viene convertito in ^{4}He a temperature interessanti la catena p-p.

Perciò agli effetti di una eventuale arresto della fase gravitazionale delle stelle solo le reazioni del deuterio possono avere un certo peso in stelle di massa inferiore a quella del Sole.

Per stelle di massa maggiore anche l'energia proveniente dalla catena p-p è soverchiata da quella prodotta dalla contrazione gravitazionale. La massa stellare passa quindi dalla fase contrazionale a quella termonucleare relativa al ciclo del C-N superando e scavalcando la fase p-p.

Seguendo questo processo sembrerebbe potersi attendere che per masse assai più grandi di quella del Sole anche la fase C-N possa essere coperta da quella gravitazionale. Ma eseguendo i calcoli con le formule di sopra (corrette come diremo subito) si vede che ciò non è possibile perchè il ciclo del C-N interviene sempre a superare energeticamente la fase gravitazionale. Ciò è dovuto all'effetto della pressione di radiazione che impedisce alle grandi masse di raggiungere temperature centrali molto elevate. Levée nei suoi modelli non ha tenuto conto della pressione di radiazione, ma si può osservare che nel caso in cui il rapporto β fra la pressione del gas e quella totale rimane costante attraverso la stella, le sue formule si trasformano in quelle che tengono conto

della pressione di radiazione semplicemente moltiplicando μ per β. Basta infatti dare a P il significato di pressione totale e sostituire μ con $\beta\mu$. Il passaggio relativo alle variabili omologicamente invarianti non cambia, e il sistema di equazioni differenziali cui esse soddisfano rimane inalterato.

Il considerare β costante attraverso la stella è il caso del modello standard di ben nota validità. Con le formule di sopra così corrette riferiamoci ad esempio a una massa dell'ordine di 100 $M_\odot$ considerata come un limite superiore delle masse e assumiamo per essa [56] $\beta = 0.65$. La temperatura centrale della fase di passaggio risulta $T_c = 3.8 \cdot 10^7$ °K. A questa temperatura la vita media del ciclo del C-N è dell'ordine di 10^7 anni mentre il tempo scala della stella risulterebbe inferiore di almeno due ordini di grandezza. Ciò significa che durante l'evoluzione contrazionale precedente la fase di passaggio all'equilibrio termonucleare, nella quale la temperatura centrale è più bassa e il tempo scala ancora più breve, non può mai verificarsi il caso che al centro si formi un nucleo di solo He; pertanto la fase gravitazionale non può procedere fino all'innesco delle reazioni di Öpik-Salpeter senza essere stata prima sostituita dalla fase C-N. Le reazioni Öpik-Salpeter dunque possono innescarsi solo dopo che la stella dalla fase gravitazionale è passata a quella termonucleare del C-N e dopo che quest'ultima, trascorso un tempo sufficiente, si è esaurita lasciando che il nuovo sopravvento della fase contrazionale porti la temperatura centrale al valore necessario.

La natura delle fonti energetiche vista in funzione del processo evolutivo stellare secondo le linee esposte, pone le basi per una teoria della formazione degli elementi a lunga scala dei tempi e porge un sostegno alla recente analisi dettagliata e completa fatta da Fowler e G. e M. Burbidge [10].

Dal punto di vista dell'evoluzione stellare e della importanza della contrazione gravitazionale quale fonte energetica nei primi stadi di tale evoluzione sono importantissimi gli ammassi NGC 2264 e 6530 studiati da Walker [57] i cui diagrammi H-R indicano che mentre le stelle più calde e luminose occupano la zona normale della sequenza principale, quelle meno luminose ne occupano una più alta. Ciò può essere interpretato come dovuto al fatto che mentre il tempo scala della fase contrazionale è, per le prime, assai piccolo, (tanto da consentire a tali stelle di avere già raggiunto la fase nucleare), per le seconde è maggiore e perciò, data la particolare giovinezza di tutto l'ammasso, queste ultime non hanno ancora raggiunto la loro sequenza principale.

Il punto in cui la sequenza si stacca da quella normale (main sequence) indica l'età dell'ammasso relativo, che risulta dell'ordine di $3 \cdot 10^6$ anni.

Resta da chiedersi come mai negli ammassi di popolazione 2 le stelle che

---

[56] S. Chandrasekhar: *An introduction to the study of stellar structure* (Chicago 1938), p. 229.

[57] M. F. Walker: *Ap. Journ.*, **125**, 636 (1957).

li compongono non hanno una massa maggiore di (1.1 ÷1.2) volte quella del Sole. Si può rispondere con un motivo semiempirico così: SANDAGE ([47-48]), basandosi sulla funzione di luminosità osservata dell'ammasso globulare M3 e sulla teoria di Schönberg e Chandrasekhar ([43]) prima e di Hoyle e Schwarzschild ([42]) poi, applicata al ramo della sequenza principale del diagramma H-R relativo allo stesso ammasso, trova che le stelle occupanti l'altro ramo orizzontale e verticale del diagramma dovrebbero essere quelle che, originariamente nella sequenza principale, hanno compiuto gran parte del loro processo evolutivo. Tali stelle, riportate alla sequenza principale a ritroso della traccia evolutiva teoricamente calcolata, dimostrano una massa non superiore a 1.25 $M_\odot$.

Se non si ricorre al lavoro di HOYLE e SCHWARZSCHILD, difficilmente si comprende come stelle di massa così piccola possano avere avuto una evoluzione tanto diversa da quella solare. Resta da domandarsi come mai nell'ammasso M3 non si trovano stelle di massa maggiore di 1.25 $M_\odot$. Si può cercare una risposta facendo riferimento a un lavoro della MASSEVITCH ([58]) la quale studiando la dispersione del diagramma H-R per stelle di popolazione 1 ha messo in evidenza che quando si tiene conto di una eventuale composizione chimica diversa da stella a stella, non solo il punto rappresentativo di ciascuna è diverso nel diagramma H-R ma, a seconda della zona di quest'ultimo in cui ci si trova, si può passare da una stella stabile a una instabile al solo cambiare della composizione chimica. Così ad esempio la sequenza principale di stelle aventi un contenuto di elementi pesanti uguale a 0.01 è limitata superiormente per raggiunto limite di stabilità, il punto limite trovandosi molto vicino a quello rappresentativo del Sole e perciò relativo a una massa ad esso assai vicina.

Poichè le stelle dell'ammasso hanno tutte un contenuto di elementi pesanti molto basso non meraviglia nè il fatto di trovare nell'ammasso M3 il limite di 1.25 $M_\odot$ per la massa delle stelle componenti nè un processo evolutivo come quello proposto da Sandage, poichè scarso contenuto di metalli significa basso coefficiente di opacità e in definitiva rapido processo evolutivo.

Pertanto, che le reazioni di Öpik-Salpeter si inneschino nell'estremo limite superiore del diagramma H-R di certi ammassi, potrebbe essere cosa più che probabile. Forse ciò non accade nell'ammasso M67 il cui diagramma H-R invece si potrebbe interpretare ammettendo che quelle reazioni si inneschino alla fine del ramo orizzontale. Confrontando i due diagrammi M3 e M67 si dovrebbe concludere che le masse delle loro stelle non sono molto differenti (*) e quindi la sola diversa composizione chimica dovrebbe essere la maggiore responsabile della differenza dei diagrammi e in definitiva della possibilità che le stesse reazioni termonucleari si possano innescare in zone rappresentative diverse del diagramma H-R. La probabile differenza di composizione chimica

([58]) A. G. MASSEVITCH: *V^e coll. Int. d'Astr.* (Liège, 1954), p. 170.

(*) Poichè la zona di scostamento dalla sequenza principale è la medesima.

degli ammassi M3 e M67 è stata messa in evidenza spettroscopicamente e fotometricamente e anzi è a questo proposito suggestivo che mentre nel secondo il contenuto di metalli è probabilmente normale, nel primo è assai scarso.

9. – Le stelle variabili.

Nel campo delle stelle variabili la situazione non è più chiara. Non si sa fino a qual punto la variabilità delle giganti (dalle Cefeidi alle irregolari) è causata da una instabilità del modello stellare oppure è dovuta a un gioco opportuno di una qualche sorgente di energia.

La teoria delle stelle pulsanti sembra però abbastanza persuasiva nell'interpretare le oscillazioni di tali stelle come dovute a una instabilità oscillatoria dell'edificio stellare.

Ma la difficoltà cui va incontro è la seguente: le ampiezze delle oscillazioni nella zona centrale non risultano sufficienti a provocare, nella fase di compressione, un aumento di temperatura tale che le sorgenti di energia termonucleare possano rifornire energeticamente la stella e farle mantenere l'energia di pulsazione. In altre parole il tempo necessario per aumentare le ampiezze delle oscillazioni, anche nel caso che la dissipazione di energia sia la minima possibile, è superiore di molti ordini di grandezza a quello richiesto per smorzare tali oscillazioni per effetto di questa dissipazione di energia.

Ciò risulta dalla impossibilità di trovare un modello pel quale il coefficiente K del termine immaginario nell'espressione della frequenza $\sigma = \sigma_0 + iK$, risulta nullo o negativo

$$K = -\int_0^{2\pi/\sigma_0} \mathrm{d}t \int_0^M \frac{\delta T}{T}\left[\delta\varepsilon - \frac{\mathrm{d}\delta(4\pi r^2 F(r))}{\mathrm{d}m}\right]\mathrm{d}m$$

t = tempo; T = temperatura; $F(r)$ = flusso di energia che attraversa un cm² alla distanza r dal centro; δ indica l'ampiezza di variazione, durante l'oscillazione, della grandezza cui è premessa.

Secondo Cowling [59] il particolare tipo di sorgente di energia potrebbe contribuire a trovare le cause di instabilità ma i tentativi compiuti da Cox [60] su modelli aventi la zona esterna al nucleo in equilibrio radiativo e quelli di Schatzman [61] sul modello della Dumezil-Curien [41] e infine quelli di Rabinowitz [62] che più propriamente esamina modelli di giganti rosse aventi tale

---

([59]) T. G. Cowling: *M. N.*, **94**, 768 (1934); **96**, 42 (1935).
([60]) J. P. Cox: *Ap. Journ.*, **122**, 286 (1955).
([61]) E. Schatzman: *Ann. d'Astrophys.*, **19**, 51 (1956).
([62]) I. N. Rabinowitz: *Ap. Journ.*, **126**, 386 (1957).

zona in equilibrio convettivo, indicano che non è possibile, senza fare ricorso a qualche processo fisico che sembra trascurato, rendere conto della instabilità constatata di certe stelle anche nel caso in cui la sorgente di energia sia quella del ciclo del C-N.

Specialmente il lavoro di quest'ultimo autore appare persuasivo in quanto sono considerati casi estremi di modelli fra cui verosimilmente le variabili si modellano. Sembra, da un interessante lavoro di LONGE ([63]), che tale processo dimenticato possa essere costituito dalla viscosità turbolenta la quale produce non solo l'effetto di ridurre K ma anche quello di uniformare la distribuzione delle ampiezze relative col risultato di rendere le variazioni di temperatura al centro assai più elevate e di far sì che il termine $\delta\varepsilon$ del tasso di generazione di energia sia più importante di quello calcolato a prescindere dai fenomeni di viscosità.

Prima di poter concludere in tal senso occorrerebbe però continuare il calcolo effettuato dal Longe.

La situazione si fa più grave se si considerano le variabili nane dalle Novae e Supernovae alle Novoidi (SS Cygni, Z Camelopardalis, U Germinorum) alle Flares e Flash stars.

Secondo SCHATZMAN il fenomeno delle Novae e Supernovae origina per effetto di un'onda d'urto la quale, prodotta nell'interno di una nana bianca (in cui, secondo l'evidenza osservativa, hanno origine questi fenomeni) si propaga velocemente verso la superficie. Subito dietro il fronte d'onda la temperatura è portata, in maniera repentina, a un valore dell'ordine di 10^8 gradi ed è capace quindi di ridurre notevolmente la vita media delle reazioni termonucleari. Fra queste la più sensibile al fenomeno è l'ultina reazione della catena p-p: $^3He(^3He, 2p)^4He$ la quale, a causa della vita media sufficientemente alta in condizioni di temperatura normale, consente la continua presenza statistica di una certa percentuale di ^3He.

Appena l'onda d'urto passa, la temperatura sale fino al valore detto, la vita media della precedente reazione si riduce a valori molto bassi e viene prodotta una notevole quantità di energia che raggiunge la superficie in maniera violenta.

Questa teoria è assai suggestiva ma per la sua attendibilità occorre la continua efficacia della catena p-p la quale deve fornire la percentuale di equilibrio del ^3He necessaria.

Ora ci sono serie ragioni per dubitare dell'efficacia di tale catena. Abbiamo infatti visto per quali ragioni il MESTEL e MASANI considerano le nane bianche prive di sorgenti di energia termonucleare.

Il fenomeno delle Novae e Supernovae sarebbe dovuto secondo MESTEL ([26]) all'innesco nelle Nane Bianche del ciclo del C-N quando e se, durante la loro

([63]) P. LONGE: *Extr. Bull. Soc. Roy. des Sc.*, no. 7, 8, 9, 10 (Liège, 1956).

vita, accade che la temperatura centrale raggiunge la temperatura critica di innesco. Secondo l'Autore di queste pagine ([27]) invece le Novae dovrebbero originare dalle Nane Bianche quando, durante la loro vita, raggiungono la temperatura sufficiente all'innesco della reazione p-p e le Supernovae quando, in seguito all'innesco della reazione p-p, la temperatura sale fino a fare innescare anche il ciclo C-N; le stelle Novoidi dovrebbero trovare il loro posto dalla parte dei fenomeni meno violenti che caratterizzano le Novae.

Per quanto riguarda le flares e le flash stars, la notevolissima variazione di luminosità e la brevità dei « bursts » obbliga a porre la sorgente energetica alla superficie delle stelle, sebbene appaia assai difficile individuare il tipo di sorgente capace di manifestarsi in proporzioni così elevate e così all'improvviso sulla loro superficie.

Ambartsumian parla di una energia trasportata da materia « prestellare » o « intrastellare » intendendo indicare praticamente un tipo di energia finora sconosciuto. Ma anche per la forma piuttosto vaga con la quale si esprime, non si può attribuire un valore scientifico preciso a una tale espressione. Tanto più che secondo l'Autore questa materia prestellare dovrebbe sostituire addirittura nelle stelle della sequenza principale le reazioni termonucleari già viste. Il che non è accettabile perchè almeno il ciclo del C-N deve bene innescarsi nelle stelle a sinistra del sole nel diagramma H-R e dare una quantità di energia in accordo con la loro luminosità. Veramente Ambartsumian svela il proprio pensiero sulla natura di tale materia quando dice che la « disintegrazione di essa può spiegare la presenza del Tecnezio scoperto da Merril ([65]) in molte stelle di tipo S ». Siamo quindi ancora sul piano nucleare e d'altra parte l'Autore lo dice esplicitamente ([66]) quando parla di materia di densità dell'ordine di quella nucleare, in uno stato tuttora sconosciuto. L'espressione è ancora vaga e oscura; sembra che l'Autore pensi al fluido neutronico originario da cui ebbe origine il mondo attuale secondo la teoria α, β, γ di Alpher, Bethe, Gamow ([67]).

È chiaro che un'espressione così generica non può costituire una base di discussione proficua e si presta a obbiezioni ovvie, per cui G. R. e M. Burbidge ([68]) hanno preferito esaminare l'eventuale manifestarsi di una « macchia calda », come la chiamano, derivante dalla trasformazione in energia cinetica dell'energia magnetica di una zona di dimensioni opportune, sede di un campo magnetico rapidamente variabile.

Una tale interpretazione è stata appena accennata dagli Autori e meriterebbe una analisi più dettagliata per vedere se può adattarsi a tutte le partico-

([64]) V. Kourganoff: *Suppl. Nuovo Cimento*, **4**, 273 (1955).
([65]) P. W. Merril: *Ap. Journ.*, **116**, 21 (1952).
([66]) V. A. Ambartsumian: *The Obs.*, **75**, 72 (1955).
([67]) R. A. Alpher, H. A. Bethe and G. Gamow: *Phys. Rev.*, **73**, 803 (1948).
([68]) G. R. Burbidge e M. Burbidge: *The Obs.*, **75**, 212 (1955).

larità delle osservazioni specie per le flash stars la cui rapidità non solo di salita al massimo, ma anche di ritorno al minimo, forse male si adatta a una interpretazione termica se non di una zona molto superficiale.

A nostro avviso l'interpretazione dei BURBIDGE dovrebbe essere rivista tenendo conto di quella complessa fenomenologia che ha avuto oggi un così notevole impulso e che va sotto il nome generico di « scariche nei gas ». Dopo quanto si è riusciti a conoscere dagli studi teorici e da quelli eseguiti nei vari laboratori specialmente a proposito dell'energia nucleare controllata, appare assai probabile che in certe stelle possano verificarsi condizioni fisiche che provocano, in superficie, l'innesco di reazioni termonucleari in grande quantità.

La notevole instabilità dei fenomeni di scarica bene si adatta all'interpretazione della brevità dei fenomeni osservati, per cui il principale compito di una tale teoria dovrebbe essere semmai quello di studiare perchè queste scariche si verificano, almeno in misura sufficiente, preferibilmente nelle stelle degli ultimi tipi della sequenza principale.

Sottolineiamo l'interessante tentativo compiuto in tal senso da SEVERNY ([69]) studiando i flares del Sole. Egli calcola che, nel caso esaminato, la pressione elettromagnetica, la quale per effetto Pinch tende a contrarre il gas entro cui avviene una scarica elettrica, può superare il gradiente di pressione del gas stesso per cui quest'ultimo effettivamente si restringe. Il fenomeno viene arrestato da un'onda d'urto che si manifesta a un certo momento della contrazione. Non appena il fronte dell'onda d'urto incontra il fronte del gas che si restringe si manifesta un surriscaldamento improvviso che porta la temperatura del plasma fino a 10^7 gradi e possono così innescarsi le reazioni termonucleari.

A parte il meccanismo specifico che produce tali « bursts » è importante rilevare con HERBIG ([70]) che le stelle in cui si manifestano, insieme alle cosidette stelle del tipo T Tauri (di tipo spettrale avanzato (M), di bassa luminosità, spesso associate con nebulosità e aventi alcune righe spettrali in emissione) sono probabilmente l'analogo, dalla parte opposta nella sequenza principale, delle stelle O e BO; stelle cioè assai giovani anch'esse, di piccola massa, addirittura ancora in fase gravitazionale. Ciò si deduce fra l'altro dal fatto che nell'intorno di molti ammassi e associazioni giovani si trova un gran numero di tali tipi di stelle. Anche certe variabili irregolari, pure di tipo spettrale avanzato, che si trovano immerse o nelle immediate vicinanze di nebbie cosmiche potrebbero essere associate all'evento astronomico delle associazioni e alla stessa fase dell'evoluzione stellare; quando ciò fosse definitivamente accertato si potrebbe concludere che le flare stars sono l'esempio più tipico del fenomeno assai vario e complesso della fase contrattiva di una stella di piccola massa.

([69]) A. B. SEVERNY: *Isv. Astr. Obs. Mosca*, **20**, 22 (1958).
([70]) G. H. HERBIG: *Ric. Astr.*, **5**, 127 (1958).

Per di più, se con AMBARTSUMIAN ([71]) si pone attenzione al fatto che almeno in certe catene e filamenti stellari le stesse nebbie cosmiche nelle quali le giovani stelle (di tipo O e B e T Tauri) sono immerse risultano instabili e deve essere loro attribuita una età dello stesso ordine di quella di tali stelle (qualche milione di anni), bisogna concludere che, dal punto di vista osservativo, non è assolutamente possibile escludere che qualche stella sia addirittura più vecchia della nebulosa stessa in cui è immersa e occorre tenersi pronti ad affrontare il problema dell'origine stellare e della materia interstellare secondo principi essenzialmente diversi da quelli seguiti finora.

Questi ultimi accettano la presenza di materia interstellare come un dato originario e sostanzialmente studiano l'inizio del formarsi di una stella come il risultato del fenomeno di instabilità gravitazionale, già analizzato da JEANS ([72]) che si ha quando una perturbazione contrattiva interessante una notevole parte di materia interstellare di opportuna densità e temperatura non si propaga elasticamente al resto della nube con la velocità del suono, come accade quando l'azione delle forze gravitazionali è trascurabile, ma continua a contrarsi se tali forze sopravvengono in misura apprezzabile.

I casi cui si è prima accennato potrebbero essere molto significativi nel lasciare aperta la possibilità di una interpretazione diversa e anzi addirittura opposta, per cui molto opportuno risuona il richiamo a una più cauta posizione che AMBARTSUMIAN rivolge da quando ne ha intuito l'esigenza con la scoperta delle associazioni stellari, con l'analisi delle variabili flare, ma che finora non è stato nè precisamente formulato nè precisamente compreso per mancanza di una sufficiente messe di osservazioni chiarificatrici. Oggi è necessario però tenerlo presente poichè queste ultime si vanno accumulando e definendo e potrebbero portare ben presto l'Astronomia di fronte al suggestivo problema della creazione stessa della materia e del suo formarsi continuamente nel tempo.

Per riassumere si può presentare il prospetto seguente il quale illustra sinteticamente quanto sembra potersi dire oggi riguardo alla specificazione dei vari processi energetici che alimentano i diversi tipi stellari e i principali fenomeni delle stelle variabili:

Stelle a destra del Sole nel diagramma H-R (popolazione 1).	Catena p-p se valgono le regole di selezione di Gamow-Teller. Ciclo del C-N se valgono le regole di selezione di Fermi e se vi è un livello di risonanza nella quarta reazione del ciclo alle energie di (20÷30) keV.
Stelle a sinistra del Sole nel diagramma H-R (popolazione 1).	Ciclo del C—N.

([71]) V. A. AMBARTSUMIAN: *Rev. of Mod. Phys.*, **30**, 944 (1958).
([72]) J. H. JEANS: *Astronomy and cosmogeny* (Cambridge, 1928), p. 337.

Stelle nane bianche e in genere stelle di piccola luminosità situate al termine e sotto la sequenza principale nel diagramma H-R.	Raffreddamento della massa stellare.
Stelle Giganti di popolazione 1.	Ciclo del C-N in un nucleo centrale convettivo molto caldo e di peso molecolare medio maggiore della zona esterna. Un eventuale livello di risonanza nella quarta reazione del ciclo favorirebbe in questo senso la soluzione del problema.
Stelle Giganti di popolazione 2.	Crescita del nucleo centrale di ^{4}He, degenere, e, alla fine del ramo, formazione di elementi più pesanti del ^{4}He.
Stelle di ammassi molto giovani.	Contrazione gravitazionale.
Variabili di popolazione 1.	Come le giganti di popolazione 1.
Variabili di popolazione 2.	Come le giganti di popolazione 2.
Novae e Supernovae	Innesco della catena p-p per le prime e della catena del p-p seguita dall'innesco del ciclo del C-N per le seconde; oppure per entrambe innesco della reazione ^{3}He+^{3}He.
Novoidi.	Innesco della catena del p-p in stelle di piccola degenerazione.
Flare e Flash stars.	Processi nucleari associati e scariche nei gas nelle regioni superficiali delle stelle di piccola massa e di giovane età?

Per quanto riguarda una dettagliata esposizione delle formule relative alle reazioni termonucleari vedi, ad esempio, oltre la bibliografia citata ([1,5]), i seguenti testi:

L. H. Aller: *Astrophysics* (1954).
J. A. Hynek: *Astrophysics* (New York, 1951).
A. Masani: *Questioni di astronomia* (Genova, 1957).
A. G. W. Cameron: *Stellar Evolution*, CRL-41 (Chalk River, Ontario, 1957).

SUPPLEMENTO AL VOLUME XI, SERIE X
DEL NUOVO CIMENTO

N. 1, 1959
1° Trimestre

Observation of High Energy Jets with Emulsion Chambers.

I. - Transverse Momentum of the π^0-Meson.

O. Minakawa, Y. Nishimura, M. Tsuzuki and H. Yamanouchi
Kobe University

H. Aizu and H. Hasegawa
Rikkyo University

Y. Ishii and S. Tokunaga
Saikyo University

Y. Fujimoto, S. Hasegawa, J. Nishimura and K. Niu
Institute for Nuclear Study (Tokyo University)

K. Nishikawa
Wakayama Univerity

K. Imaeda and M. Kazuno
Yamanashi University

(ricevuto il 17 Luglio 1958)

1. – Introduction.

Since the pioneer works of BRADT, PETERS and KAPLON (1) and LEPRINCE-RINGUET (2), a number of works (3) have been made on jet showers by means of nuclear emulsions. The double cone structure of the jet shower was found and interpreted in terms of the Lorentz-transformation from the center of mass system to the laboratory system. Thus the half-angle method was invented and extensively applied to get information on the parameter of the Lorentz-transformation. In this way, a lot of data were accumulated on the energy-multiplicity relation, and many analyses were made on a possible nucleonic cascade process or a model of pluro-multiple production in a nucleus (4).

In a kinematic analysis of this kind, there always remained some ambiguity in determining the parameter of the Lorentz-transformation in spite of various attempts made to avoid the difficulty. Though the energy of a jet shower could be determined within an order of magnitude in this way, practically no information was obtained on an important dynamical quantity in the center of mass system, such as the energy spectrum of the produced particles. Thus it may be said that no conclusive results for the detailed mechanism of the multiple production were attained by the works in this direction.

It appears to be natural to consider that the investigation of the dynamics will be possible only after the establishment of the above kinematics. But a different approach to the dynamics should not be overlooked, which does not depend essentially on the details of the kinematics of jet showers.

An investigation on the dynamics of multiple production was first attempted by the Bristol group, by measuring the composition of shower particles, *i.e.*, the ratio of the number of produced π-mesons to that of K-mesons (5). Unfortunately, the technical difficulties in the mass determination of particles produced in the higher energy region and the poor statistics of jets with extremely high energy made the results far from conclusive. Only recently some reliable

---

(1) H. L. BRADT, M. F. KAPLON and B. PETERS: *Phys. Rev.*, **76**, 1735 (1949); *Helv. Phys. Acta*, **23**, 24 (1950).

(2) LEPRINCE-RINGUEST, BONSSER, FONG, JAUNDEAV and MORELLET: *Comptes Rendus* **229**, 163 (1949).

(3) Complete references will be found in E. LOHRMANN: *Nuovo Cimento*, **5**, 1074 (1957).

(4) F. C. ROESLER and C. B. A. MCCUSKER: *Nuovo Cimento*, **10**, 127 (1953); W. HEITLER and C. H. TERREAUX: *Proc. Roy. Soc.*, **664**, 929(1953); G. COCCONI: *Phys. Rev.* **93**, 1107 (1954); Y. TERASHIMA: *Prog. Theor. Phys.*, **13**, 1 (1955).

(5) R. R. DANIEL, J. H. DAVIES, J. MULVEY and D. H. PERKINS: *Phil. Mag.* **43**, 753 (1952).

results were obtained after a long controversy among various laboratories ([6]).

Another important quantity for the dynamical properties of jet shower was pointed out by one of us in 1956 ([7]). This is the transverse momentum of the produced shower particles with respect to the shower axis. Besides its significance for an understanding of the dynamics of multiple-production, the measurement of the transverse momentum has an advantage compared to that of other measurements. It is invariant under the Lorentz transformation from the laboratory to the center of mass system.

In the preliminary analysis ([7]) of the existing data of various high energy phenomena, a very interesting feature of the transverse momentum was noticed. The order of magnitude of the transverse momentum was deduced from a few data on jet showers in nuclear emulsions, on the spatial distribution of μ-mesons underground, and on the behavior of the soft component near the shower axis in an air shower. All of the deduced values agreed with each other and came out to be between few hundred MeV/c to a few GeV/c, though the pertaining energy regions differ by considerable amounts. As the above experiments were not designed for the study of the transverse momentum, it was not possible to discuss this problem in a more precise way.

This circumstance compelled us to make an accurate and extensive investigation on the transverse momenta of jet showers by means of nuclear emulsions. To make this experiment possible, the existing difficulties in the energy determination in the extremely high energy region must be overcome.

The current methods for the energy determination in nuclear emulsion are based on either the multiple scattering, the half angle of secondary showers, size of electron cascade, etc. None of them is free from defect and can be used for our present purpose. For example, the scattering method becomes less reliable at higher energies and is not free from some unknown systematic errors, such as a spurious scattering. The method of cascade showers can not be used extensively, because, in many cases, the cascades from different γ-rays of π^0-meson decay become mixed together and cannot be separated without ambiguity.

The emulsion chamber was found suitable for our purpose. This is a pile of plates of nuclear emulsion and of various materials. It was first constructed by KAPLON, PETERS and RITSON ([8]) for use in an attempt to study the dependence of jet showers on the mass number of the target nucleus. We found

---

([6]) F. A. BRISBOUT, C. DAHANAYAKE, A. ENGLER, Y. FUJIMOTO and D. H. PERKINS: *Phil. Mag.*, **1**, 605 (1956); M. KOSHIBA and M. F. KAPLON: *Phys. Rev.*, **97**, 193 (1955); D. LAL, YASH PAL and RAMA: *Nuovo Cimento Suppl.*, **12**, 347 (1954).

([7]) J. NISHIMURA: *Soryushiron Kenkyu* (in Japanese), **12**, 24 (1956); Z. KOBA: *Proc. of the VI-th Rochester Conference*, **4**, 43 (1956).

([8]) M. F. KAPLON, B. PETERS and D. M. RITSON: *Phys. Rev.*, **85**, 900 (1952).

that the development of cascade showers can be controlled by choosing suitable materials for the chamber. Thus it is possible to observe separately each cascade shower from different γ-rays. Then, using such a chamber, the energy of the individual γ-ray can be measured with good accuracy and, furthermore, can be checked by the kinematical relation in the π^0-meson decay into two γ-rays.

In the summer of 1955 a pilot experiment was made by the Kobe group. One emulsion chamber was constructed and exposed to cosmic-rays in the stratosphere. It consisted of 18 carbon plates, each 5 mm thick, 7 lead plates each 3 mm thick, and two dozen G-5 emulsion plates 6 in. $\times$ 4 in. $\times$ 200 μm. After the scanning, one jet event was found with four separated cascade cores which is suitable for our analysis.

The final form of our emulsion chamber project was determined in the discussion at the high energy cosmic-ray symposium in February of 1956 held at the Research Institute for Fundamental Physics, Kyoto University ([9]). At this meeting, an idea on the transverse momentum and the results of this pilot experiment were presented, and the importance of this proposal was discussed from various points of view. The advantage of the emulsion chamber over the usual emulsion stack was examined carefully. Finally the collaboration scheme was organized among six laboratories on this project.

The actual balloon flights were made in the summer of 1956. 17 chambers and 7 polyethylene balloons were constructed for this project. Out of them, 13 chambers were recovered with successful exposure. After the scanning, 16 events were found with good separation in cascade cores and with energy greater than several times 10^{12} eV.

In this paper, which covers the first part of this project, a report is given on the measurement of the transverse momentum of π^0-mesons in a jet of energy $\sim 10^{13}$ eV, together with the detail of the design of our chambers. Some of these results have been already presented in the VII-th Rochester and the Varenna Conferences ([10]). Other works on this project will be published in our subsequent papers.

2. – Experimental procedure.

2·1. *Design of the emulsion chamber.* – The most important point in the design of our emulsion chamber is to develop the secondary cascade showers originated from γ-rays of the produced π^0-mesons with a large spatial

---

([9]) *Soryushiron Kenkyu* (in Japanese), **12**, 1 (1956).

([10]) S. HAYAKAWA: *Proceedings of the 7-th Rochester Conference*, XI-3 (1957); THE JAPANESE EMULSION GROUP: *Suppl. Nuovo Cimento*, **8**, 761 (1958).

separation, so that measurements of the energy and direction can be made for individual cascade showers. The following combination of materials appears to be most suitable for thispurpose: low atomic number material in the upper half of the chamber as producing layer and high Z material below as detection layer.

γ-rays from the neutral π^0-mesons emitted by jet showers produced in the low Z material layer penetrate through without any materialization. Thus, when the γ-rays attain the high Z material layer and start to develop the cascade shower, they have already traveled far enough to have sufficient spatial separation from each other. A schematic illustration is shown in Fig. 1.

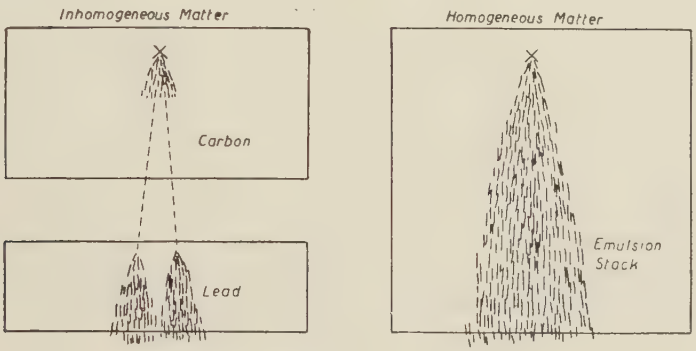

Fig. 1. Principle of our chamber.

The calculation of electron cascade showers for this design is given in the Appendix III. The adopted types of emulsion chambers are of two kinds, which are shown in Fig. 2. Type A is the standard one, consisting of 10 carbon

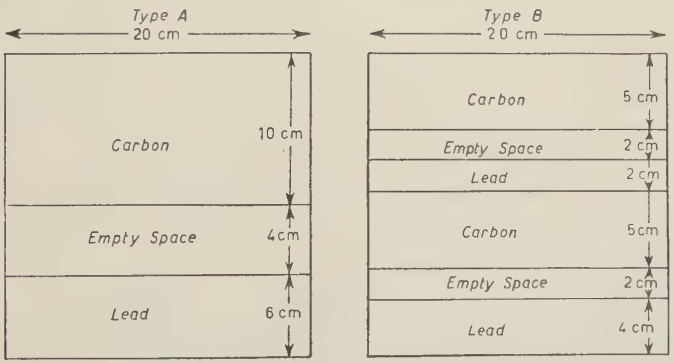

Fig. 2.

plates each 8 mm thick as shower producing layer at the top, an empty space of 4 cm height, and 7 lead plates each 5 mm thick as cascade shower

detector at the bottom. A G-5 emulsion plate of 6 in. $\times$ 8 in. $\times$ 200 μm is put under every layer of material

The type B chamber consists of two cycles of the same combination of materials as the type A. This type of chamber is expected to be effective for the observation of successive nuclear interactions. It has also a wider sensitive solid-angle than type A.

A chamber of either type has the dimensions 20 cm $\times$ 15 cm $\times$ 20 cm, and the weight is about 27 kg. We constructed 9 chambers of type A and 8 chambers of type B.

2·2. *Balloon flights.* – Seven polyethylene balloons were constructed (*) for use in the exposure of the chambers. The balloon is of pyramidal shape, and its volume is 5 600 m^3, which makes floating at high altitude possible with a pay load of about 200 kg. Particular attention was paid to the problem of attaining sufficient strength to withstand the expected large shock at the moment of launching the heavy load. The balloon is designed to be able to withstand a force of 1 ton.

The balloon flights were carried out in the summer of 1956, because in Japan the condition of the upper air current is suitable for long floating only in the summer season. Table I lists the balloon flights made in our project. Several typical balloon trajectories are shown in the Fig. 3.

Fig. 3. – Map of balloon flights.

(*) We are indebted to FUJIKURA Co. Ltd. (Tokyo) for constructing these balloons, and to TOYO RAYON and FUJIKURA Co., Ltd. for giving the parachutes for these balloon flights.

TABLE I. - *Balloon flights.*

Flight No.	Launching place	No. of chambers	Height and time of level flight	Remark
1	SHIZUOKA	2	25 Km 6h	success
2	»	3	(23 Km)	balloon burst
3	»	3	(23 Km)	»
4	KOBE	3	23 Km 7h	success
5	»	4	21 Km »	»
6	»	4	21 Km »	»
7	»	4	(10 Km) »	launching failure

2·3. *Scanning.* – The scanning for showers was carried out in the emulsion plate just beneath the third lead plate in each chamber. This place is three cascade units from the top of the lead layer, when the shower travels in a vertical direction. As shown in Appendix III, it is estimated to be the best place for looking for showers and ascertaining whether a shower has a multi-core structure or not.

The criterion for scanning is to pick up all shower events with more than ten parallel tracks in a microscope field. In each scanned plate, about two hundred cascade showers were found which have energies greater than several times 10^{10} eV.

All shower events thus found are again carefully examined to see whether they have a multi-core structure or not. There are about one to four events per scanned plate which have a distinct multi-core structure. On the whole, about twenty events were picked up as suitable showers for our analysis on the transverse momentum. These events had estimated primary energies larger than several times 10^{12} eV.

3. – Analysis of the event.

Showers with multi-core structure are analysed in the following way. A target diagram of the shower tracks is plotted for each cascade in the emulsion plate under each lead layer. The number of the tracks within a circle of radius r, taking the centre of the cascade as its centre, is determined and plotted as a function of the depth of the lead layer. The cascade transition curve thus obtained is compared with the theoretical one, and the energy of the primary γ-ray is estimated.

An improved calculation of three dimensional cascade theory is prepared for the present purpose in which a higher precision is required than that of the current cascade theory. The details and the precision of this cascade

function are shown in Appendix I. Analytical calculations are carried out without Landau's approximation, and the effects of the backing glass and the space between the lead plates are also taken into account in the numerical calculations. The errors of the theoretical curves are expected to be at most $(20 \div 30)\,\%$ in absolute value. An example of the procedure is shown in the analysis for one event (T.H. 4) in Fig. 4.

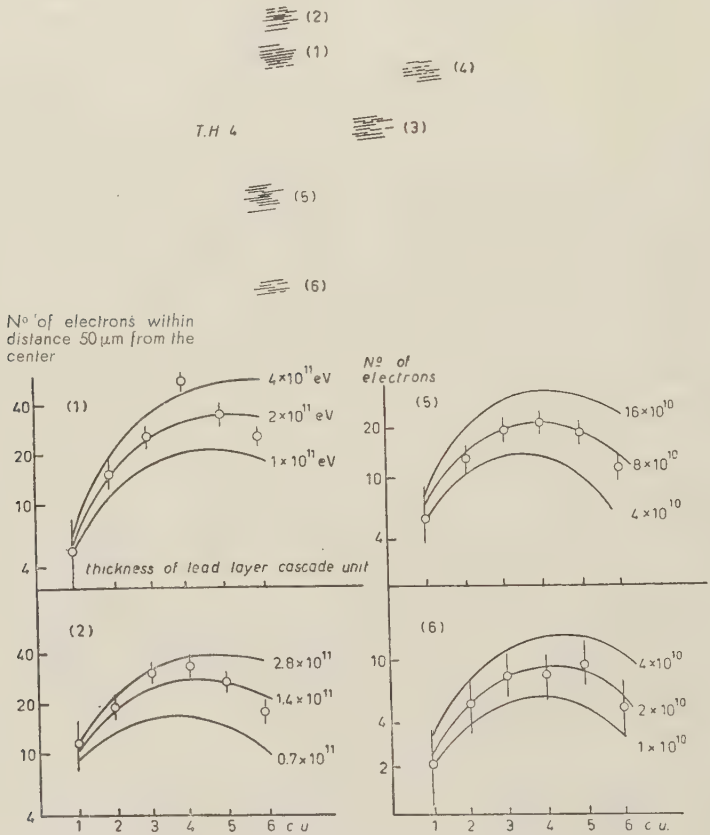

Fig. 4. – Transition curves of cascade showers in T.H.4. From these curves the energies of the primary γ-rays are estimated as

$$E_1 = (2.0 \pm 0.30)\cdot 10^{11}\ \text{eV} \qquad E_4 = (0.5 \pm 0.31)\cdot 10^{11}\ \text{eV}$$
$$E_2 = (1.4 \pm 0.76)\cdot 10^{11}\ \text{eV} \qquad E_5 = (0.8 \pm 0.18)\cdot 10^{11}\ \text{eV}$$
$$E_3 = (1.0 \pm 0.20)\cdot 10^{11}\ \text{eV} \qquad E_6 = (0.2 \pm 0.07)\cdot 10^{11}\ \text{eV}$$

The relative errors for the energy estimation quoted here are $1/\sqrt{N}$, where N is the number of electrons at the shower maximum.

After this analysis, a pair of γ-rays originating from a π^0-meson is picked up from all possible pairs of γ-rays by using the kinematical relation between

the opening angle and the energy of the pair of γ-rays, which is given by

$$\theta_{2\gamma} = \frac{r}{L} = \frac{m_{\pi^0} C^2}{\sqrt{E_{\gamma_1} \cdot E_{\gamma_2}}} = \frac{m_{\pi^0} C^2}{E_{\pi^0}} \left(\sqrt{n} + \frac{1}{\sqrt{n}} \right), \tag{1}$$

where:

r: separation between cascade showers measured in an emulsion plate under a certain lead layer.

L: distance from the point of origin of the jet to the plate where the separations of the cascade showers are measured.

$m_{\pi^0} C^2$: rest energy of the π^0-meson.

$E_{\gamma_1}, E_{\gamma_2}$: energy of each γ-ray, decayed from a π^0-meson.

n: $n = E_{\gamma_1}/E_{\gamma_2}$.

E_{π^0}: $E_{\pi^0} = E_{\gamma_1} + E_{\gamma_2}$ = energy of the π^0-meson.

The distance L must be measured to get the value of $\theta_{2\gamma}$. Tracing back each of the separated cascade showers in the successive lead plates, the place where the primary jet is produced can be predicted. When the predicted place happens to be in a certain carbon plate the emulsion plate just below is scanned for the charged secondaries from the primary jet.

The error in the determination of this distance is estimated to be a few % in the case when the charged secondaries of a jet shower are found, and in other cases it is 10% or so.

Using the observed values of L, E_{γ_1} and E_{γ_2}, the separation, $r_{\text{calc.}}$, is estimated from the formula (1). The ratio of the calculated separation, $r_{\text{calc.}}$ to the observed one, $r_{\text{obs.}}$, is made for all possible pairs of cascades. Out of these, we have selected those which have the ratio $r_{\text{cal.}}/r_{\text{obs.}}$ near unity, for instance 1.0 ± 0.2. These limits differ slightly depending on the measuring conditions of each cascade shower. The cascade pairs thus selected are regarded in the first step of our analysis as the decay products from the same π^0-mesons.

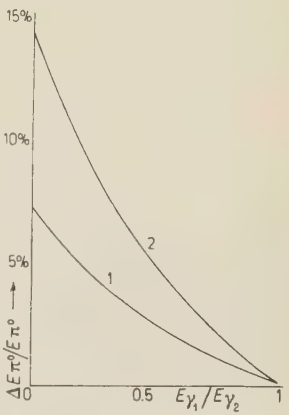

Fig. 5. – Precision of energy determination of π^0-mesons by the kinematical method. Curves 1 and 2 show the relative errors of this determination when the errors of E_{γ_1} and E_{γ_2} are 10% and 20%.

Of course, there may be some false pairs selected by the above method. In order to reject such miscoupled pairs, an examination of the consistency of the identification of pairs into π^0-mesons is made on each jet shower.

Usually a unique combination of pairs is found in this way for a shower of small multiplicity, say with less than 4 π^0-mesons.

After selecting pairs of γ-rays from π^0-mesons as above, the energy of the π^0-meson can be determined more accurately by using again the kinematical relation (1). The accuracy of this energy determination is quite good, and the error introduced by this method is in general about 10%. This is because the errors of E_{γ_1} and E_{γ_2} affect the results only slightly, as shown in Fig. 5.

In order to get the values of the transverse momenta of these π^0-mesons, the position of the shower axis must be known. We assume that the centre of a jet shower is the energy-weighted average position of the observed π^0-mesons. Then the value of the transverse momentum of each π^0-meson is obtained. Corrections for the error due to deviation of the assumed shower axis from the true axis are made in the next section. An example of the above analysis for event T.H. 4. is shown in Fig. 6. A statistical test is made to see whether

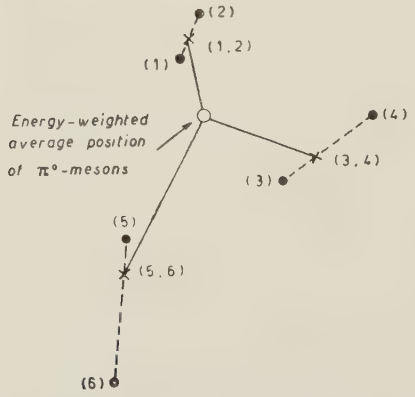

Fig. 6. - Coupling of 2 γ-rays and determination of energies of π^0-mesons. The most probable combination is the coupling of (1, 2), (3, 4) and (5, 6). The ratio $r_{\text{calc.}}/r_{\text{obs.}}$ for these combination is as follows:

	most probable		next probable	
	couple	R	couple	R
	(1, 2)	0.70 ± 0.11	(1, 3)	0.23 ± 0.03
$R = r_{\text{calc.}}/r_{\text{obs.}}$	(3, 4)	0.70 ± 0.13	(2, 4)	0.32 ± 0.06
	(5, 6)	0.93 ± 0.22	(5, 6)	0.93 ± 0.22

Taking the most probable combination, we get the energies of π^0- mesons. The energies of the π^0-mesons thus obtained and the transverse momenta of these π^0-mesons are shown in the following Table:

	E	P_T
(1, 2)	$(2.14 \pm 0.22) \cdot 10^{11}$ eV	(480 ± 39) MeV/c
(3, 4)	$(0.96 \pm 0.09) \cdot 10^{11}$ eV	(308 ± 24) MeV/c
(5, 6)	$(0.85 \pm 0.13) \cdot 10^{11}$ eV	(411 ± 52) MeV/c

TABLE II.

Event	No. of cores	Origin	E_0 (eV)	P_T (MeV/c)
H.A.1.	7	A	10^{13}	272
				252
				225
				284
S.H.1. (*)	14	Carbon	10^{14}	(*)
T.H.1.	6	A	10^{13}	116 ± 23
				361 ± 73
				284 ± 57
T.H.2.	4	Carbon	$4 \cdot 10^{12}$	286
T.H.3.	5	Carbon	$2 \cdot 10^{12}$	289 ± 80
				381 ± 108
				661 ± 185
T.H.4.	6	Carbon	$4 \cdot 10^{12}$	481 ± 38
				308 ± 24
				411 ± 52
K.I.1.	4	Carbon	$4 \cdot 10^{12}$	210
				260
				260
Ya.N.1.	4	Carbon	$5 \cdot 10^{12}$	192
Yo.N.1. (*)	16	A	10^{14}	(*)
Yo.N.2.	4	A	$1.3 \cdot 10^{12}$	300 ± 100
Yo.N.3.	2	Carbon	$5 \cdot 10^{12}$	146
T.O.1.	6	Carbon	$6 \cdot 10^{12}$	171
				315
				337
T.O.2.	5	Carbon	$7 \cdot 10^{12}$	285
				186
				143
Y.T.1.	4	Carbon	$7 \cdot 10^{12}$	600 ± 30
S.T.1. (**)	8	A	$7 \cdot 10^{12}$	121 78 183
				248 230 173
				31 42 53
				348 300 234
S.T.2. (**)	11	Carbon	$1.2 \cdot 10^{13}$	470 450 577
				316 78 93
				210 561 190
				414 198 600
				475 476 485
S.T.3.	4	Carbon	$3.5 \cdot 10^{12}$	280
S.T.4.	6	Carbon	$9 \cdot 10^{12}$	514
				289
				518
H.Y.1.	6	Lead	$5 \cdot 10^{12}$	196
				146
				62

A: Outside of chamber.
(*) These showers will be analysed in a subsequent paper.
(**) Combination of the pairs of γ-rays can not be determined uniquely.
E_0: Energy of the primary which is estimated as ten times the total energy of the π^0-meson.

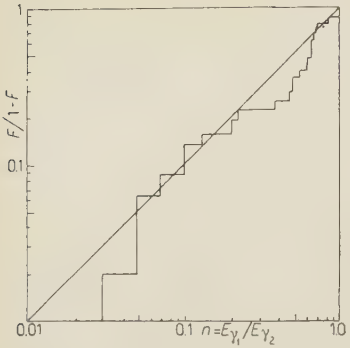

Fig. 7. – F-plot for π^0-decay.

in the above analysis we have miscoupled or not. The method is similar to that of the F-plot ([11]).

As the γ-rays decay isotropically in the rest system of the π^0-meson, we get the relation,

$$\frac{F}{1-F} = n ,$$

where F is the fraction of the number of pairs of γ-rays with energy ratio less than n.

Then, if we plot $\ln (F/(1-F))$ versus $\ln n$, the data should be on a straight line as shown in Fig. 7.

The result is consistent with the line within the statistical errors, and this is evidence for the consistency of our analysis.

4. – Experimental results.

4·1. *Table of the events.* – The following is the table of shower events for which the measurements on the transverse momenta are made. In total in 16 jet showers we obtained 49 π^0-mesons with measured transverse momenta.

4·2. *Spectrum of the transverse momentum.* – The histogram of the observed values of the transverse momentum is shown in Fig. 8. As is seen, most of the data are confined within a narrow interval of (100 ÷ 600) MeV/c, and none is found beyond 700 MeV/c.

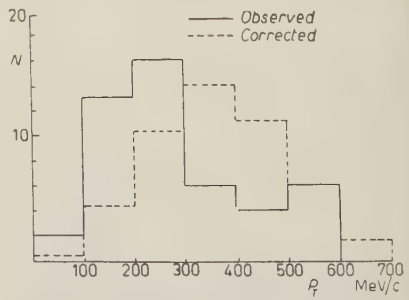

Fig. 8. Spectrum of the transverse momenta of the π^0-mesons.

A correction is to be applied to this histogram for a possible error in the position of our assumed shower axis. This is because we measured the transverse momenta of the π^0-mesons with reference to the shower axis determined as shown in the preceding section. There we assumed the vector sum of the transverse momenta of all observed π^0-mesons in a jet to be zero. This procedure underestimates on the average the magnitude of the transverse momentum.

This correction can be calculated in a statistical way with an assumption

([11]) N. M. Duller and W. D. Walker: *Phys. Rev.*, **93**, 215 (1954).

that the distribution function of the transverse momentum is symmetric around the true shower axis and is independent of other physical quantities of a jet shower. In Appendix IV, detailed calculations are shown for obtaining an expected value of the true distribution function of the transverse momentum from the histogram of the observed values. The magnitude of the correction depends on the multiplicity and the energy-partition among π^0-mesons in an observed jet. By this correction the average value of the transverse momentum is increased by about 30%. In Fig. 8, a corrected histogram is shown and compared with the observed one.

4·3. *Relation of the transverse momentum to other physical quantities.* – To study whether or not the magnitude of the transverse momentum varies depending on some other physical quantity, the whole event is divided into groups and the average values of the transverse momentum are compared among these groups.

Table III.

	Average of estimated primary energy	Root mean square of transverse momentum
High energy primary	$8.4 \cdot 10^{12}$ eV	(407 ± 32) MeV/c
Low energy primary	$3.8 \cdot 10^{12}$ eV	(365 ± 30) MeV/c

First, the showers are divided into two groups according to the magnitude of their estimated primary energy. The average transverse momentum is calculated and compared.

Table IV.

	Average of energy of π^0-meson	Root mean square of transverse momentum;
High energy π^0-mesons	$3.1 \cdot 10^{11}$ eV	(397 ± 32) MeV/c
Low energy π^0-mesons	$0.9 \cdot 10^{11}$ eV	(380 ± 30) MeV/c

A possible dependence of the transverse momentum on the energy of the produced π^0-meson itself is also interesting to know. This has a close connection with the dependence on the emission angle θ of secondary particles, as there is the relation $\theta = P_T/P$. The data are classified into two groups according to π^0-meson energy and the following result is obtained.

This procedure may have a bias against finding any appreciable difference,

because the assumption on the shower axis in our analysis tends to minimize the difference in a statistical way. The following analysis is made to estimate the effect without bias. First, the observed π^0-mesons are divided into two groups depending on whether or not they have energy greater than $1.6 \cdot 10^{11}$ eV. There are 18 π^0-mesons of the high energy group in 8 jet showers and 16 of the low energy group in 6 jet showers. For the measurement of the transverse momentum of a high energy π^0-meson, the shower axis is determined only from the high energy π^0-mesons in the same jet. A similar treatment is also made for a low energy π^0-meson. The standard correction procedure is applied for these two groups. In this way, the result is free from the assumption that the transverse momentum distribution is the same in both groups. This analysis gives us the following results.

TABLE V.

	Average energy of π^0-meson	Root mean square of traverse momentum
High energy π^0-mesons	$3 \cdot 10^{11}$ eV	(450 ± 50) MeV/c
Low energy π^0-mesons	$0.9 \cdot 10^{11}$ eV	(405 ± 40) MeV/c

Last, a study is made to see whether or not the distribution functions of the transverse momentum of individual showers differ. Of course, even if a difference does exist in an elementary collision process, this might not appear in our experiment because the target nucleus is carbon in most cases. The dispersion of the data is estimated in an individual shower and also among showers. The mean square deviation of the observed transverse momentum is calculated in each shower with three or more π^0-mesons. This gives a measure of the dispersion of the data in an individual shower. This result is compared with that expected from the original distribution derived at the beginning of this section.

TABLE VI. – *Ratio of the average mean square deviation of transverse momentum in an individual shower to that of the original distribution function.*

Observed value	0.48 ± 0.11
Expected value	0.60

It seems to be consistent that the distributions in individual showers are in agreement.

5. – Summary and discussions.

The experimental results obtained here can be summarized in the following way. The spectrum of the transverse momentum of π^0-mesons in jets with energy $(10^{12} \div 10^{14})$ eV is obtained. It is rather a narrow distribution which has a maximum at around 400 MeV/c with the width of about 200 MeV/c. No data are obtained beyond 700 MeV/c. A possible dependence of the transverse momentum on either the primary energy or the π^0-meson energy is examined. These analyses tell that the average transverse momentum does not show any significant difference between groups classified according to the above property. A possible difference in the distributions of the transverse momentum for individual showers is examined, and we find that the difference is not significant beyond the statistical fluctuation.

The above experimental results agree with the results of our preliminary analysis in 1956. Of course, the final answer must await the investigation of a wider range of energy and different kinds of particles.

After our proposal about the importance of the transverse momentum, various experiments have been made in this direction. The most extensive investigation among these is that of the Bristol group ([12]). They used large stacks of nuclear emulsion and analysed thirty events of jet showers found in them. Energies of charged particles in the outer cone of the jets were measured by the multiple scattering method. For the γ-rays from the decay of produced π^0-mesons in their inner cone, information of their energy is obtained by observing relative scattering of tracks of the electron pairs and size of the cascade showers. To the secondary stars produced by particles in the inner cone they applied the half-angle method, so that they could give an estimation for the energy of the producing particles. By measuring the energies of the secondary particles with the various methods mentioned above, they obtained the spectrum of the transverse momenta in thirty jet showers.

As they stated in their paper, the measurement of multiple scattering of outer charged particles introduces some bias of missing particles with large transverse momentum, because the tracks with significant magnitude of multiple scattering will be those of energies below a certain cut-off value which depends on the geometry of the track and the distortion of the emulsions. The half-angle method, which is based on forward-backward symmetry in the center of mass system, may be legitimately used only in the cases of nucleon-nucleon collision, and has no theoretical reasons to be extrapolated to collisions of other kinds. Therefore the results on π^0-mesons are more reliable than those obtained by the above two methods.

([12]) B. Edwards, J. Losty, D. H. Perkins, K. Pinkau and J. Reynolds: *Phil. Mag.*, **3**, 237 (1958).

Comparing the experimental data on π^0-mesons of our group with those of the Bristol group, the difference between both experimental methods must be considered.

In their relative scattering measurement of the electron pairs, information is obtained only for the particle of lower energy of the pair, so that they estimate the total energy of the pair simply by multiplying by a factor 10 the value of this low energy one. Since the distribution of energy disparity between pair electrons is almost flat, the above procedure introduces a large error in their energy determination of the individual pair. Thus the error will largely affect the shape of the observed distribution of transverse momentum, though it may not much disturb the mean value. While in our case, the energy measurement of individual γ-rays is made in a more accurate way, say with an error of $10\,\%$. But our observed distribution of transverse momentum is obtained after applying a statistical procedure to eliminate an uncertainty in the determination of the position of the shower axis.

Another point to be considered is a difference of the experimental conditions. In our experiment γ-rays with energy greater than a certain cut-off energy ($\sim 5 \cdot 10^{10}$ eV) are picked up irrespectively of their energy, while in the Bristol case those whith emission angle smaller than a certain value are taken irrespectively of their energy. In general the spectrum of the transverse momentum will be different in the two cases, even if the spectrum is independent of the emission angle or the energy. If we assume that the angular distribution of produced particles is $\theta\,\mathrm{d}\theta/\theta$ ([12,13]), a calculation shows that the spectrum obtained under our condition should be multiplied by a factor $1/P_T$ for direct comparison with that of the Bristol group.

Fig. 9 shows the results of the Bristol group for the charged particles together with our data for comparison. An agreement of both data appears rather good considering the above remarks and the different constitution of the measured particles. For the transverse momentum of π^0-mesons, it seems appropriate to compare the mean values of both groups. After multiplying $1/P_T$ to our spectrum as shown above, we get (325 ± 20) MeV/c for the mean value of the transverse momentum of π^0-mesons within a finite solid angle. This value can be directly compared with that of the Bristol group, (520 ± 160) MeV/c. Both results seem to be consistent with each other.

GRAMENITZKIJ and others ([14]) made an analysis similar to that of Bristol on their α-primary jet of energy $8 \cdot 10^{13}$ eV. CIOK and others ([15]) also analysed one event of energy $\sim 10^{14}$ eV in their emulsion stack. MILEHIN and RO-

([13]) S. HASEGAWA, J. NISHIMURA and Y. NISHIMURA: *Nuovo Cimento*, **6**, 979 (1957).

([14]) I. M. GRAMENITZKIJ, G. B. JUDANOV, E. A. ZAMCHALOVA and M. N. ŠCHERBAKOVA: *Journ. Exp. Theor. Phys.* (*U.S.S.R.*), **32**, 936 (1957).

([15]) P. CIOK, M. DANYSZ, J. GIERULA, A. JURAK, M. MIĘSOWICZ, J. PERNEGR, J. VRÁNA and W. WOLTER: *Nuovo Cimento*, **6**, 1409 (1957).

SENTHAL ([16]) analysed one shower event in a report of DE BENEDETTI and others ([17]). These results seem to be not in contradiction with the data of ours or Bristol.

Attention must be paid, also, in the experiments on extensive air showers, because the energy of the participating particles in an air shower is much

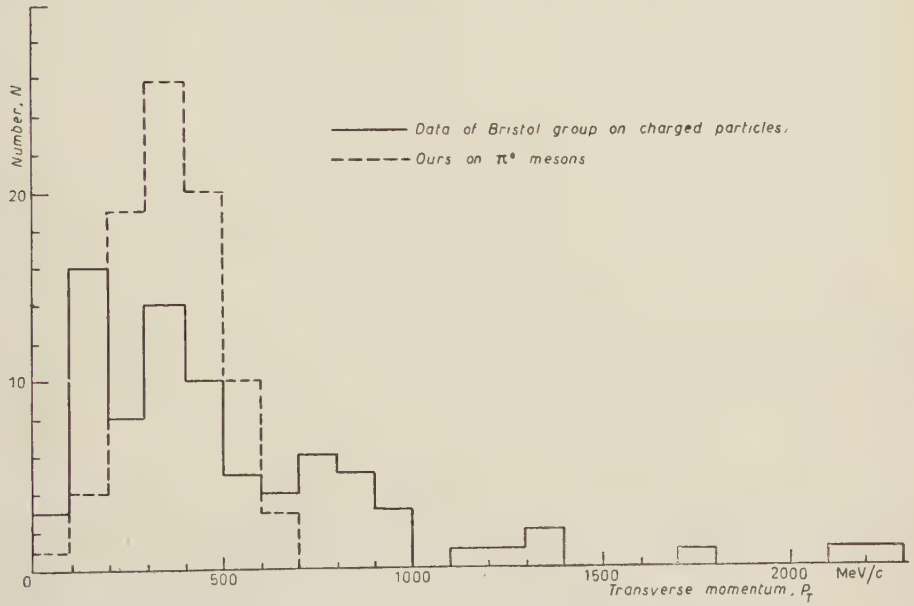

Fig. 9. – Spectrum of transverse momentum of secondary particles.

higher than that of the events observed in nuclear emulsion. However, in these air shower cases, the measurement is usually made only in an indirect way, so that their analysis and the interpretation of the data is to be looked at with reservation. The experiment of the Moscow group ([18]) on the lateral distribution of the soft-component and of the N-component made clear the structure of the shower core to some extent. According to their conclusion, the core part has a diameter of ~ 1 m at sea level or mountain altitude, and contains some extremely high energy N-component particles. This results make it possible to get information on the transverse momentum in the range of primary energy (10^{13} : 10^{16}) eV, which gives us a value of the order of 1 GeV/c.

([16]) T. A. MILEHIN and I. L. ROZENTAL: *Journ. Exp. Theor. Phys.* (*U.S.S.R.*), **33**, 197 (1957).

([17]) A. DE BENEBETTI, C. M. GARELLI, L. TALLONE and M. VIGNOE: *Nuovo Cimento*, **4**, 1142 (1956).

([18]) N. A. DOBROTIN, G. T. ZACEPIN, S. I. MIKOLOKIJ and G. B. HRISTIANSEN: *Suppl. Nuovo Cimento*, **3**, 634 (1956).

The experimental study of the dynamics of multiple production of particles stimulated the theoretical work in this field of physics. The measurements on the transverse momentum and the ratio of the number of produced π-mesons to that of K-mesons lead KOBA to a critical study of the current theories on the multiple production of mesons ([19]). He made a calculation following the idea of LANDAU ([20]) in which the inter-relation between the transverse momentum and the π/K ratio is made clear. The interpretation is also made in connection with the temperature of the created meson cloud and the meson-meson interaction. The Fermi theory ([21]) is shown to disagree with the values of the parameters found in this way.

This study might be just at the entrance of the dynamics of the multiple production. So far, the transverse momentum of the produced particle seems to be fairly constant over a wide range of energies, and it is suspected to be an important quantity for our understanding of the phenomenon. Much information on jet showers could be derived by using this property of the transverse momentum; for instance, the energy of the secondary particle can be estimated immediately by only measuring the production angle of this particle.

* * *

It is a pleasure for us to thank Professor S. KIKUCHI for his continuous interest during the course of this work. We wish to acknowledge the members of the Meteorological Institute, the Maritime Safety Agency, the Police Office and the Press Asahi for their kind arrangement for the balloon flights, including recovery of the exposed emulsion chambers.

Thanks are also due to the staff of Kobe, Shizuoka and Rikkyo Universities for launching and tracing the balloons, and to Miss T. HASEBE, Mrs. E. MIKUMO, Mrs. Y. NISHIMURA and Mrs. T. ODA for their skilful scanning. Dr. CONZET kindly read our manuscript before publication and corrected our English. We are grateful to the members of the Symposium of Extremely High Energy Phenomena in 1956 for their encouraging discussions.

APPENDIX I

Three dimensional electron shower theory without Landau's approximation.

In our older calculation ([22]) for the three dimensional electron shower theory, an analytical solution for the lateral distribution function is derived using

([19]) Z. KOBA: *Prog. Theor. Phys.*, **15**, 461 (1956).
([20]) L. D. LANDAU: *Proc. Acad. Science of U.S.S.R. Phys.*, Section **17**, 51 (1953).
([21]) E. FERMI: *Prog. Theor. Phys.*, **5**, 570 (1950).
([22]) J. NISHIMURA and K. KAMATA: *Prog. Theor. Phys.*, **7**, 185 (1952)

Landau's approximation. In this approximation the effect of multiple Coulomb scattering is only taken into account and the contributions of single and plural scatterings are neglected. When it is applied to a problem of the single charged particle without energy loss, it yields the well known Gaussian distribution. As the contributions of the single and plural scattering are all neglected, a serious error can be found at the tail of the distribution function.

In their calculations for a single particle SNYDER and SCOTT and MOLIÈRE [23] have shown that there is a considerable error in the distribution with Landau's approximation not only at the tail but even at small angle region.

Such discrepancies are also found in the theory of angular distribution function for electron shower by CHARTRES and MESSEL [24]. Their track length angular distribution function is about 40% higher at small angle region than that obtained in Landau's approximation. Their function is derived using Molière's scattering theory and Tamm and Bele'nkij's cascade theory. It is to be regretted that their treatment is limited to only the angular distribution function, and furthermore it does not incluse the effect of ionization loss, so that it can not be used for the energy determination of γ-rays in our emulsion chambers.

As shown in our paper (Sect. 3), the energy of γ-rays must be measured as accurately as possible from the transition curves of the shower particles within radius r under the successive lead plates. The accuracy of our older theory of the lateral distribution function seems now to be insufficient for this purpose and a new lateral distribution function is sought for.

The treatment is based on Molière's scattering theory and Snyder's [25] electron shower theory. Thus our theory, the details of which will be published elsewhere (*), includes rigorously the effects of ionization loss and the contributions of single, plural and multiple scatterings.

Here we present only the final results $\Pi(E_0, r, t)$ which gives the total number of electrons within the radius r of the shower developed by a single γ-ray of energy E_0 after passing through t cascade units. The solution is expressed in a series of inverse powers of G, which is approximately equal to the logarithm of the number of collisions of an electron passing through the matter of one cascade unit, and is given by

$$\Pi = \Pi^{(0)} + \frac{1}{G}\Pi^{(1)} + . \qquad \text{(A1.1)}$$

For $\varepsilon r/K \ll 1$, we have

$$\Pi^{(0)} = \frac{1}{2\pi i}\int_{-i\infty}^{i\infty} \frac{\mathrm{d}S}{S}\left(\frac{E_0 r}{K}\right)^s \Gamma\left(1-\frac{S}{2}\right) \mathcal{M}\left(-\frac{S}{2}, 0, 0, S, t\right) \qquad \text{(A1.2)}$$

---

[23] H. S. SNYDER and W. T. SCOTT: *Phys. Rev.*, **76**, 220 (1952).

[24] B. A. CHARTRESS and H. MESSEL: *Phys. Rev.*, **104**, 517 (1956).

[25] H. S. SNYDER: *Phys. Rev.*, **76**, 1563 (1949).

(*) A full account has been recently published by K. KAMATA and J. NISHIMURA: *Suppl. Prog. Theor. Phys.*, **6**, 93 (1958).

and

$$\text{(A1.3)}\quad \Pi^{(n)} = \frac{1}{4\pi i}\int_{-i\infty}^{i\infty} \mathrm{d}S \left(\frac{E_0 r}{K}\right)^S \Gamma\left(1-\frac{S}{2}\right)\left[\left\{\psi\left(\frac{S}{2}+1\right)\right\}\mathcal{M}\left(-1-\frac{S}{2}, 1, 0, S, t\right) - \right.$$
$$\left. - \frac{\mathrm{d}}{\mathrm{d}p}\mathcal{M}\,(p, 1, -2p-2-S, S, t)\,\Big|_{p=-1-\frac{S}{2}}\right],$$

where $\mathcal{M}$ is given by

$$\mathcal{M} = \lim_{(\xi - t)\to 0} N\,.$$

Here N is defined by the equation:

$$\sum_{n=0}^{p} {}_pC_n \left(-\frac{1}{G}\right)^n L^{(n)}(S+2p+2u-2q)N(p-n, n+u, q, S, t) =$$
$$= \left(\frac{\partial}{\partial t}+\sigma\right)\left[p\left\{(\xi-t)^2 1\left(-\frac{1}{G}\ln\,(\xi-t)^2\right)\right\}N(p-1, u, q, S, t) + \right.$$
$$+ u(\xi-t)^2 N(p, u-1, q, S, t) + (S+2p+2n+q)qN\cdot$$
$$\left.\cdot(p, u, q-1, S, t) - \frac{2}{G}pqN(p-1, u+1, q-1, S, t)\right]$$

with

$$N(0, 0, 0, S, t) = S^{\frac{1}{2}} M(S)\left[\exp\left[\lambda_1(S)t\right] - \exp\left[\lambda_2(S)t\right]\right]$$

and

$$(L^n(S+2p+2u-q) = \frac{\mathrm{d}^n}{\mathrm{d}S^n}\left[\frac{\partial^2}{\partial t^2} - (\lambda_1(S+2p+2u-q) + \right.$$
$$\left. + \lambda_2(S+2p+2u-q))\frac{\partial}{\partial t} + \lambda_1(S+2p+2u-q)\,\lambda_2(S+2p+2u-q)\right].$$

G : 12.9 for lead,

$$K = \frac{21\,(G)^{\frac{1}{2}}}{2(\ln 181 Z^{-\frac{1}{3}})^{\frac{1}{2}}}\text{MeV} = 19.1\ \text{MeV/c},$$

ε : critical energy of the material, 7.2 MeV for lead,

r : distance from the shower axis, measured in cascade units.

It should be noted that the distribution is a function of only t and $E_0 r/K$ for $\varepsilon r/K \ll 1$, which is a very convenient expression to be applied for actual purpose. This circumstance may easily be interpreted in the following way.

In the linear cascade theory, the number of electrons with energy larger than E is expressed by a function of E_0/E and t. On the other hand, the average energy of an electron lying at the distance r from the shower axis is approximately given by K/r. Then the number of electrons within the circle of radius r is given by a function of only $E_0 r/K$.

The first term of the series (A1.1), $\Pi^{(0)}$, representing the contribution of the Coulomb multiple scattering, is just of the same form as our old lateral distribution function except a slight difference in the definition of K. The second, third and higher terms represent the contributions of single and plural scattering. It can be proved that the series (A1.1) converges very rapidly, and it is sufficient to take the contribution up to the second term for our present purpose.

The following points are taken into account in the actual numerical calculations.

1) The approximation for $t \gg 1$ can not always be used, which means that we can not neglect the terms containing

$$\exp[\lambda_1(s)t], \quad \exp[\lambda_1(s+1)t], \quad \exp[\lambda_2(s)t], \quad \exp[\lambda_2(s+1)t], \quad \ldots,$$

against $\exp[\lambda_1(s)t]$ appearing in $\mathcal{M}(t)$.

2) The distribution function calculated for homogeneous matter can not be directly applied to the case of our emulsion chamber, because there is one nuclear plate between the lead plates. An extension of our theory to inhomogeneous matter is made.

Numerical calculations are made for $E_0 = 10^{10}$ eV $\div 10^{13}$ eV, $r = 5\ \mu\text{m} \div \div 200\ \mu\text{m}$, and $t/n = 1 \div 24$, where $1/n$ is the cosine of the zenith angle, and for n, we take the values 1, 1.5, 2, 3, and 4. The error included in our calculation is expected to be at most $(20 \div 30)\%$.

Appendix II

Experimental test on the accuracy of the cascade shower theory.

The identification and measurement of the energy of the π^0-mesons are based in our analysis on the three dimensional shower theory and the kinematical relation of $2\,\gamma$-rays of a π^0-meson decay. Though the cross check from both methods seems to be sufficient for the experimental confirmation of the accuracy of our energy measurement, an independent test on the accuracy of the cascade theory is also desirable.

The precision of the cascade shower theory given in Appendix I is examined in the following two ways. One is the measurement of the double core events found in our emulsion chambers, while the other is the comparison of our theoretical curve with the experimental data of Pinkau [26] on the electron showers initiated by a single γ-ray in an emulsion stack.

The scanning of our emulsion chambers, has yielded about 10 showers with distinct double core structure. We measure the distance between two cores of a selected event in every available emulsion plate, so that the angle of

[26] K. Pinkau: *Phil. Mag.*, **2**, 1389 (1957).

divergence is obtained. The target diagrams of shower particles under the successive lead plates are plotted, and the energy of each γ-ray can be estimated from their transition curves.

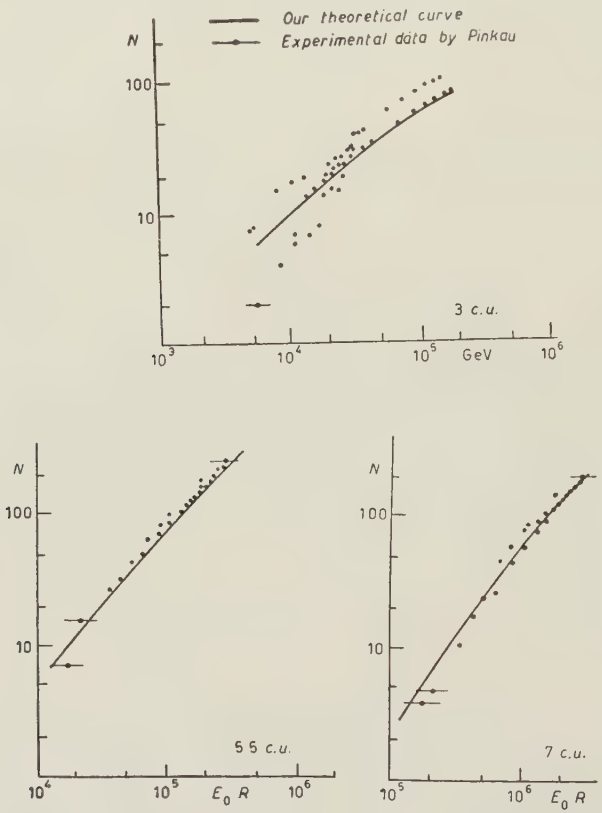

Fig. 10. – Comparison with Pinkau's data. E_0 is the energy of the primary γ-ray.

By examining the observed value of opening angle and energy of each double core event, all the events can be classified into the following two groups. One is the group of showers, in which the opening angle is not significantly different from zero and the two cores appear to be parallel within our experimental accuracy. They can be interpreted as some electromagnetic phenomena, such as an electron pair created outside the emulsion chamber.

The other is the group of showers, in which the measured opening angle is significantly different from zero. These are the showers which we used for the calibration.

In Table VII the results of analyses are presented for the double core events, three of which M.K.1, T.O.6 and Ya.N.2 are interpreted as the decay of a single π^0-meson. The comparison is made between the observed value of the opening angle and the expected value calculated from the cascade theory and

the kinematics. An agreement in the above three cases shows that there is no serious systematic error in our cascade function.

TABLE VII. – *Showers with double core structure.*

Events	Energy of γ-rays estimated from their cascade showers (eV)		Distance between two cores (μm)	Opening angle of two γ-rays (rad)	
	E_1	E_2		obs.	cal.
M.K.1	$(1.5\pm0.5)\cdot10^{11}$	$(1.5\pm0.5)\cdot10^{11}$	60	$(1.15\pm0.2)\cdot10^{-3}$	$0.9\cdot10^{-3}$
T.O.6	$(3.0\pm0.4)\cdot10^{11}$	$(5.0\pm1.3)\cdot10^{10}$	330	$(2.1\pm0.4)\cdot10^{-3}$	$1.1\cdot10^{-3}$
Ya.N.2	$(2.0\pm0.3)\cdot10^{11}$	$(7.0\pm0.15)\cdot10^{10}$	100	$(1.4\pm0.5)\cdot10^{-3}$	$1.2\cdot10^{-3}$
Yo.N.2	$(5.0\pm1.0)\cdot10^{11}$	$(2.0\pm0.6)\cdot10^{11}$	144	$(0.4\pm0.9)\cdot10^{-4}$	$4.5\cdot10^{-4}$
T.O.7	$(4.0\pm1.3)\cdot10^{10}$	$(4.0\pm1.3)\cdot10^{10}$	370	$(0.2\pm0.6)\cdot10^{-3}$	$3.5\cdot10^{-3}$

The other test is made by comparing the theoretical results with the experimental data of PINKAU on the cascade showers. He observed several events of cascade showers initiated by a single γ-ray in an emulsion stack, and a scattering measurement was made on every shower track. As a result, an approximate value is obtained for the total energy of these showers, and at the same time, their shower transition curves are constructed by counting the number of shower tracks within a certain distance from the shower axis. These two data offer us a possibility of testing our cascade function.

As was stated in Appendix I, the three dimensional cascade function depends on the primary energy E_0 and the distance from the center R only through the product E_0R. In Fig. 10, both experimental and theoretical curves are plotted with the shower particle number as the ordinate and the parameter E_0R as the abscissa for several values of the distance traversed. An agreement in the absolute value seems fairly good particularly around the shower maximum ($S=1$) in which we are mainly interested.

APPENDIX III

Design of the emulsion chamber.

In Sect. 2 is shown that our emulsion chambers are designed to observe separately cascade showers from each γ-ray. Here we present in some detail the argument which is used for the design of these chambers.

Now we consider a simple case in which a π^0-meson of energy E_0 is produced at a distance l from the lead layer and an observation is made on the

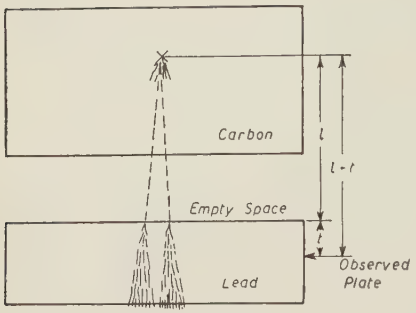

Fig. 11. – Illustration of a π^0-meson decay. $n = (l + t)/t$.

cascade showers of these two γ-rays at the depth t in the lead layer. The ratio of the two lengths, $t + l$ and t,

$$n = (t + l)/t\,,$$

(l and t measured in the cascade unit of lead, ~ 0.5 cm), is introduced as a parameter (see Fig. 11). It is clear that the separability of these cascade showers becomes better with increasing n. A quantitative treatment for this separability is made as follows.

At the place of the observation, the two showers 1 and 2, are assumed to have their centers at the point A and C. The distance R between A and C is related to the opening angle of 2 γ-rays in the decay of the π^0-meson, assuming its energy is equally divided, and is given by

$$R = \left(\frac{2m_{\pi^0}C^2}{E_0}\right) nt\,.$$

The middle point between A and C is named B. To have a quantitative estimate on the separability of showers 1 and 2, we draw three circles, a, b and c, with radii of $R/4$ and with their centers at A, B and C as shown in Fig. 12. Let the number of particles in the circles a, b and c be N_a, N_b and N_c respectively, and we define the quantity Σ

$$\Sigma = \frac{N_a - N_b}{(N_a + N_b)^{\frac{1}{2}}} = \frac{N_c - N_b}{(N_c + N_b)^{\frac{1}{2}}}\,.$$

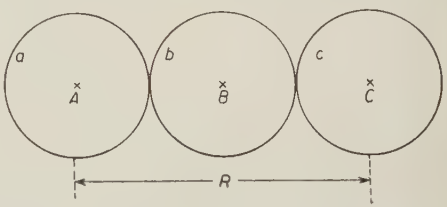

Fig. 12. – A and C are the centers of the showers 1 and 2 respectively, and B is the middle point of the distance between A and C.

Σ is called the « separability parameter » which measures how distinctly we can identify the two cascade showers beyond the fluctuation in the number of showers tracks.

In the calculation of the above parameter Σ, the lateral distribution function is approximated as,

$$N(mR) \sim \left(\frac{\mu C^2}{K} \cdot 2nmt\right)^s \exp\left[\lambda_1(s)t\right],$$

where $N(mR)$ is the number of electrons within a distance mR from the center, and s the age parameter. By using this approximation, an explicit expression can be obtained for the separability parameter Σ as follows,

$$\Sigma(t, n) = N(t)^{\frac{1}{2}} f(s) n^{s/2}\,,$$

where $N(t)$ is the number of electrons of the shower 1 in the circle a for the case of $n=1$, *i.e.* in homogeneous matter. The age parameter s is a function of t and n. In Fig. 13, the numerical values of the separability Σ are plotted with varying t and n. As shown in this figure, Σ has a broad maximum, the height and position of which increases with increasing t. From these curves, suitable values can be determined for the size of the empty space, and the thickness of the lead and carbon layers in our emulsion chamber.

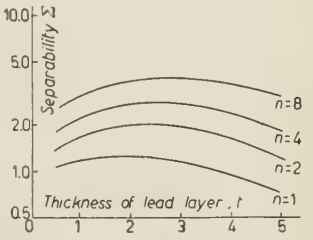

Fig. 13. – Separability Σ as a function of t and n.

Another condition to be considered here is a requirement on the accuracy in the measurement of energy on each cascade shower. If the error is required to be smaller than 25%, the number of shower particles N_a or N_c in the above defined circles a or c should be larger than 20. This condition can be satisfied by making the parameter n larger than 2, as is seen from Fig. 14.

If we fix the value of the parameter n as 2 for our emulsion chamber, the separability parameter Σ has a maximum at $t=3$ with its value about 2. This means that the probability of missing to detect the core structure of the shower is about one in twenty. It should be remarked that the above discussions are made for a simplified model, *i.e.*, a decay of a single π^0-meson into two γ-rays of equal energy. In actual showers, however, a number of π^0-mesons will be produced with different energies, and in their decay into γ-rays the energy will not be equally divided. Furthermore, a fluctuation in the cascade shower may not be of the Poisson type as we assumed here. All these complications are expected to increase slightly the optimum value of n so that the value $n \sim 4$ is chosen for the design of the chamber of type A. For the type B chambers, the value $n \sim 2$ is adopted to observe more events by making use of wide solid angles.

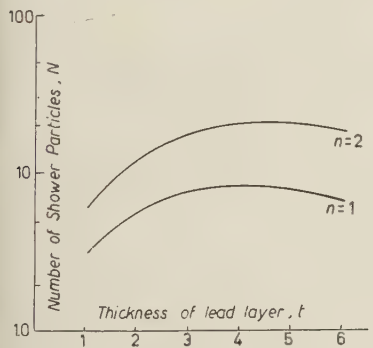

Fig. 14. – Number of shower electrons within a circle a or c defined in Fig. 12.

Appendix IV

Statistical treatment to eliminate the ambiguity of the position of the shower axis.

In our measurement of the transverse momenta P_T of the π^0-mesons, the shower axis is assumed to be equally directed as the energy weighted average direction of the observed π^0-mesons. This means that the vector sum of the observed transverse momenta in a jet is always put equal to zero.

Of course, this is just an approximate procedure, and the correction factor should be calculated.

In the following calculation the relation between the true and observed distribution is derived assuming first independence of the transverse momentum P_T of other quantities. After a Bessel transformation we get the relation between the moments of P_T for both distribution functions. Thus we can construct the true distribution function from the observed data.

Suppose we have n π^0-mesons in a shower, discriminating them with a suffix, j $(j = 1, 2, ..., n)$. Let $\boldsymbol{P}_{Tj}$ and $\boldsymbol{P}'_{Tj}$ be the true and observed values of the transverse momentum of the j-th meson respectively, then we have

$$\boldsymbol{P}'_{Tj} = \boldsymbol{P}_{Tj} - \frac{P_j}{\sum_k P_k} \left(\sum_k \boldsymbol{P}_{Tk}\right), \tag{A4. 1}$$

where P_j is the momentum of the j-th meson.

Suppose $\prod_j f(\boldsymbol{P}_{Tj})\,\mathrm{d}\boldsymbol{P}_{Tj}$ and $F(\boldsymbol{P}'_{T1}, \boldsymbol{P}'_{T2}, ..., \boldsymbol{P}'_{Tn}) \prod \mathrm{d}\boldsymbol{P}'_{Tj}$ to be the distribution functions of the true and observed values of the transverse momenta.

Then the relation between both distribution functions is given by

$$F(\boldsymbol{P}'_{T1}, ... \boldsymbol{P}'_{Tn}) = \int ... \int \prod_{j=1}^{n-1} \mathrm{d}\boldsymbol{P}_{Tj}\, \mathrm{d}\boldsymbol{P}_{Tn}\, \delta\left(\boldsymbol{P}'_{Tj} - \left(\boldsymbol{P}_{Tj} - \frac{P_j \sum \boldsymbol{P}_{Tk}}{\sum P_k}\right)\right) \cdot$$
$$\cdot \delta\left(\boldsymbol{P}'_{Tn} - \sum_l^{n-1} \boldsymbol{P}'_{Tl}\right) f(\boldsymbol{P}_{Tj}) f(\boldsymbol{P}_{Tn}) .$$

Multiplying $\exp[i\boldsymbol{t}_j \boldsymbol{P}'_{Tj}]$ on the both sides of the above formulae and integrating with respect to $\boldsymbol{P}'_{Tj}$ we get

$$\int ... \int \prod_{j=1}^{n-1} \mathrm{d}\boldsymbol{P}'_{Tj} \exp[i\boldsymbol{t}_j \boldsymbol{P}'_{Tj}] F(\boldsymbol{P}'_{T1} ... \boldsymbol{P}'_{Tn}) =$$
$$= \int ... \int \prod_{j=1}^{n} \mathrm{d}\boldsymbol{P}_{Tj} \exp\left[i\left\{(\boldsymbol{t}_j - \boldsymbol{t}_n)(1 - x_j) - \sum x_k (\boldsymbol{t}_k - \boldsymbol{t}_n)\right\} \boldsymbol{P}_{Tj}\right] \cdot f(\boldsymbol{P}_{Tj}) =$$
$$= \int ... \int \prod_j \mathrm{d}\boldsymbol{P}_{Tj} \exp[i\boldsymbol{\zeta}_j \boldsymbol{P}_{Tj}] f(\boldsymbol{P}_{Tj}) , \tag{A4.2}$$

where we put

$$x_j = \frac{P_j}{\sum P_k}$$

and

$$\boldsymbol{\zeta}_j = (1 - x_j)(\boldsymbol{t}_j - \boldsymbol{t}_n) - \sum_{k \neq j} x_k (\boldsymbol{t}_k - \boldsymbol{t}_n) = (1 - x_j)\, \boldsymbol{T}_j - \sum_k x_k \boldsymbol{T}_k . \tag{A4.3}$$

We have only $n - 1$ independent vectors $\boldsymbol{T}_k$. Not all $\boldsymbol{\zeta}_j$ are now independent of each other, because the centre of the transverse momenta is taken as the shower axis, which reduces the degrees of freedom. Hereafter we have $\boldsymbol{\zeta}_n$ as the dependent vector, so that the $\boldsymbol{\zeta}_n$ is represented from (A4.3)

by the formula

$$\zeta_n = -\sum_{j}^{n-1} \frac{x_j}{x_n} \zeta_j \,, \tag{A4.4}$$

where we use the relation

$$\sum x_k = 1 \,.$$

From (A.4.4), the formula (A4.2) becomes

$$G(\zeta_1 - \zeta_n, \ldots \zeta_j - \zeta_n, \ldots 0) = \prod_j^n g_j(\zeta_j)\, g_n\left(\sum_i^{n-1} \frac{x_i}{x_n} \zeta_i\right), \tag{A4.5}$$

where

$$G = \frac{1}{(2\pi)^n} \int \ldots \int F(\boldsymbol{P}'_{T1} \ldots \boldsymbol{P}'_{Tn}) \exp\left[i\boldsymbol{P}'_{Tj}(\zeta_j - \zeta_n)\right] \prod_j \mathrm{d}\boldsymbol{P}'_{Tj} \tag{A4.6}$$

and

$$g_j = \frac{1}{2\pi} \int f_j(\boldsymbol{P})_{Tj} \exp\left[i\zeta_j \boldsymbol{P}_{Tj}\right] \mathrm{d}\boldsymbol{P}_{Tj} \,.$$

Here we assume the true distribution of the transverse momentum to be symmetric with respect to the shower axis and independent of the energy of the secondary particle, so that

$$f_1(\boldsymbol{P}_{Ti})\, \mathrm{d}\boldsymbol{P}_{Ti} = \ldots = f_n(\boldsymbol{P}_{Tn})\, \mathrm{d}\boldsymbol{P}_{Tn} = f(P_T) 2\pi P_T \mathrm{d}P_T \,. \tag{A4.7}$$

Then, we get

$$G(\zeta_1 - \zeta_n, \ldots \zeta_{n-1} - \zeta_n,\ 0) = \prod_j g_j(\zeta_j)\, g_n\left(\sum_i^{n-1} \frac{x_n}{x_i} \zeta_i\right), \tag{A4.8}$$

where

$$g(\zeta_j) = \frac{1}{2\pi} \int f(\boldsymbol{P}_{Tj}) \exp\left[i\boldsymbol{\zeta}_j \boldsymbol{P}_{Tj}\right] \mathrm{d}\boldsymbol{P}_{Tj} = \int_0^\infty J_0(P_{Tj}\zeta_j) f(P_{Tj}) \cdot P_{Tj} \mathrm{d}P_{Tj} \,, \tag{A4.9}$$

and

$$G = \int \ldots \int \prod_j^{n-1} J_0\left\{P_{Tj} \cdot (\zeta_j - \zeta_n)\right\} F(P'_{T1}, P'_{T2} \ldots, P'_{Tn}) P'_{Tj} \mathrm{d}P'_{Tj}\, P'_{Tn} \mathrm{d}P'_{Tn} \,. \tag{A4.10}$$

In order to obtain the information about g by using Eq. (A4.8), we first put $\zeta_1, \ldots, \zeta_n$ to zero except ζ_j and ζ_n.

Then from eq. (A4.4)

$$\zeta_n = -\frac{x_j}{x_n} \zeta_j \,.$$

Since

$$g(0) = 1$$

we get from eq. (A4.8)

$$G_1\left(\frac{x_j}{x_n}\zeta_j, \frac{x_j}{x_n}\zeta_j, \ldots, \zeta_j\frac{x_j}{x_n}\zeta_j, \ldots\right) = g(\zeta_j)\, g\left(\frac{x_j}{x_n}\zeta_j\right). \tag{A4.11}$$

We expand both sides of the equation (A4.11) into the power series of ζ^{2n}. Then we get the relation between the moments of the true and observed distribution by equating the coefficient of both sides of these series, because these coefficients are functions of the moment.

Another approach to get the solution of the equation (A4.8) is as follows. First we put $\zeta_1, \ldots, \zeta_n$ to be egual except ζ_j, then

$$\zeta_j = -\sum_{i\neq j}^{n}\frac{x_i}{x_j}\zeta_i - -\frac{(1-x_j)}{x_j}\zeta_1 ,$$

and we get the relation

$$G\left(0, 0, \ldots \frac{\zeta_1}{x_j}, \ldots 0, 0\right) - g\left(\frac{(1-x_j)\zeta_1}{x_j}\right) g^{n-1}(\zeta_1) . \tag{A4.11'}$$

Expanding both sides of (A4.11) into a power series of ζ^{2n} as before, we get the relation for the moment,

$$\begin{cases} \langle P_T'^2\rangle = C_{2,2}\langle P_T^2\rangle , \\ \langle P_T'^{2n}\rangle = C_{2m,2n}\langle P_T^2\rangle^m + C_{2m,2m-2,2}\langle P_T^{2m-2}\rangle\langle P_T^2\rangle - \\ \qquad + C_{2m,2m-4,2,2}\langle P_T^{2m-4}\rangle\langle P_T^2\rangle^2 + C_{2m,2m-4,4}\langle P_T^{2m-4}\rangle\langle P_T^4\rangle + \\ \qquad + (\text{all possible combinations of factors having the correct dimension}). \end{cases} \tag{A4.12}$$

The coefficients $C_{2m,2n}, \ldots$ are a polynomial of $2m$-th power of x with coefficients depending on the shower multiplicity n.

The above equations show that the correction factor varies with x and n. This means that the amount of information obtained from the measurement of a single π^0-meson differs according to the shower multiplicity and the energy partition, so that the data should be properly weighted.

For example, we get the weighted average $\langle P_T^{2n}\rangle$ putting

$$\langle P_T^2\rangle = \frac{\sum_j W_j\left(\frac{\langle P_{T_j}'^2\rangle}{C_{22j}}\right)}{\sum_j W_j},$$

where the weight W_j,

$$W_j = \frac{\langle P_{T_j}'^2\rangle^2}{\langle P_{T_j}'^4\rangle - \langle P_{T_j}'^2\rangle^2} .$$

From equation (A4.12), the above formula is written now,

$$W_j = \frac{C_{22j}^2 \langle P_{Tj}^2 \rangle^2}{C_{44j}\langle P_{Tj}^4 \rangle + (C_{42j} - C_{22j}^2)\langle P_{Tj}^2 \rangle^2} .$$

A similar weight function is also derivable for $\langle P_T^{2n} \rangle$, but they are somewhat compliated.

In applying the above formula for the actual analysis, we first calculate W_j using the values of $\langle P_T^{2n} \rangle$ derived from the experimental data with equal weight.

Second, we get the values of the weighted $\langle P_T^{2n} \rangle$ using the above $\langle P_T^{2n} \rangle$. After this calculation, these values are compared with those used for calculating $\langle P_T^{2n} \rangle$, and if there are any significant differences between them, we iterate further. The convergence of this iteration is very good, and one or two iterations are sufficient for our practical purpose.

The weighted $\langle P_T^{2n} \rangle$ thus obtained are shown in Table VIII.

TABLE VIII. – *Moments of the traverse momentum.*

$\langle P_T^2 \rangle$	15.0 ± 1.7	$(10^8$ MeV/c$)^2$
$\langle P_T^4 \rangle$	335 ± 140	$(10^8$ MeV/c$)^4$
$\langle P_T^6 \rangle$	$10\,600 \pm 8\,000$	$(10^8$ MeV/c$)^6$

SUPPLEMENTO AL VOLUME XI, SERIE X
DEL NUOVO CIMENTO

N. 1, 1959
1° Trimestre

A proposito della "Fisica dei corpi ponderabili" di Amedeo Avogadro.

E. PERUCCA

Istituto di Fisica del Politecnico di Torino

(ricevuto il 19 Gennaio 1959)

Nella mia rievocazione di AMEDEO AVOGADRO, tenuta a Torino in occasione della celebrazione del 1° Centenario della sua morte, e pubblicata nel *Supplemento* al Vol. VI, Serie X, del *Nuovo Cimento*, 1957, pag. 10-27, ponevo la questione se la famosa *Fisica dei corpi ponderabili*, dall'AVOGADRO stesso data alle stampe a « Torino, presso la Stamperia Reale », tra il 1837 e il 1841, fosse stata pubblicata a spese del Re Carlo Alberto. A crederlo spingeva soprattutto la frase con la quale nella dedicatoria AVOGADRO « umiliava » l'opera a Sua Maestà: « Compiuto ora questo lavoro..., io mi fo animo ad umiliarlo a V.S.R.M., omaggio ben dovuto a quel Sovrano Protettore e fautore munificentissimo di ogni nobile studio... ».

Posso oggi rispondere esaurientemente alla domanda posta: infatti il prof. NICOLÒ RODOLICO — che qui ringrazio — mi ha recentemente segnalato che tra le « Carte che appartennero a Carlo Alberto » e ora si conservano presso la Biblioteca del Re, l'opera di AVOGADRO — come il RODOLICO stesso aveva ricordato in *Carlo Alberto negli anni di regno 1831-1843*, Vol. II, Firenze, Le Monnier, 1936, pag. 386 — è annoverata appunto tra quelle che il Re fece stampare a sue spese.

Direttore responsabile: G. POLVANI

Tipografia Compositori - Bologna

Questo fascicolo del *Supplemento* è stato licenziato dai torchi il 14-III-1959